POLITECNICO DI TORINO

Corso di Laurea Magistrale in Ingegneria per l'Ambiente e il Territorio

Tesi di Laurea Magistrale

Application of shallow geothermal energy systems to pressure reduction stations of the natural gas pipeline network

Relatore

Ing. Alessandro Casasso

Correlatori

Ing. Bruno Piga

Ing. Edoardo Ruffino

Candidato

Amerigo Musti

Marzo 2021

ABSTRACT

Climate change and fossil fuel depletion are urging all industrial sectors to reduce the use of non-renewable energy sources and replace them with renewables. The management of gas pipeline networks and, in particular, gas pressure reduction stations (PRS) represent a niche with good potential to increase energy efficiency. PRSs are plants connecting the international high-pressure pipeline network, operating at about 60 bar and managed by the State-owned company SNAM, to the local low-pressure network, operating at about 5 bar and managed by local companies. The expansion operated at PRS causes a temperature drop of gas, even below 0 °C, which could damage pipelines. Therefore, PRSs need to warm up natural gas upstream the expansion valve. The heat is generally provided by gas boilers, with consequent fossil fuels consumption and pollutant emissions into the atmosphere, but also the risk of fires and explosions. Alternative solutions for gas preheating at PRS have therefore been sought and, among them, heat pumps. Indeed, heat pumps combine the benefits of eliminating combustion on site and reducing overall greenhouse gases (GHG) emissions.

This thesis presents the case study of a PRS in Magliano Alfieri (NW Italy), managed by the local utility EGEA, which delivers about 16.5 million Sm^3 of gas per year. The line-heater consumes about 18500 Sm^3 of gas per year (i.e., about 180 MWh/y), implying GHG emissions of about 40 tCO_2 equivalent. Natural gas thermodynamic processes and properties were studied to determine inlet and outlet temperatures at the shell and tube heat exchanger and the overall heat transfer coefficient. Calculations on the preheating system led to an estimation of 40 kW as peak thermal power needed by the PRS.

The option to replace the gas boiler with a geothermal heat pump was evaluated. Since the site lies on an alluvial plain, an open-loop system was proposed. Although the local stratigraphy and hydrogeological setting were not studied widely so far, merging different datasets allowed to derive an acceptable conceptual model of the site. A single-well pumping test performed at an existing borehole led to an estimation of transmissivity and hydraulic conductivity. Based on the results of these elaborations, the open-loop system was simulated with a numerical flow and heat transport model implemented on the finite-element code FEFLOW. Modelling results confirmed the operational sustainability of the open-loop system. As an alternative, a closed-loop system was designed adopting the Eskilson method implemented on Earth Energy Designer (EED). A payback time of 7 and 10 years was found for the open-loop and the closed-loop geothermal systems, respectively, with a reduction of GHG emissions of more than 70% in both cases.

The work carried out in this thesis sheds light on the potential to implement renewable energy sources in the gas distribution network, reducing its impacts on environment and increasing its sustainability and safety.

TABLE OF CONTENTS

SCOPE OF WORK

In this study, the application of shallow geothermal energy systems is proposed to replace gas-fired line-heaters used in pressure reduction stations of the natural gas distribution network.

Natural gas is transported through buried pipelines at high pressure (60 bar) from production sites. Before its use in industries or buildings, the pressure of natural gas must be reduced to a lower value (5 bar). This action is performed in pressure reduction stations, where natural gas is expanded from high to low pressures through the use of throttling valves. The expansion process induces a temperature drop due to the Joule-Thomson effect. Temperatures below 0°C, however, could induce the formation of methane hydrates that may damage pipes. For this reason, before the pressure reduction step, a natural gas preheating system is usually required in order to provide the necessary heat.

The aim of this thesis is to study the feasibility of using a groundwater heat pump or vertical boreholes heat exchangers to perform gas preheating. The use of geothermal energy resources can be an alternative and innovative solution to reduce greenhouse gases emissions due to the large amount of fossil fuel consumption by conventional boilers, but also to reduce the risk of fires and explosions at natural gas pressure reduction stations.

The rest of the work is structured as follows.

In *Chapter 1* (Introduction) the most important literature themes are briefly presented: a short review of the basic theory of geothermal energy and heat transport mechanisms, the low-enthalpy geothermal systems and the ground source heat pumps. Then, the natural gas distribution network is described, with specific reference to the Italian pipeline network, and the case study is introduced.

Chapter 2 analyses the approaches adopted to study the problem. In this section, the plant design is presented for the different configurations. First of all, the design of the conventional preheating system is addressed through the sizing of the methane boiler and the shell and tube heat exchanger. Then, a groundwater flow and heat transport model is set for the open-loop configuration and implemented with the software FEFLOW. Subsequently, the closed-loop geothermal system is sized with the Earth Energy Designer (EED) software.

Chapter 3 presents the results of the work. Different methodologies, used for the design of the two novel systems, are validated. Furthermore, consumed energy, costs, and CO_2 emissions are compared with the conventional plant configuration.

Conclusions and final considerations are reported in *Chapter 4*.

1 INTRODUCTION

This Chapter presents an overview of all the major issues concerning this study.

In the C*hapter 1.1* the heat transport mechanisms and the geothermal energy uses are analysed. In particular, the low-enthalpy geothermal systems are described, and the basic processes of heat pumps operation are explained, with a focus on the heat exchangers. Moreover, two kinds of installations are examined: vertical boreholes ground heat exchangers in closed-loop configurations and groundwater heat pumps in open-loop geothermal systems.

In the *Chapter 1.2*, the natural gas pipeline network is presented, with details on the Italian one. In particular, pressure reduction stations and pre-treatments of the natural gas are analysed, as they are the focus of this thesis. The main processes examined in this work are the rapid expansion in the regulator and the preheating of gas.

Chapter 1.3 is focused on the description of the case study, the "Alba4" pressure reduction station (PRS). In this section, the geographical framework is presented, but also the gas thermodynamic processes and the input operational parameters of the PRS are described, with particular attention on the shell and tube heat exchanger.

1.1 GEOTHERMAL ENERGY

Geothermal energy is the heat naturally originated and stored in the earth. It can be found at very high depths or in the shallow ground. In the first case, geothermal heat is mainly used for electrical energy generation in power plants; on the other hand, geothermal energy stored in the lower underground and in the aquifers can be used for heating and cooling, with the help of heat pumps. Geothermal energy sources can be classified as:

- low-temperature (T < 90 °C) or low-enthalpy resources;
- middle-temperature (T ≈ 90-150 °C) or medium-enthalpy resources;
- high-temperature (T > 150 °C) or high-enthalpy resources.

Deep geothermal technologies are only available in certain zones, whereas geothermal heat pumps could be used virtually everywhere. Besides electricity production, geothermal energy is also used to heat and cool buildings. The potential of geothermal resources is very large and it is expected to grow in the next years; the road map to 2050 is shown in the *Fig. 1.1* below.

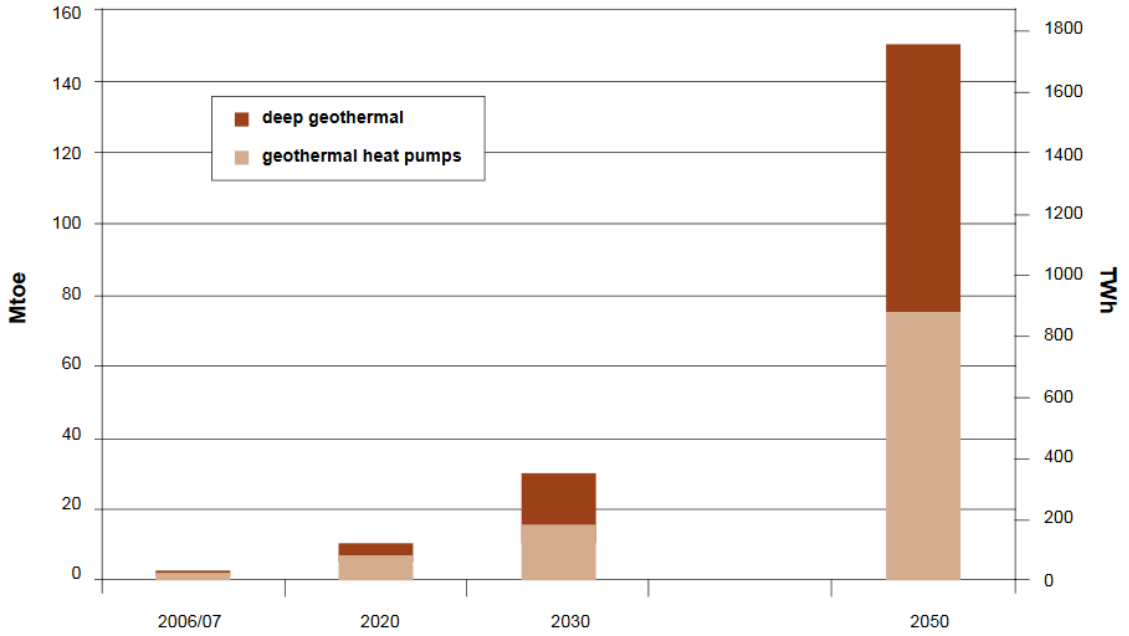

Fig. 1.1 Heating potential of geothermal energy in EU (*from [1]*).

The heat budget in the underground is represented in *Fig. 1.2.* At low depths, is composed of absorbed, reflected, and irradiated heat, temperature changes of the ground (sensible heat exchange), and heat exchanges related to weather conditions (wind, precipitations, etc.). At large depths, the main contributions are the radioactive decay (involving elements which are present in the rocks) and the geothermal heat flux (which comes from the mantle on which the earth crust floats).

Heat transport in porous media occurs through three distinct mechanisms, that are shown in *Fig. 1.3*:

1) Conduction: thermal exchange in a medium due to the temperature gradient and random particles collisions. Conductive heat transport is governed by Fourier's law, similar to Fick's law for molecular diffusion:

$$J_{C,x} = -\lambda \frac{\partial T}{\partial x} \tag{1.1}$$

where $J_{C,x}$ is the conductive flux (Wm^{-2}), and λ is the thermal conductivity ($Wm^{-1}K^{-1}$).

2) Advection: energy transfer by a moving fluid. The advective flow J_A (Wm^{-2}) is proportional to the Darcy velocity:

$$J_A = -v_e n_e \rho_w c_w T \tag{1.2}$$

where v_e (ms^{-1}) is the effective (average) water velocity in the pores, n_e (-) is the effective porosity, the aquifer fraction in which water flows, ρ_w (kg m^{-3}) and c_w (J $kg^{-1}K^{-1}$) are the water density and its specific heat.

Heat moves in porous media like a solute subject to sorption and, hence, to retardation: there is an equilibrium between fluid temperatures and the solid phase. The propagation velocity v_{th} (ms^{-1}) of the thermal plume is defined as follows:

$$v_{th} = \frac{v_e}{R_{th}} \tag{1.3}$$

where R_{th} (-) is the retardation coefficient and depends on the thermal capacity ρc (Jm^{-3}K^{-1}) of the porous medium:

$$R_{th} = 1 + \frac{(1-n_e)\rho_s c_s}{n_e \rho_w c_w} = \frac{\rho c}{n_e \rho_w c_w} \tag{1.4}$$

where the subscripts s indicate the soil matrix.

3) Dispersion: heat transport due to the heterogeneity of the flow field. Thermal dispersion J_D (Wm^{-2}) occurs only in presence of groundwater flow:

$$J_D = -\rho_w c_w \alpha_x v_e \frac{\partial T}{\partial x} \tag{1.5}$$

where α_x(m) is the thermal dispersivity, it is scale-dependent and it has two distinct values for longitudinal and transverse directions. The dispersion spreads the thermal plume through time along and perpendicularly to the flow direction.

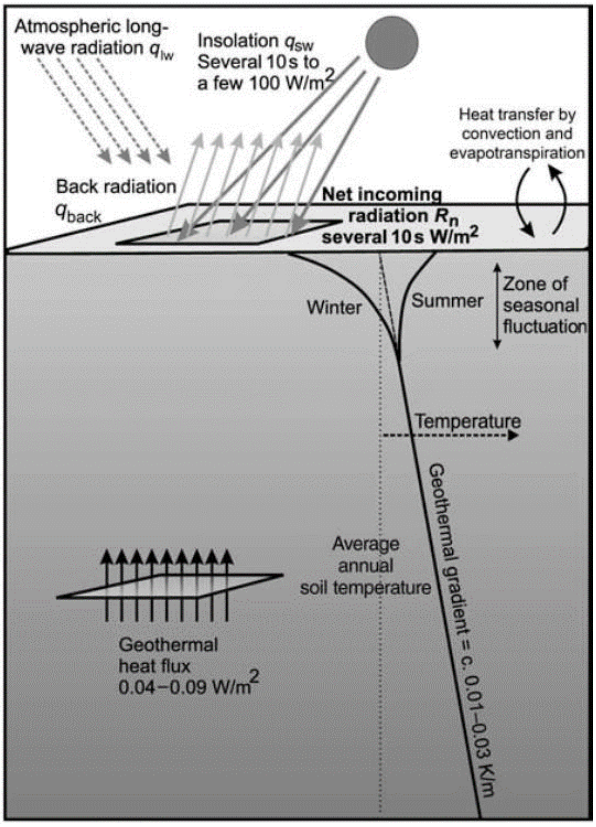

Fig. 1.2 Heat balance in the underground (*from [2]*).

The above-described heat fluxes are combined in the heat conservation equation:

$$\frac{\partial T}{\partial t} + D_x \frac{\partial^2 T}{\partial x^2} + D_y \frac{\partial^2 T}{\partial y^2} + D_z \frac{\partial^2 T}{\partial z^2} - v_{th} \frac{\partial T}{\partial x} = \frac{H}{\rho c} \tag{1.6}$$

where H (Wm^{-3}) is the thermal source (> 0) or sink (< 0), D_x (m^2s^{-1}) is the dispersion coefficient along the groundwater flow direction x, D_y and D_z (m^2s^{-1}) are the thermal dispersion coefficients transversally to groundwater flow:

$$D_x = \frac{\lambda}{\rho c} + \alpha_L v_{th} \tag{1.7}$$

$$D_y = D_z = \frac{\lambda}{\rho c} + \alpha_T v_{th} \tag{1.8}$$

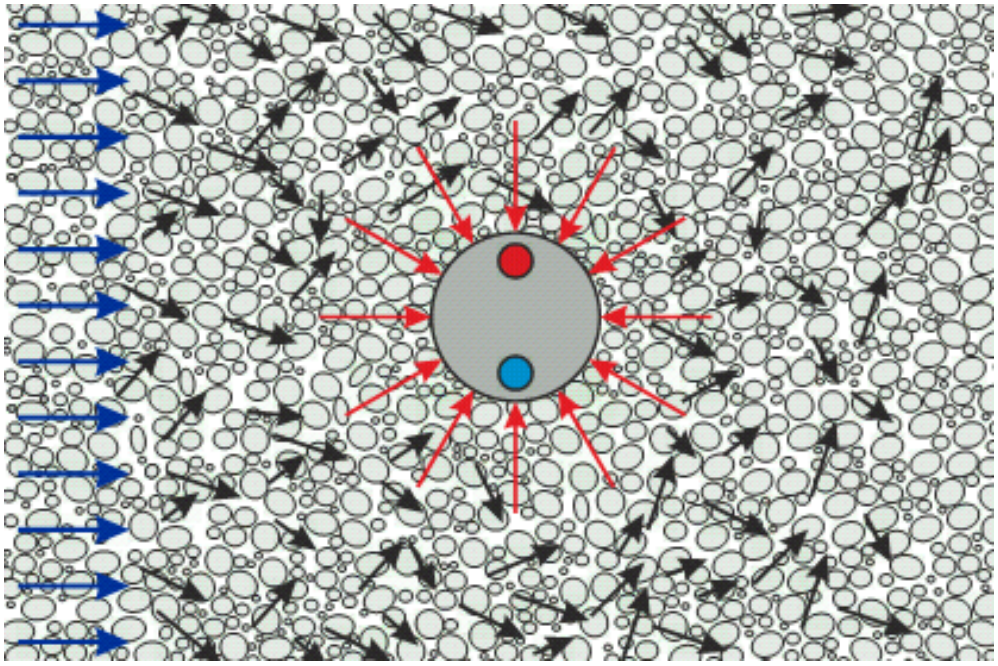

Fig. 1.3 Heat transport mechanisms in a porous medium (conduction in red, advection in blue and dispersion in black).

1.1.1 LOW-ENTHALPY GEOTHERMAL SYSTEMS

Low-enthalpy geothermal resources have been used since the end of the last century. In recent years, geothermal energy consumption has seen a continuous growing, thanks to its high efficiency, sustainability and increasing competitiveness.

The utilization of low-enthalpy geothermal systems is made possible by using ground-source heat pumps (GSHP), i.e., heat pumps which use the underground as a heat source (for heating) or sink (for cooling). The main advantage with respect to the air is that the ground temperature at relatively low depths is almost constant throughout the year, that is, warmer than air during winter and cooler than air during summer. As shown in the *Fig. 1.4* below, the amplitude of temperature oscillations throughout the year (and the day) diminishes as depth from ground surface increases.

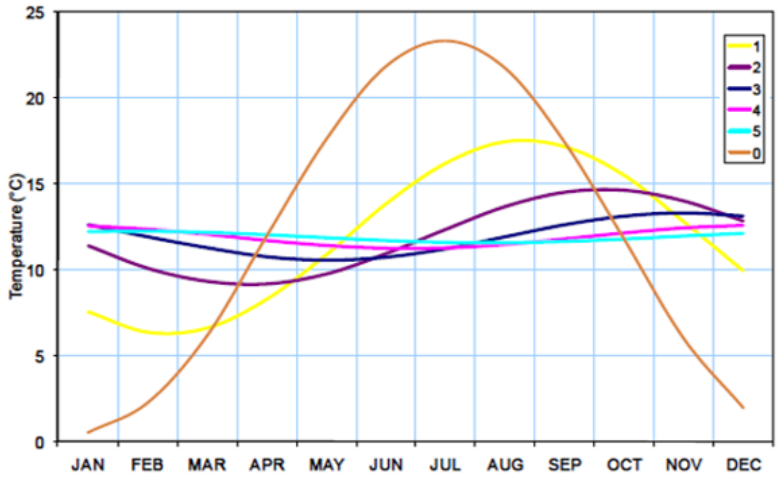

Fig. 1.4 Temperature oscillations from 0 to 5 m depth in Turin (Italy).

A low-enthalpy geothermal energy system consists of three main elements:

- the heat pump;
- the ground heat exchanger;
- the heating/cooling system of the building.

Thermal energy transfer processes take place by mean of a heat carrier fluid, which flows through tubes that connect heat pumps with ground heat exchangers.

Open and closed-loop configurations are used for heat extraction or heat rejection from/in the underground. Closed-loop systems consist of heat exchangers installed either horizontally or vertically in the ground, while open-loop systems directly use the groundwater or superficial waters.

In *Fig. 1.5* is shown a schematic representation of low-enthalpy geothermal energy systems.

There are several environmental and energy benefits associated with the use of geothermal heat pumps:

- no pollutant emissions on site;
- reduction of greenhouse gases (GHG) emissions;
- reduction of primary energy consumption;
- peak shaving during summer;
- demand side management;
- no fuel storage;
- reduction of visual impacts;
- low noise.

Geothermal heat pumps are widely being used for heating and cooling houses in several regions of the world. Besides the suitability of installing these systems for different building applications, they also have a high use potential in the industrial sector. The waste heat available in most industries can make the utilization of low-enthalpy geothermal resources unfavourable, since the heat production costs have a prevailing role in the choice of energy sources. On the other hand, the use of geothermal heat pumps can contribute to primary energy resources savings for industrial applications with low-heating process demand. Thus, the utilization of low-temperature geothermal systems can help reduce fossil fuels consumption in such industries, covering a relevant fraction of the heat demand with a renewable energy source (RES).

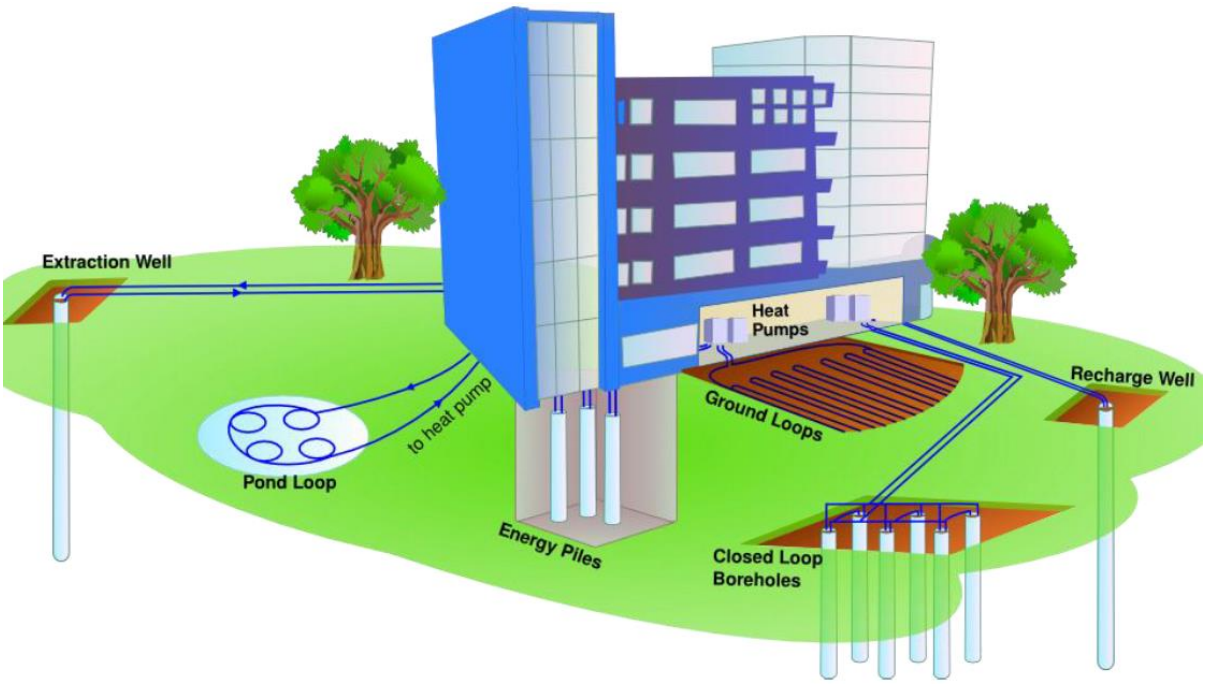

Fig. 1.5 Low-enthalpy geothermal energy systems (source *Polytechnic of Turin*).

1.1.2 HEAT PUMPS

Heat pumps are devices that absorb heat from a cold source and release it to a hot sink: they transfer heat in the direction opposite to spontaneous thermal energy transport. As a result of the second principle of thermodynamics (Kelvin's formulation), this transformation cannot be performed without the use of external energy. In fact, heat pumps require energy in form of mechanical work or heat. In the first case it is a vapour compression heat pump, while in the second an absorption heat pump. Therefore, heat pumps can be divided into two groups according to their functioning principle:

- Vapour compression: the increase of pressure (and thus, temperature) is provided by a mechanical compressor, which consumes electrical energy;
- Absorption: the mechanical compressor is replaced by a thermal source and a binary mix of fluids (aqueous solutions of BrLi or NH_3), in which the most volatile acts as a refrigerant, while the least volatile is a solvent.

The operation process of vapour compression heat pumps is based on the ideal reverse Carnot cycle, which consists of four main phases:

1) isothermal evaporation: heating fluid absorbs heat and passes from saturated liquid to saturated vapour phase;
2) isentropic compression: pressure increases and the saturated vapor is superheated;
3) isothermal condensation: fluid releases heat and condenses to a saturated liquid;
4) isentropic expansion: pressure and temperature decrease and the fluid comes back to initial conditions.

The real vapour compression cycle differs from the above-described ideal one, because compression and expansion always result in an entropy variation. A vapour compression heat pump is therefore composed of the following components: an evaporator, a compressor, a condenser and an expansion valve, as schematically represented in *Fig. 1.6*.

The heat carrier fluid which flows in this circuit is called refrigerant. The heat pump uses the ability of the volatile fluid to absorb and release thermal energy in transitions of phase, from liquid to vapour in the evaporator, and vice versa in the condenser. The characteristics required for a good refrigerant are the following:

- high latent heat of vaporization/condensation ("large bell" on the p-h diagram);
- far below the critical point at the operating temperatures;
- low evaporation and condensation pressure;
- high gas density entering into the compressor;
- non corrosive, non-flammable, and non-toxic;
- stability and chemical compatibility with the heat pump materials and lubricant;
- null or low ozone depleting potential (ODP) and global warming power (GWP).

Regarding these properties, a refrigerant widely adopted is the hydrofluorocarbon R-134a, whereas another substance is R-717, known as ammonia and used in large-scale systems.

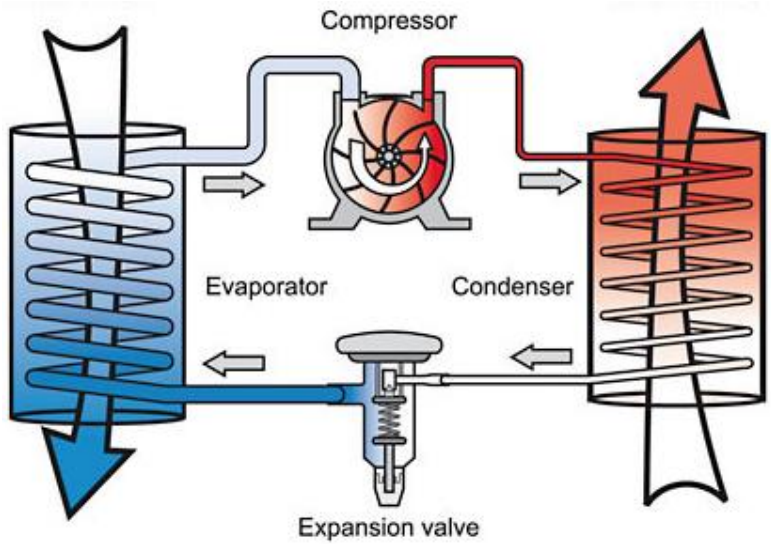

Fig. 1.6 Heat pump work principle and components (*from [3]*).

The energy efficiency of the heat pump is called coefficient of performance (COP) and it is defined as the ratio between the useful effect of the heat pump and the work spent by the compressor. COP is used when the useful effect is heating, while the EER (Energy Efficiency Ratio) is used in the case of cooling. The efficiency depends on the temperature difference between the cold source and the hot sink. In fact, temperature and humidity conditions may affect the performance of a heat pump: if the temperature difference increases, the required pressure difference increases too, and more electricity is needed to compress the heat carrier fluid, thus the overall efficiency decreases. In order to reduce the compressor work and the required energy, the refrigerant flows through insulated pipes. Reference values for COP are about 4 for ground-coupled heat pumps and 4.8 for groundwater heat pumps.

Generally, heat pumps can be used either in heating or cooling mode, therefore, the useful effect is different for the two operation processes:

- for heating: heat is delivered in the condensation phase;
- for cooling: heat is abstracted in the evaporation phase.

During evaporation and condensation, the fluid experiences a phase transition at constant temperature. Thus, the condenser and the evaporator are used to lose or gain, respectively, a certain amount of latent heat involved in the change of phase between liquid and vapour. Evaporators or condensers can be considered as heat exchangers where the temperature does not change from inlet to outlet, on one side, as shown in *Fig. 1.7*.

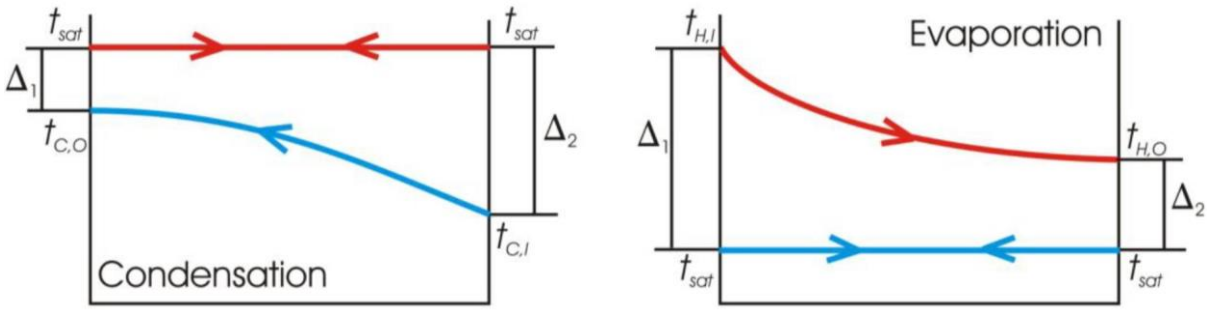

Fig. 1.7 Condensation and evaporation temperature profiles for a pure refrigerant (*from [4]*).

1.1.2.1 HEAT EXCHANGERS

A heat exchanger is a device used to transfer heat between two fluid streams at different temperatures which are separated by a solid wall. Heat always flows from the warmer medium towards the colder one: the thermal power released by the hot stream must be equalled by that absorbed by the cold stream and the heat losses.

Heat exchangers are classified in different typologies according to type of construction and flow arrangement. The basic configuration is the concentric tube, in which the two fluids flow in the same or opposite directions. If the mode is parallel-flow, the hot and cold streams move in the same direction, and enter and leave at the same ends. Instead, if the arrangement is counterflow, the two fluids flow in two opposite directions: one enters into a side, while the other at the opposite, and vice versa.

Generally, the counter-current flow mode is more effective than the co-current one: indeed the outlet temperature of the cold fluid can be higher than the hot fluid one, as shown in *Fig. 1.8*. Therefore, to achieve the same heat transfer rate, it is necessary to provide a smaller heat exchange area for the counterflow configuration. In the case of parallel-flow, there is a large temperature difference between the hot and the cold fluid at the inlet, and a minimum temperature difference at the outlet; while, for the counter-current arrangement, the temperature distribution between the two fluids is quite constant from inlet to outlet of the heat exchanger, as represented in *Fig. 1.8* below.

Another configuration typically used are the shell and tube heat exchangers. The main components are an external tank (the shell) and internal pipes (tubes). Two typologies are possible:

- Flooded: the heating fluid flows in the tubes and the refrigerant in the shell;
- Dry or direct expansion: the refrigerant flows into tubes and the heating fluid in the shell.

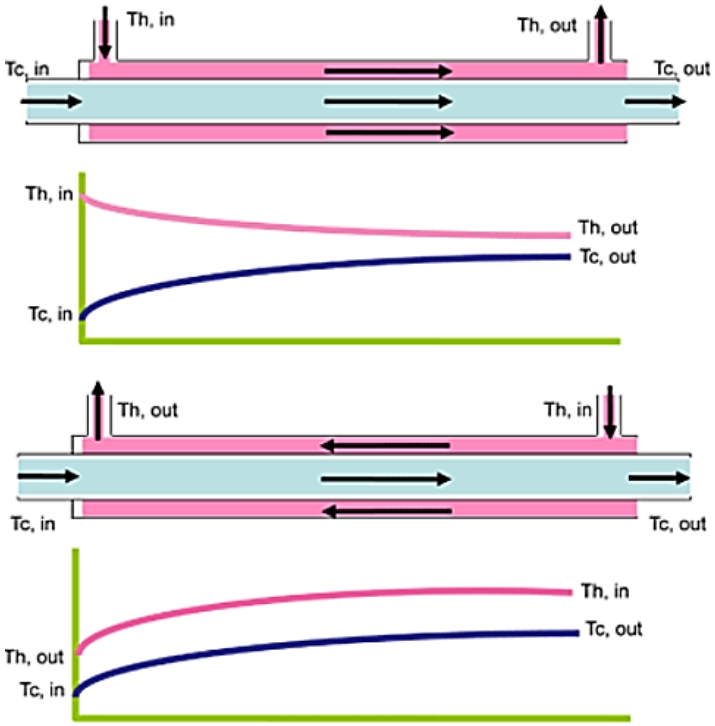

Fig. 1.8 Flow directions and temperature distributions associated with concentric tube heat exchangers: parallel-flow, over, and counterflow, under (*from [5]*).

Different types depend on the number of passes, either for the shell and tubes; for example, *Fig. 1.9* presents a heat exchanger with a single shell and two tube passes, or "U" pattern. In order to increase the convection coefficient, baffles are usually adopted. Baffles create a cross-flow velocity relative to the pipes which increases turbulence and, hence, the convection heat transfer of the shell-side fluid. Moreover, the baffles work as a physical support for pipes, and reduce the tube vibrations.

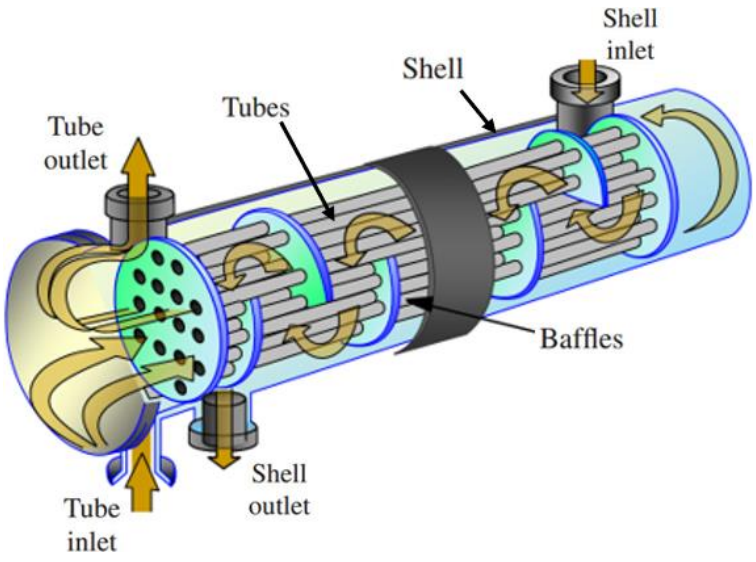

Fig. 1.9 Shell-and-tube heat exchanger (*from [6]*).

1.1.3 CLOSED-LOOP GEOTHERMAL SYSTEMS

Closed-loop geothermal systems rely on a mainly conductive heat transfer between the ground and the heat carrier fluid which circulates in a closed hydraulic loop, releasing or absorbing heat to/from the ground (depending on whether cooling or heating operation mode is used). Ground heat exchangers are divided in three main categories, as shown in *Fig. 1.10*:

A) shallow horizontal collectors like earth coils, serpentine and geothermal baskets;
B) borehole heat exchangers (BHE), which are the most commonly used configuration;
C) geothermal piles and geo-structures, which are pipes integrated in the foundations.

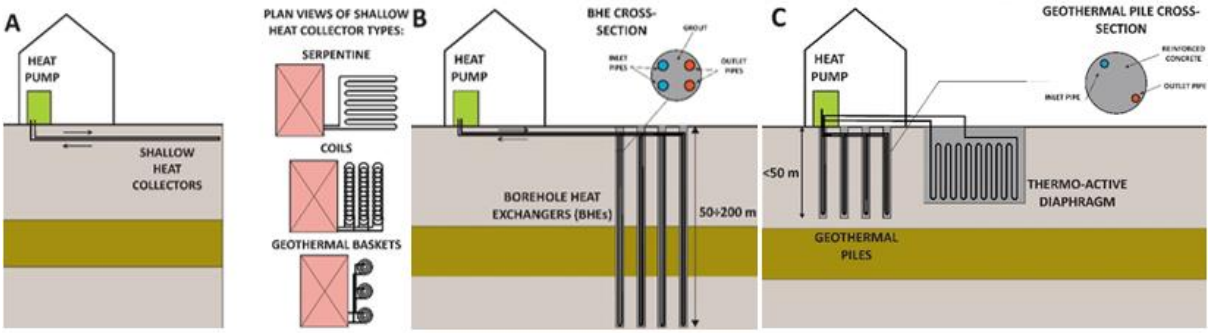

Fig. 1.10 Closed-loop ground heat exchangers classification (*from [7]*).

The borehole heat exchangers consist of polyethylene pipes installed in vertical boreholes which are backfilled with thermal grout. These vertical heat exchangers exploit the ground temperature, which is approximately constant below the 10 m depth. BHEs are very diffused as they can be installed almost everywhere and their design and management are simpler than open-loop systems. Borehole heat exchangers have also proved better performance in comparison with other heating or cooling systems such as air-source heat pumps.

Closed loop geothermal systems are generally composed of several boreholes. Increasing the BHEs number leads to a higher efficiency but also to a higher initial investment cost. For this reason, it must be defined a thermo-economic trade-off. The most efficient BHEs configuration is an L shape array, however, the line, "U" or rectangular arrangements are also possible.

Vertical heat exchangers occupy less land area and have higher efficiency compared to horizontal ones. Indeed, horizontal heat exchangers are installed at low depth and, hence, they still undergo some temperature variation depending on the season and some thermal conductivity variation of the soil due to the variable moisture.

Typical boreholes lengths are about 50-200 m. The longer the borehole, the higher the energy obtainable but, also, the higher the initial investment costs. The B/H factor is the ratio of the spacing between the boreholes and their depth: for optimal configurations, it is recommended to be in the range of 0.05-0.2.

Regarding the boreholes diameter, smaller ones lead to higher energy transfer efficiency; on the other hand, larger boreholes diameters involve larger thermal exchange surfaces and a consequent greater heat transfer rate per unit length. Therefore, a trade-off approach must be adopted to determine the right boreholes diameter. Diameters in the range of 100-150 mm are usually adopted.

Heat pumps are connected to the underground via U-pipes inserted into the boreholes. These tubes are in high density polyethylene and they can be 1U, 2U or coaxial configurations, as represented in the *Fig. 1.11*. Their nominal external diameters are 25, 32 or 40 mm, while the nominal pressure resistance is to 10 or 16 atm. Pipes U-junction is very important because it avoids sharp bends and hydraulic head losses. At the bottom there is a small container to collect any waste accidentally fallen in the tubes and a ballast of 20-50 kg. Pipe spacers have to hold tubes at sufficient distance, minimizing thermal exchange between inlet and outlet pipes and keeping the vertical tubes layout.

Geothermal grout is generally used to fill the boreholes and guarantee a perfect sealing between pipes and ground. It can be a premixed Portland concrete with bentonite, quartz sand or specific additives. Grout has a low viscosity because of higher water content than common concrete. It has several functions such as mechanical tubes protection, hydraulic sealing of aquifers and good thermal exchange between the borehole and the ground (about 2 W/(mK)). The geothermal grout must be injected from the bottom and in pressure to prevent air voids, however it is necessary to verify pipes damages before grouting. This check could be performed with a flow test, which measures the pressure drop between going and back, and, then, compares computed and measured hydraulic pressure losses.

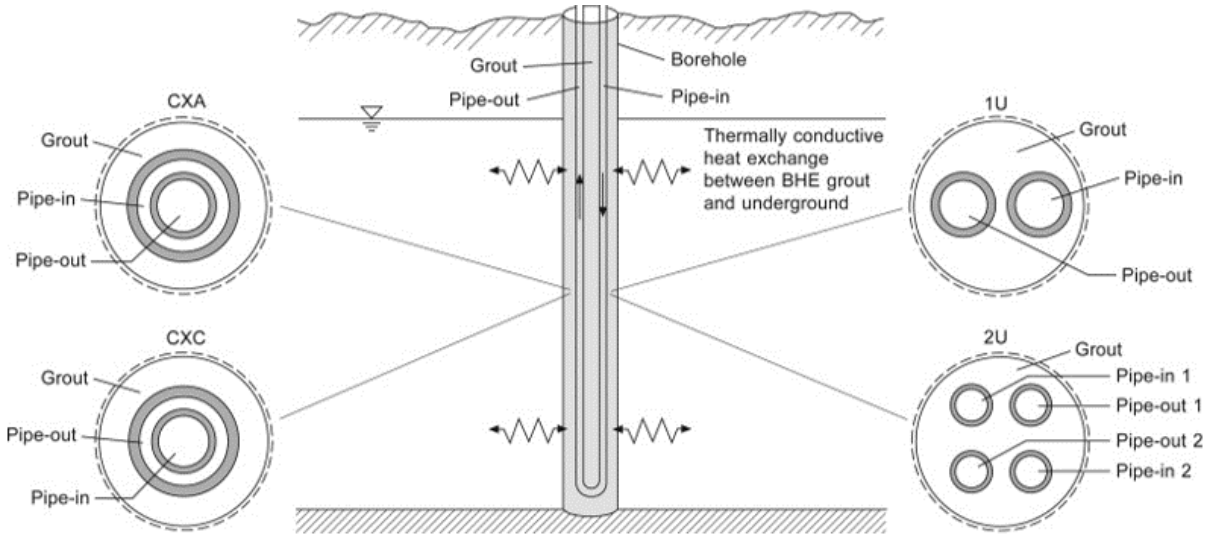

Fig. 1.11 Different BHE configurations in the form of single or doubled U-shaped pipes and coaxial pipes with annular or centered inlet (*from [8]*).

The heat carrier fluid is a solution of water and antifreeze, such as calcium chloride, propylenic glycol, or ethylene glycol. When choosing a heat carrier fluid, the main properties to consider are the corrosivity, the flammability, the toxicity, the viscosity and last but not least, its price. Heat carrier fluid concentrations are about 25-35%, the higher the antifreeze concentration, the lower the solidification temperature, but the higher the viscosity and the electrical energy required by the pump. In a vertical closed-loop configuration, pumps work is in the order of 5-10% of the overall electricity demand of the geothermal system.

The thermal power exchanged by vertical BHEs and the soil thermal properties determine the working fluid temperature. Considering a fixed yearly cycle of thermal load, the temperature of the heat carrier fluid undergoes a drift, i.e., a decreasing trend for heating-dominated loads or an increasing trend for cooling-dominated loads. Therefore, borehole heat exchangers are more efficient in the early years of operation.

Ground-coupled heat pumps (GCHP) systems may cause problems or environmental impacts due to their installation. Some critical issues are the following (*from [7]*):

- drilling site space management (e.g., the accessibility for the drilling equipment);
- anthropic activities such as landfills or contaminated sites;
- hydrogeological features (possible interferences with confined or artesian aquifers);
- geochemical alterations of groundwater quality used for potable purposes.

1.1.4 OPEN-LOOP GEOTHERMAL SYSTEMS

In open-loop geothermal systems, heat is exchanged directly with the groundwater, which is firstly pumped up and later reinjected into the aquifer or sent to surface waters (e.g., lakes, rivers, or canals). As shown in *Fig. 1.12*, groundwater is abstracted from a well and, then, discharged in different ways, depending on the system design or local law prescriptions:

- Well doublet, which has both the extraction and the injection well.
- Groundwater heat pump with reinjection into surface waters.
- Standing column, which has a single well for both operations.

The most common open-loop configuration is the well doublet system, which consists of a supply well with the pump, the groundwater heat pump (GWHP), and a recharge well. In response to pumping, a hydraulic head variation of the aquifer static level occurs: there is a depletion at the extraction well and a piezometric level rise at the injection well, as represented in *Fig. 1.13*. The drawdown in the aquifer is proportional to the pumped flow rate, which is limited by the aquifer hydraulic properties. This alteration must be assessed in the authorization procedure to ensure it is sustainable in the long term system operation.

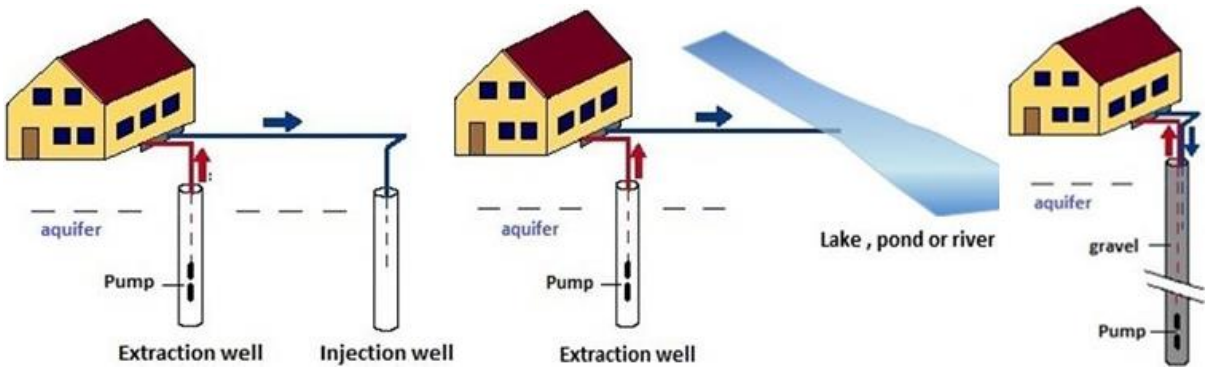

Fig. 1.12 GWHP systems (from left to right): well doublet, surface water and standing column.

Another issue to be considered is related to thermal impacts. The temperature difference between the abstracted water and the reinjected one is limited by regulations and also imposed by heat exchangers manufacturers. However, when water is discharged with a different temperature from that of the aquifer, it may originate a zone of thermally altered flow, called thermal plume. The plume propagation could interfere with downstream groundwater uses and also with the supply well. Thermal recycling occurs when a fraction of the reinjected flow rate returns to the extraction well, leading to a progressive thermal alteration over time. This phenomenon can result in a significant loss of the system efficiency. Therefore, because of its temporal evolution, the thermal plume should be modelled to ensure no water well and no geothermal system is impacted by the GWHP.

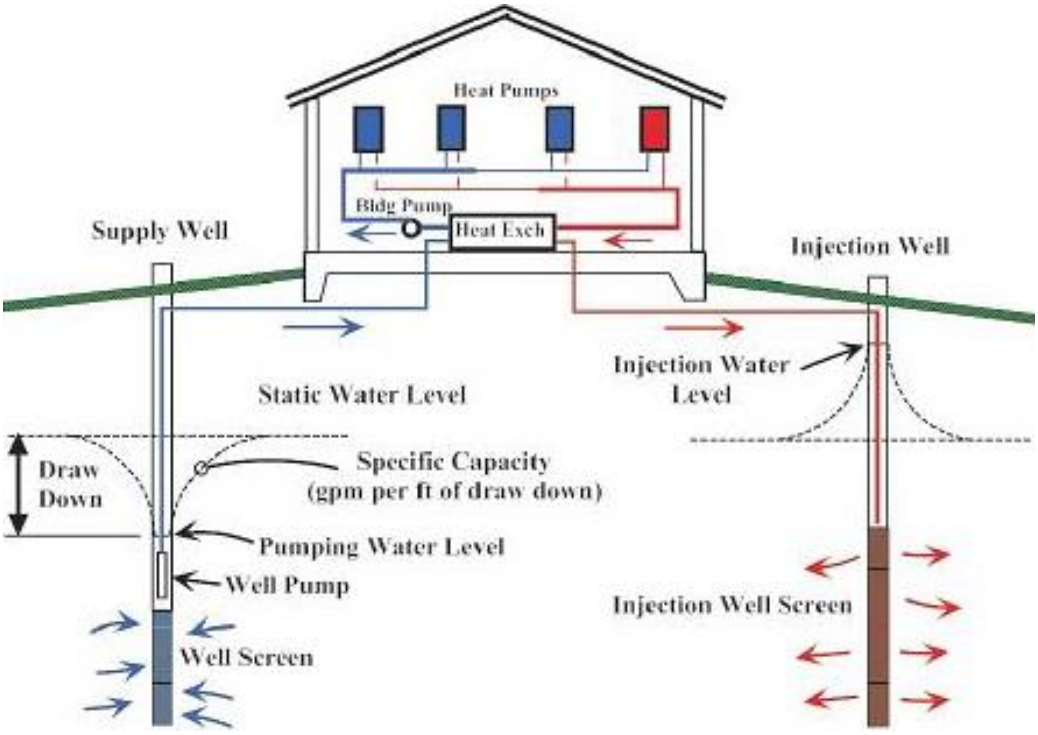

Fig. 1.13 Open-loop with abstraction and reinjection wells (source *Polytechnic of Turin*).

There are some benefits when using open-loop systems instead of closed-loop ones: they have higher COP and EER values (due to the larger thermal conductivity of the groundwater compared to that of the antifreeze solution in boreholes), opportunity of performing free cooling and scale economy advantages. On the other hand, GWHPs have also several constraints such as expensive and time-consuming site characterization, well authorisation required, more maintenance operations needed, the need for a sufficiently productive aquifer, and available area for wells spacing.

1.1.4.1 WATER WELLS

Water wells are used to extract water from aquifers both for potable and geothermal purposes. The most popular drilling techniques used for water wells are: percussion, rotary with direct circulation and rotary with reverse circulation, as represented in *Fig. 1.14* below.

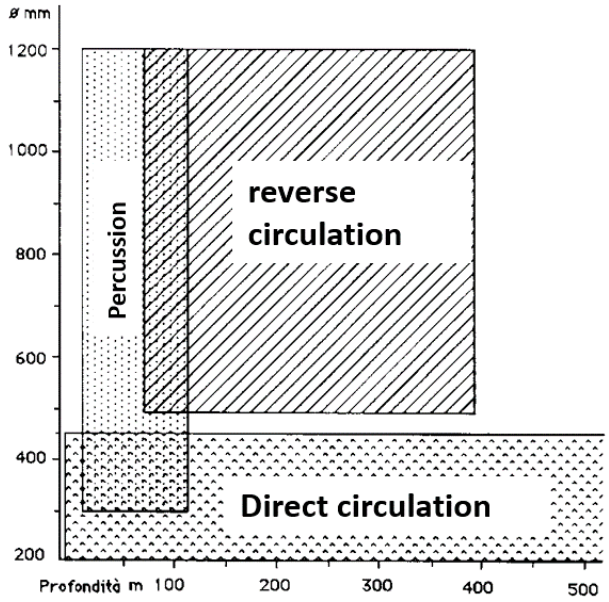

Fig. 1.14 Water well drilling techniques.

Percussion (cable tool) is suitable for large-diameter wells at small depths (< 100 m). The utilization of this drilling technique consists in a "hammer" repeatedly dropped. In fact, the percussion has the following main functions: penetrating the material, reaming the sides of the hole, crushing the geology into fine particles and then mixing them with water.

In rotary with direct circulation technique, the drilling mud or water is injected from the rig, debris rise by floating from the anulus. This perforation method is used for small-diameter wells of all depths, it works on every kind of ground and can face artesian aquifers and shallow gas layers. Moreover, inclined drilling and high drilling speed are possible. On the other hand, it is not so effective for coarse sediments and provides incomplete borehole information.

Drilling with rotary reverse circulation, debris are abstracted from the rig pipe. This technique is generally used for large-diameter and deep wells, it utilizes low viscosity mud and is also advised for coarse sediments. This method provides accurate borehole information, however, it needs large available spaces and consumes a considerable amount of water.

There are some basic requirements for water well designing:

- the pump;
- the diameter of the well pipe (casing and screen);
- the screen diameter and type;
- the gravel pack.

The choice of the proper pump should provide a sufficient flow rate and an adequate hydraulic head. The most widespread well pipes material are PVC (especially for monitoring wells), Zinc or carbon-bitumen steel and stainless steel. Pipes consist in two main segments: the casing, which crosses the non-aquifer layers, and the screen which crosses the aquifer layers. The casing, at least up to the pump depth, should be large enough to host the pump. The screens can be of different typologies: torch or milled slots, bridged slots, wire wrap or Johnson. The screen diameter, the opening type and the screened length should guarantee the hydraulic efficiency of the well. Indeed, the screens are characterized by a certain yield R ($ls^{-1}m^{-1}$), determined as follows:

$$R = \frac{Q}{L} = \pi D \alpha v_{opt} \tag{1.9}$$

where Q (ls^{-1}) is the flow rate, L and D are the screen length and diameter, α (dimensionless) is the share of the lateral surface open to flow, and v_{opt} is the optimal entrance velocity of water at the screen, which should be chosen according to the aquifer lithology.

The gravel pack should be coarse enough to be permeable and to avoid entering into the screen openings, but, not too coarse in order to avoid the entrance of the aquifer sediments. So, it is necessary to evaluate the aquifer composition with grain size distribution curves. Gravel pack thickness is proportional to the well diameter, and it is in the range of 50-150 mm.

Water wells can become preferential pathways of contamination, from the ground to the aquifer and between different aquifers. Therefore, sealing is necessary on the shallowest part (> 1 m) and when crossing different aquifers, in the casing sections. The materials used for grout seal are concrete and bentonite in form of pellet.

In order to avoid its clogging, the well development is performed: it consists in a perturbation introduced into the well to displace fine particles around it. The well development can be carried out in different modes such as bailer, hydraulic jetting or air lift.

Lastly, the purge is an over pumping which removes fine particles from the well.

The components of a drilled water well are shown in the *Fig. 1.15* below.

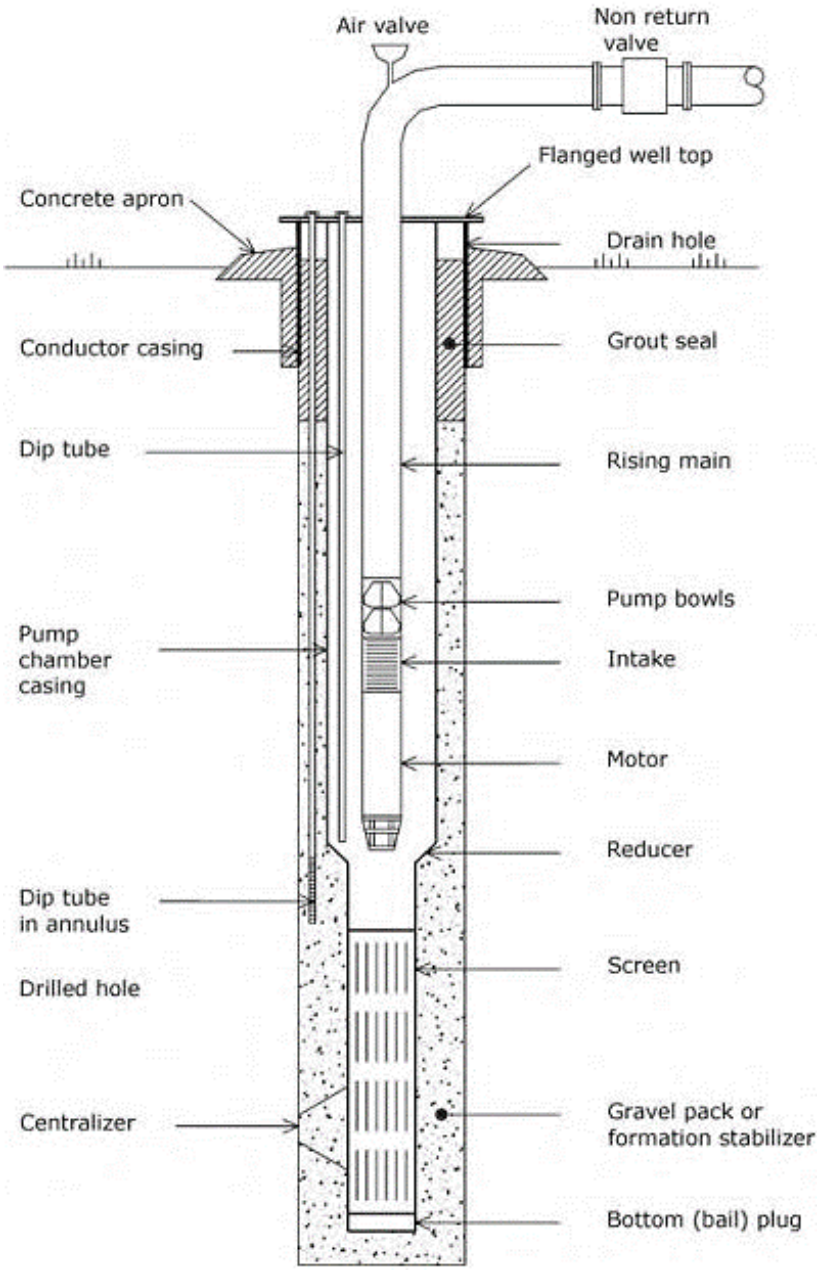

Fig. 1.15 Drilled water well components (*from [9]*).

1.2 THE NATURAL GAS DISTRIBUTION NETWORK

The ever-increasing demand for energy, coupled to limited fossil fuels resources, results in an inevitable improvement and upgrading of the energy-consuming facilities. Natural gas has become the main fuel used in the global mix, following the lower use of coal and oil. Natural gas is a complex mixture of hydrocarbons, of which methane is the major component, with a minor share of inorganic compounds. The larger part of natural gas is consumed in the domestic and industrial sectors, because of its ease of use and high energy efficiency, as well as lower greenhouse gases emissions compared to other fossil fuels. In addition to covering residential and commercial needs, natural gas plays also a leading role in the electrical energy generation. Therefore, this fuel has become essential in the national energy policies for the transition to a clean and sustainable scenario in many countries, as shown in *Fig. 1.16*. In Italy, natural gas is widely consumed for different purposes: especially for the power generation, for heating demand and also other activities, such as sanitary water production and cooking. Therefore, a continuous supply of natural gas is very important.

Natural gas is transported from the wellhead to consumption points with a very long pipeline network, and, before reaching its end-users, it is treated several times with physical and chemical processes such as compression, filtration, expansion and odorization. The smart integration between the gas distribution sector and renewable energy sources is a strategic action to achieve. Natural gas is often transferred through several countries (also overseas) by means of a dense international infrastructure which reaches the main distribution nodes. However, the delivering of natural gas from production points to end-consumers is an energy-consuming and costly process.

In the design of the natural gas distribution network it is important to pursue an acceptable compromise between the costs of transporting the gas and those of the entire infrastructure. In fact, in order to reduce pipeline diameters and to efficiently transport the natural gas, the latter is compressed before being injected into the distribution network. However, the natural gas pressure must decrease when the pipelines get closer to the end-users. Therefore, there is a large number of pressure reduction stations distributed along the pipeline network: these reducing plants work at different pressure levels and, generally, a significant fraction of energy is lost in the expansion process.

In the pressure reduction stations, the natural gas pressure drop is generally achieved with the use of the throttling valves: these devices can perform an isenthalpic transformation without any power usage. Another possibility, in order to increase the system efficiency, is to use energy recovery technologies: for example, the turboexpander electric generators, which enable to convert the pressure energy into electricity and send a part of it to the grid. Other research works and studies are underway to find innovative solutions for the energy recovery in natural gas pressure reduction stations.

Before the expansion process takes place, the natural gas must be preheated. In fact, preheating the gas avoids the methane hydrates formation that could cause damage to the pipelines and the valves. On the other hand, the thermal plants consume high amounts of fuel. To optimize the operation of preheating systems in pressure reduction stations, it is important to select a proper thermal energy source. Conventional fossil fuels-based technologies can be used to provide the heat required by the process: water boilers or thermal oil heaters are usually employed as gas-fired line-heaters. However, these technical solutions imply large amount of pollutant emissions, safety issues due to the presence of a combustion close to a high-pressure pipeline, and high costs.

Therefore, other possibilities have been investigated in the literature, in order to achieve better performance in the operations of the pressure reduction stations, exploiting thermal system integration and energy optimisation. Concerning these issues, there are several researches in Iran, which is one of the main producers and consumers (respectively 3rd and 4th in the world ranking) of natural gas, due to its wide reserves (about 17% of the world's total gas reserves).

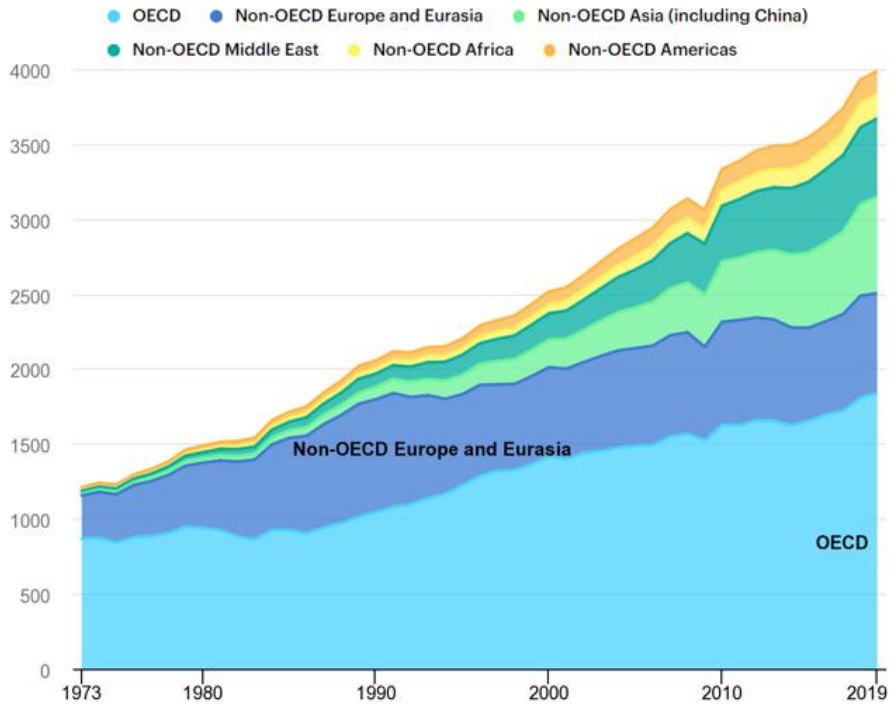

Fig. 1.16 World natural gas demand in billion cubic meters (*from [10]*).

Considering that there are many pressure reduction stations installed almost everywhere, it is worthwhile to study the feasibility of novel expansion plants configurations integrated with RES, such as solar collectors or geothermal heat pumps. This last solution is one of the potentially interesting resources ways to increase the efficiency of the systems. In fact, low-enthalpy geothermal technologies can accomplish the natural gas preheating process based only on RES, reducing carbon emissions. However, it is a very challenging objective.

1.2.1 STRUCTURE OF THE ITALIAN GAS PIPELINE NETWORK

Since the 70s', natural gas has been used in order to satisfy the needs of many industrial and residential users all over the country, through a huge and complex distribution network.

In Italy, an important guideline related to the legislation of natural gas is the DM 24/11/1984: it contains law requirements (and their subsequent modifications) for protection from risks of explosion and fire hazard during storage, transport, delivery and usage of natural gas, with density lower or equal to 0.8 kg/m^3 (relative to air). The decree has been revised and, nowadays, this matter is governed by technical regulations found in two national documents: DM 16/04/2008 and DM 17/04/2008.

The whole natural gas supply chain is composed by several sections at different pressure levels: storage plants, compression units, transportation pipes, pressure reduction stations and distribution lines, as represented in the scheme in *Fig. 1.17*. The Italian natural gas pipelines network ("Rete Nazionale Gasdotti") has a total length of around 33000 km, with 13 recompression units.

The structure of the Italian pipeline grid is mainly divided in two distribution levels:

- the national transport network, formed by high-pressure and large-diameter pipelines, which includes the systems involved in the natural gas distribution from the injection points to the regional grid and the storage sites;
- the regional pipelines network, which is at medium-pressures, also includes the local low-pressure delivering, and the supplying of power plants and industrial or domestic consumers.

The natural gas distribution system, both at national and regional levels, is mainly managed by SNAM ("Società Nazionale Metanodotti") with a total annual amount of gas supplied into the network of about 75 billion m^3. Instead, concerning the local distribution, the situation is very fragmented and there are several groups active in the sector such as Italgas, Hera, A2A, Iren and so on. This does not support an efficient management of the service; although, in recent years, we are witnessing a gradual consolidation in the local distribution sector.

The interconnection points between the regional pipelines transport network and the local distribution grid, which is almost 200000 km long, are the pressure and flow regulation and metering plants called "REMI" ("cabine di regolazione e misura").

Natural gas can be transferred from production to consumption points in different ways:

- pipeline-transmitted gas;
- compressed natural gas (CNG);
- liquefied natural gas (LNG).

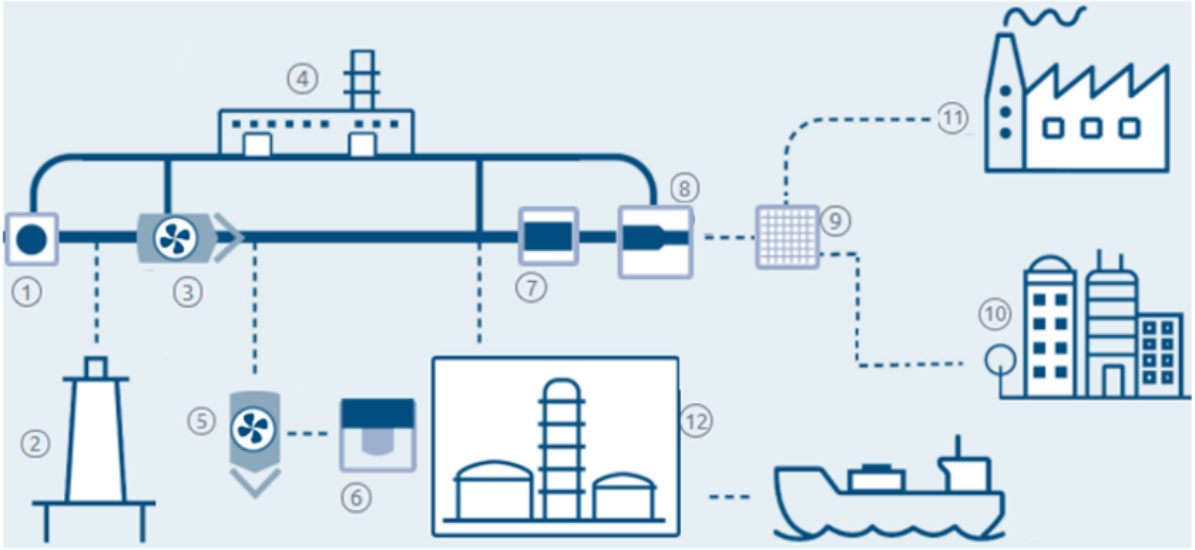

Fig. 1.17 The structure of the natural gas distribution network ***(modified from*** **[11]*).***

Natural gas pipelines are made of steel and are mainly buried underground. The gas velocity inside pipes is limited to 15 m/s, in order to reduce the noise. The authorization for the pipeline operation is given by releasing a fire prevention certificated called CPI ("Certificato Prevenzione Incendi"). Gas pipes can be divided into seven categories, depending on their suitable maximum operative pressures:

1) $P_{max} > 24$ barg
2) $12 < P_{max} \leq 24$ barg
3) $5 < P_{max} \leq 12$ barg
4) $1.5 < P_{max} \leq 5$ barg
5) $0.5 < P_{max} \leq 1.5$ barg
6) $0.04 < P_{max} \leq 0.5$ barg
7) $P_{max} \leq 0.04$ barg

The measurement unit of barg represents the difference between the absolute pressure and the atmospheric one. The national transport grid operates basically with pipelines of first, second and third types, while smaller pipes are used by local distributors.

Compression plants are located along the national pipelines network, at about 150-200 km from each other, and are generally composed of several recompression units, used to push or compress the gas. In fact, during the transportation, the pressure in pipes decreases and it must be brought back to its original value, in order to ensure the supply of the required gas flow

rate at the desired pressure level. The pressure drop depends mainly on the pipes diameter, their length and on the flow rate; minor pressure drops can occur in presence of curves, filters, valves or other line components.

Liquefied natural gas is used to efficiently transport natural gas on medium and long distances. LNG density is six hundred times higher than natural gas one at ambient pressure. LNG ships are equipped with super-insulated vessels: they guarantee the maintenance of the internal temperature below -160 °C, which is the value required to keep natural gas in the liquid form. The gas is also used as fuel for the ships, till they reach the regasification plant.

Only a small part of the natural gas consumed in Italy derives from the national reserves; the remaining is supplied through several injection points linked to international pipelines and LNG hubs. These are distributed along the Italian peninsula in the following locations:

- Gela (CL), which connects Sicily to the Libyan supply grid with the submarine pipeline called "Greenstream";
- Mazara del Vallo (TP), where the gas arrives from Algeria by means of the "Transmed" submarine pipeline;
- The Gries Pass (VB), in the North of Italy, hosts the connection to the Swiss grid through the "Transitgas" pipeline;
- Gorizia (GO), in the Northeast, where the Italian gas network meets the Slovenian one;
- Tarvisio (GO) is connected to the Austrian grid by the "Trans Austria Gas (TAG)" pipeline;
- Panigaglia (SP), in the Northwest coast, hosts a LNG regasification plant;
- Livorno (LI), has a LNG hub;
- Cavarzere (RO), in the Northeast coast, hosts the off-shore "Adriatic LNG" terminal;

The Italian national and regional natural gas pipelines network is represented in *Fig. 1.18*, in which the distribution of the injection points from the neighbouring and oversea suppliers is also shown.

Thermal energy demand, as well as natural gas consumption, is directly correlated to the average environmental temperature. Therefore, the demand is cyclical with seasonal patterns: the highest demand occurs during winter, while the lowest during summer. In this framework, storage plants are extremely important for the gas market: keeping gas reserves for high consumption periods, and compensating unexpected problems. In these sites, natural gas is stored in underground tanks or in exhaust deposits, at a maximum pressure of about 150 bar. The overall Italian storage capacity is approximately 17 billion m^3, but it will be increased in the next years.

Fig. 1.18 The Italian natural gas pipelines network (*modified from* [12]).

1.2.2 PRESSURE REDUCTION STATIONS

In order to deliver and supply natural gas, it must be transferred in high-pressure pipelines, to overcome the pressure losses related to long distances. Indeed, natural gas is transported from refineries to consumption points such as power plants, factories, and cities. However, end-consumers cannot utilize the high-pressure gas, thus, its pressure must be reduced to a desirable level in several steps before being distributed. In order to exploit this function, along the natural gas distribution network are located many pressure reduction stations (PRSs). They can be first jump reduction plants, from high to medium pressure, or second jump, from medium to low pressure, as schematically shown in *Fig. 1.19*.

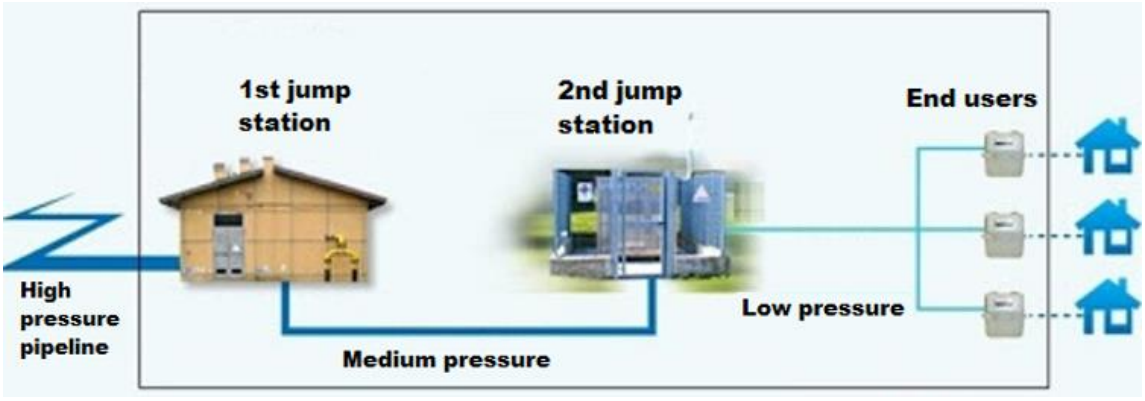

Fig. 1.19 Schematic representation of the pressure reduction steps (*modified from [13]*).

During a year the inlet natural gas to the PRSs possesses different pressure values, usually between 50 and 70 bar, consequently, there are also various pressure drops. The gas pressure depends on its flow rate: as one gets farther from the natural gas source, the pressure decreases nonlinearly. In fact, the total flow rate of the natural gas transmission pipelines is related on the removal amount of gas at several distribution points. Since a major fraction of natural gas is used for heating, removal portions from the line may be different for the final consumption sites. For these reasons, the inlet gas pressure at each PRS depends on upstream local climatic conditions: according to the geographical position of the PRS, the initial pressures may vary in different zones.

In general, the pressure reduction stations are situated in industrial areas or outside the city centre (in fact they are also called city gate stations) because they are very noisy. In pressure reduction stations, the pre-distribution treatments of the natural gas are conducted, including the following functional process units: filtering group, preheating system, pressure reducing, flow metering and gas odorization. These systems are represented in *Fig. 1.20*.

The filtration unit is normally used to protect heat exchangers, pressure regulators, and metering systems from dry gas with solid particles. The filter body is usually made of carbon steel or austenitic steel, while the filter element consists of polyester felt and can filtrate the finest particles until 5 microns.

The preheating system is used to prevent the hydrates condensation during the natural gas expansion process and to maintain the minimum temperature value required. In this phase are present economic issues and technical constraints, mainly due to two different needs: guaranteeing safety when manipulating a flammable substance, preventing risks of fires and explosions, and consuming fuel, thus releasing pollutant emissions in the environment.

The pressure reduction constitutes the main step of the whole process. In order to meet all the law requirements, there are several components: service and control regulators, block and emergency devices and discharge valves.

Flow metering can be done both downstream of the filtration system or the regulating valves. In the first case it is known as variable pressure and temperature metering, in the second it is the regulated pressure metering. In general, the metering systems consist of two main elements: the primary one is a flow meter, while the secondary is a conversion system composed of flow computer and relative accessories. The most common typologies of volumetric flow meters utilised are turbine, venturi, rotary, ultrasonic, orifice with single or double chambers. The flow metering also includes the conversion systems and the instruments used to measure the gas quality, which are the following:

- gas chromatograph;
- calorimeter;
- moisture analyser;
- density meter;
- H_2S analyser;
- flow computer.

Natural gas is odourless, therefore, in order to give it its typical and recognisable odour, an odorization system is generally installed. It is used to add a certain amount of odorant liquid to the gas in proportion to the flow rate supplied in the line.

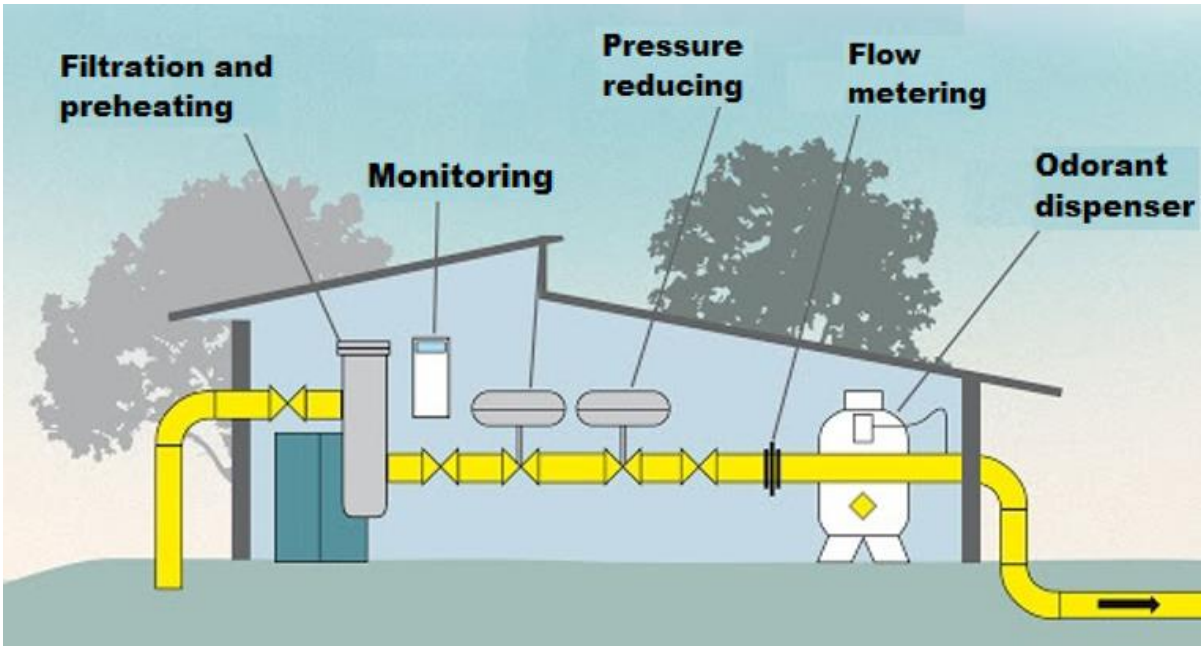

Fig. 1.20 Natural gas treatment systems in a pressure reduction station (*modified from [14]*).

An internal view of the pressure reduction station components is shown in *Fig. 1.21* below.

Fig. 1.21 Inside view of a typical pressure reduction station (*from [15]*).

1.2.3 PREHEATING AND EXPANSION PROCESSES

As imposed by the Italian legislation, a natural gas preheating system must be installed at each pressure reduction station. It is an essential part of the gas treatment, and it must be performed before the expansion process. The minimum gas temperature after preheating is subject to a specific constraint: natural gas should not leave the pressure reduction station at a temperature lower than 0 °C.

The preheating thermal duty is a function of the regulator mass flow rate and the pressure drop, thus, also of the inlet natural gas temperature which varies throughout the year. The expansion process is different for each PRS, based on the local average consumption of natural gas during the year. In fact, the natural gas demand is strongly affected by the seasonality: there is a huge difference between the maximum and minimum operation values in the coldest and warmest months, respectively.

The gas pressure reduction is usually achieved with regulators which perform an adiabatic, isenthalpic, irreversible, and quite rapid expansion process. The high-pressure of the gas can be reduced using either throttling valves or turboexpanders, which also enable the recovery of energy. However, considering fixed gas flow rates, the latter require larger thermal duty at higher operating temperatures compared to throttling valves or Joule-Thomson regulators.

Joule-Thomson valves are a particular kind of pressure expander characterised by a pneumatic control. The position of the actuator is governed by the differential pressure which acts on the diaphragm: down and upper pressures in the valve's chambers are regulated by two dedicated springs. These enable an exact control of the actuator position which depends on the pressure level set by the screw, as represented in *Fig. 1.22*. One of the main problems related to the use of throttling valves for the expansion process is the temperature drop of gas: if the gas pressure decreases, its temperature also drops due to the Joule-Thomson coefficient μ_{JT} (°C Pa^{-1}), which is one of the most important gas properties and can be defined as follows:

$$\mu_{JT} = \left(\frac{\partial T}{\partial P}\right)_h \tag{1.10}$$

where h (J kg^{-1}) is the enthalpy and it is constant.

The temperature can be reduced up to 0.5-0.6 °C per bar of pressure drop. Instead, for a turboexpander, one bar of pressure reduction leads to 1.5-2 °C of temperature decrease, approximately four times higher than the throttling valves process. Therefore, the use of turboexpanders increases the line heaters preheating power, due to the larger temperature drop. In fact, higher thermal energy is required because of the work extraction from the thermodynamic transformation. Turboexpanders are generally utilised for the production of liquefied natural gas, or in the plants for the extraction of ethane, with very low-temperature gas streams.

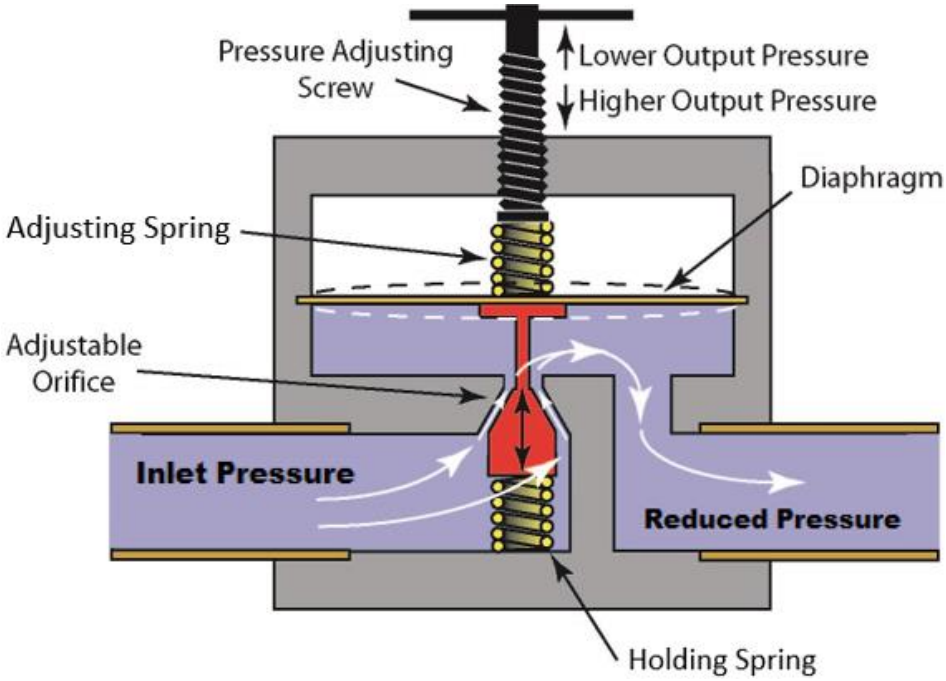

Fig. 1.22 Process scheme of a pressure reducing valve (*modified from [16]*).

Since natural gas is a real gas, on certain thermodynamic conditions as low temperature and high pressure, ice-like compounds known as "gas hydrates" are formed in the pipelines due to the Joule-Thomson effect: the temperature decreases till a point in which some natural gas components like methane, ethane, propane, and isobutane, condense into liquid or solid particles. This undesirable phenomenon happens because there are water droplets suspended in the natural gas stream: the water molecules form a cage-like structure around the smaller gas molecules. The formation of this frozen mixture of water and hydrocarbons creates an obstruction in the pipes and may damage the line components: materials embrittlement, fouling, internal erosion and corrosion, and even blocking of pipelines are the main problems of the gas hydrates condensation. For this reason, it is important to ensure that natural gas remains above the dew point and the minimum temperature below which hydrates may form. The minimum temperature required for preheating is not constant in all operating conditions. According to the outlet pressure of the expander and the natural gas composition, the hydrates condensation temperature should be calculated with thermodynamic models. Many studies and experimental researches have focused on this technical issue for natural gas pipelines and, according to the most of them, the formation of natural gas hydrates occurs at temperatures from -2 °C to -5 °C. Generally, these are very challenging threshold limits. However, there is usually a minimum allowable temperature value for gas flowing in pipes, in order to prevent this hazardous condition: in Italy, this constraint is imposed to 5 °C.

Therefore, the natural gas stream must be warmed up before pressure drops in the expander. The standard preheating temperature is in the range of 30-60 °C; the specific value is based on the operational characteristics of the system and on the composition and properties of the gas. Indirect water bath heaters are the most common typology of natural gas fired-heaters used in preheating systems. A schematic representation of a typical line-heater is shown in *Fig. 1.23*. Thermal energy is generated by burning a fraction of the inlet gas stream in the fire tubes. Then, heat is transferred to water, which acts as heat carrier fluid, and finally is transferred to natural gas, which flows through coils immersed in the water bath. The utilization of water bath indirect heaters is widely diffused in various engineering applications, including gas and oil industries, and each energy sector which uses natural gas as a fuel source. Generally, these conventional gas-fired boilers are not equipped with an automatic control system: they cannot respond to instantaneous variations of the heating demand in the natural gas distribution line. This means that their heating power is set to a fixed value for a time period. The specific setting level should be selected in order to prevent any problem occurring in extreme conditions: for example, in early morning when the external temperature decreases till its minimum value. The line-heaters consumption is directly related to the difference of temperature between the natural gas upstream and downstream. This is why gas-fired boilers constantly provide the maximum required power and, hence, consume more fuel then theoretically needed. In general, these old line-heaters have also low thermal energy efficiencies and release significant amount of CO_2, NO_x, and other pollutants emissions into the environment.

Due to the problems described above, the gas preheating system represents the main energy-consuming facility in the whole natural gas distribution network. Improving the equipment thermal efficiency or finding alternative solutions, such as renewable energy sources, is the key to reduce fossil fuels consumption and greenhouse gases emissions, in order to promote the sustainability of the pressure reduction stations.

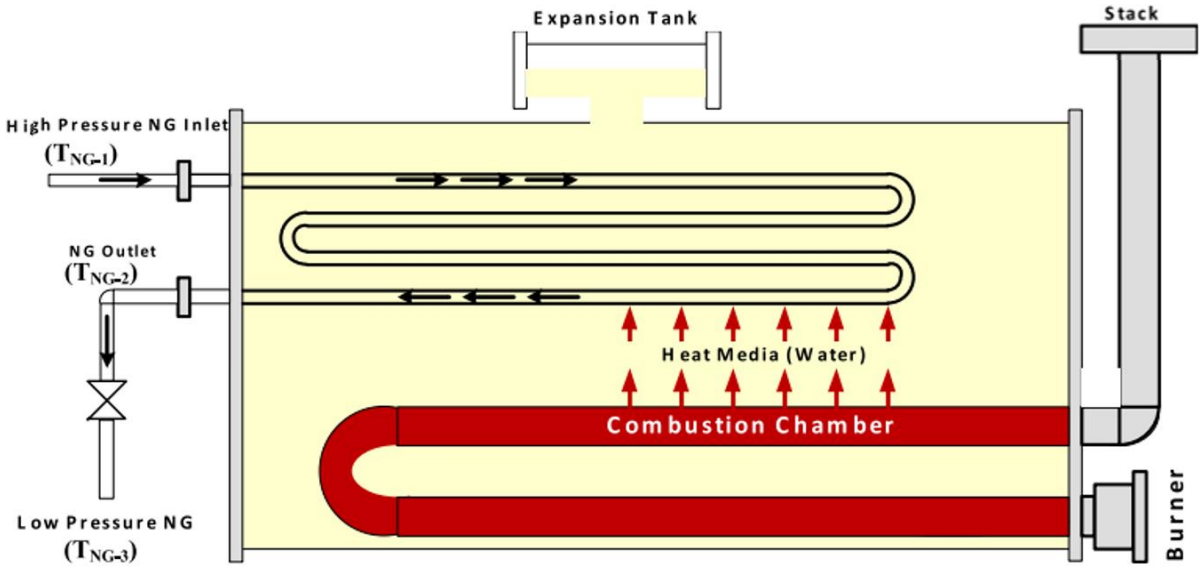

Fig. 1.23 Indirect water bath preheating system in a natural gas PRS (*modified from [17]*).

1.3 THE CASE STUDY: "CABINA REMI ALBA4"

As previously stated, this work focuses on the possibility of implementing the preheating system of a natural gas pressure reduction station with an innovative configuration based on renewable energy sources. The application of shallow geothermal systems, as a sustainable solution for providing the required heat before the expansion process, is proposed in order to replace the conventional gas boiler and eliminate in situ fuel consumption, thus, reducing carbon emissions into the environment.

For this purpose, the Italian case study of the "Alba4" plant in Magliano Alfieri was examined. This is a small pressure reduction station, managed by the local utility EGEA, in which the gas is processed before being supplied to the neighbouring houses. The main goals of the "REMI" plant are the flow rate measuring and the pressure regulation, in order to distribute the natural gas at the desired pressure value required for end-consumers. The station is shown in *Fig. 1.24*.

The gas preheating system was carefully analysed: the plant operational parameters were examined, with a focus on the shell and tube heat exchanger performance. The thermal energy demand was evaluated to ensure that the natural gas temperature will not decrease below the hydrates' formation point, to avoid pipes and equipment damage.

Fig. 1.24 External view of the Alba4 plant (source *Google Maps*).

Moreover, the territory, the subsoil and the groundwater flow of the site were also studied, in order to properly evaluate the hydrogeological and hydrodynamic properties of the shallow aquifer, which are required for the design of an open-loop geothermal system.

1.3.1 GEOGRAPHIC FRAMEWORK

The plant is located in the municipal of Magliano Alfieri, a village of 2200 inhabitants in the province of Cuneo, in the Piedmont Region (North-West of Italy). This Italian region is very interesting in terms of its geography, because of its landscapes, characterized by the Langhe and Roero hills, that are a UNESCO World Heritage Site. At the foot of this hills flows the river Tanaro, which is one of the most important tributaries of the Po river.

Magliano Alfieri is situated on the hillside, at 328 meters above the sea level, on the left bank of the Tanaro river, a few kilometres downstream of the town of Alba. The coordinates of the pressure reduction station are 44°45'28" North and 8°04'43" East. The plant is located 500 m from the Sant'Antonio hamlet and it is about 1.5 km far away from the Tanaro river. Between the site and the river we find the "Asti-Cuneo" highway (A33), as it is shown in the *Fig. 1.25*. Therefore, the boundaries of this small alluvial plain are, on the North-West, the hills or Roero and, on the South-East, the Tanaro river.

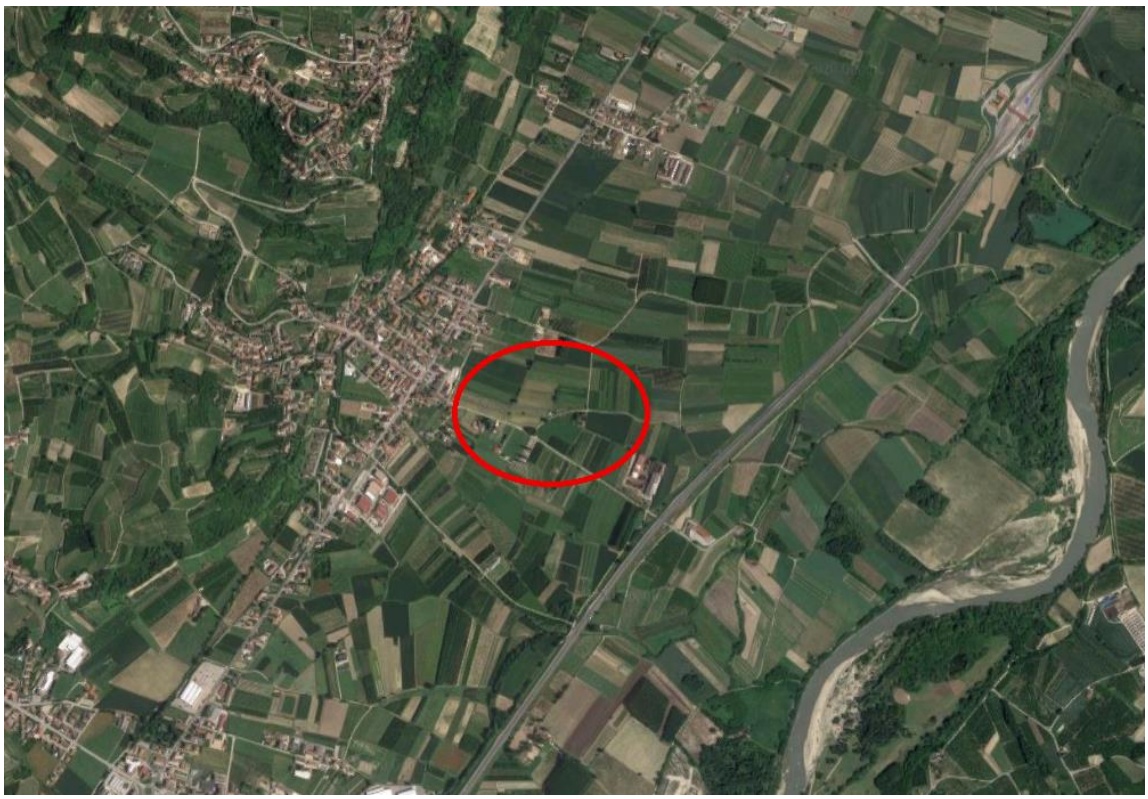

Fig. 1.25 The Alba4 plant site location (source *Google Maps*).

The prevailing land use in this plain is for agriculture, but there are also some industrial plants located along the highway. In the last 20 years, many small production sites near the river were decommissioned, because of the Tanaro river destructive flooding in November 1994.

The morphological features of the whole zone are directly marked by the evolution of the fluvial hydrographic network: indeed, the Tanaro banks are rich of natural meanders. The river flows in a valley of 1.5-2.5 km wide, from 200 to 115 m above the sea level. The floodplain is bordered on both the sides by the hills, which are about 350 m of elevation. Traces of the river modelling are visible on this area: several zones, first associated with flood phenomena, turn out to be used as agricultural lands and, thus, being modified by anthropic activities. Indeed, the plain is crossed by many small water channels that are used to irrigate the fields and the crops.

1.3.2 OPERATIONAL DATA OF THE PLANT

The examined pressure reduction station is a small plant of about 18.5 MW which supplies the natural gas to the domestic boilers located in the surrounding area. Therefore, the heating capacity and the treated flow rates are rather low compared to other pressure reduction stations situated near larger towns and cities.

A scheme of the pressure reduction line is shown in the *Fig. 1.26*. In this process, after the filter unit, natural gas is preheated and eventually depressurized at the expander, which consists in a classic throttling valve. The preheating system is composed of a gas boiler linked to a heat exchanger, as described below. The gas-fired line-heater is the only item of the whole plant equipment which consumes energy, and therefore, it is also the device that requires much operating costs. Frictions along the pipes, pressure drops in the filter unit, and also heat losses through the walls of the boiler, are negligible compared to the energy losses related to the rapid expansion in the pressure regulator.

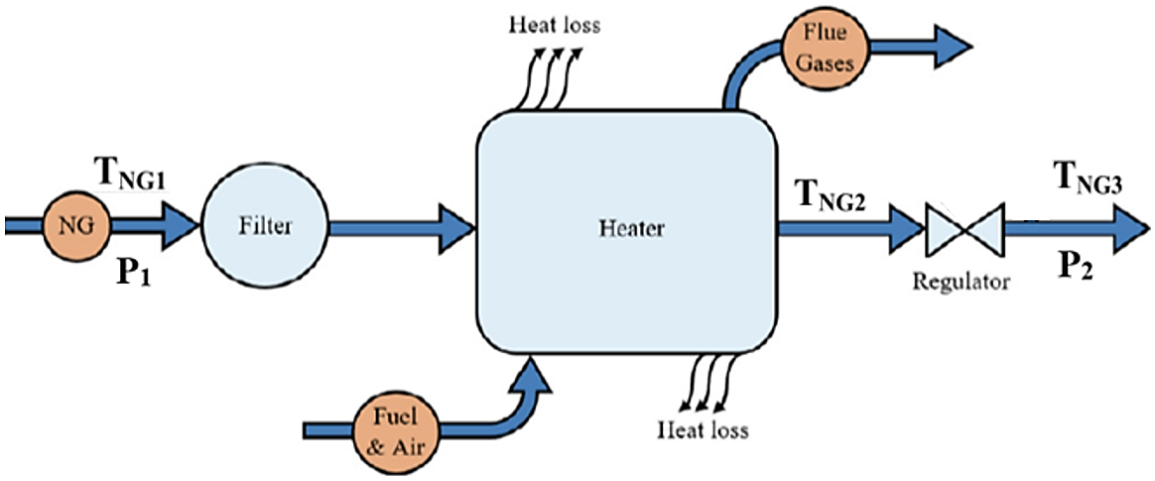

Fig. 1.26 Scheme of the pressure reduction line operation processes (*modified from [18]*).

Considering the operational data available at this station, it is possible to notice that the pressure drop between upstream and downstream gas conditions is quite high: natural gas enters with a pressure value in the range of 60-64 bar and must get out with a pressure equal to 5 bar. This high pressure drop involves a high temperature difference between the inlet and the outlet of the expander. In fact, the initial temperature could decrease almost till 0.5 °C per bar of pressure reduction, thus it can be estimated a drop of about 30 °C in this expansion process. This means that the gas stream flowing through the station requires a high thermal power to be warmed up in the preheating system. On the other hand, the heat to be supplied to the gas is also in function of its volumetric flow rate, which is quite low.

In the *Fig. 1.27*, below, is shown the graph representing the distribution of the natural gas volumetric flow rate, passing into the station during an average day of the year. The gas flow rates are lower during the night because of the lower energy demand for heating, cooking and sanitary water production. In fact, peak consumption occurs in the morning and evening hours, from 7 to 9 am and from 7 to 9 pm, when higher natural gas demands are required.

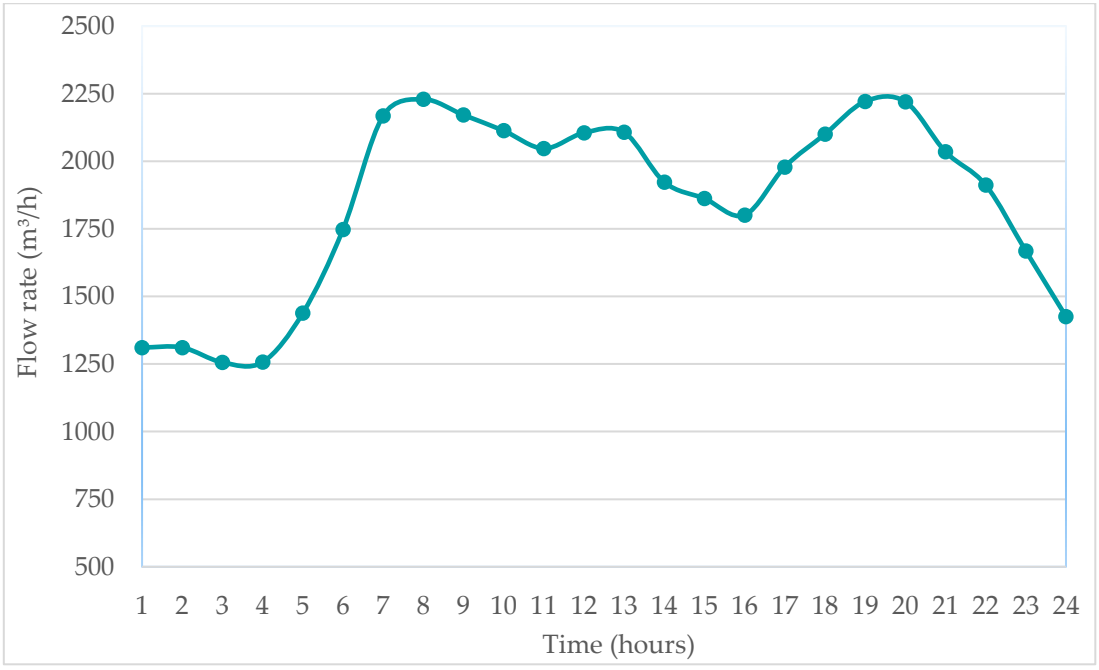

Fig. 1.27 Natural gas flow rate distribution during an average day.

The fuel demand for the preheating of natural gas stream is shown in *Fig. 1.28*. The flow rate trend is similar to that of the natural gas. However, it is possible to notice a more pronounced consumption peak in the early hours of the morning. It is due to the local climatic conditions: at dawn, ambient temperature falls down, and so does the natural gas temperature, with a consequent higher fuel energy needed by the preheating system.

The natural gas upstream pressure is not constant throughout the year because it depends on the flow rates in the pipeline and, thus, by climatic conditions: it can be assumed the average value. Instead, the downstream pressure is fixed at a constant value.

The minimum temperature of the natural gas, at the regulator outlet, is set equal to 5 °C, as imposed by the Italian legislation, considering a safety margin, to ensure that this value will always be above the hydrates forming temperature, as mentioned in the previous section.

Other parameters involved in the process are the mean and maximum volumetric flow rates of the natural gas treated during an average day of the year, equal to 1850 and 2230 m^3/h, respectively.

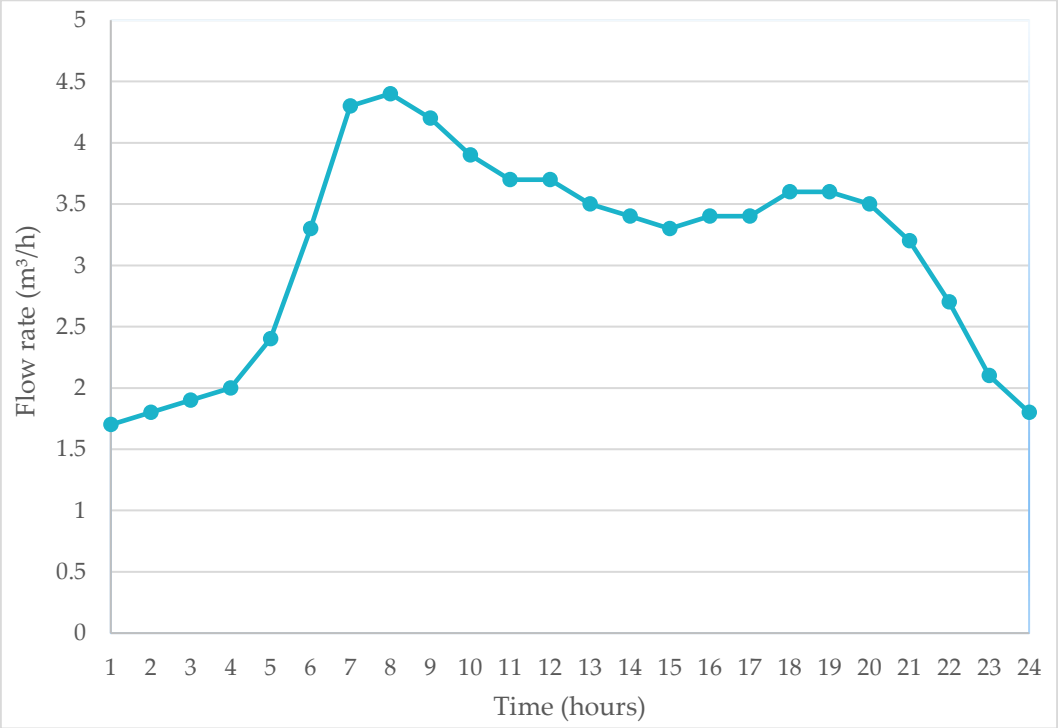

Fig. 1.28 Fuel consumption distribution for an average day.

The last necessary parameter is the inlet natural gas stream temperature to the plant, which is equal to the temperature of the soil, due to the underground transportation pipeline buried at about 1.5 m depth. Since the temperature of the shallow ground is a function of the ambient temperature, the initial temperature of the gas stream entering the station is determined by the local average temperature of the installation site. In *Fig. 1.29* are shown the mean monthly temperatures and the average annual temperature distributions in Magliano Alfieri, the latter value is just under 12 °C. As a conservative assumption, a value of 10 °C was considered for the inlet natural gas temperature at the station.

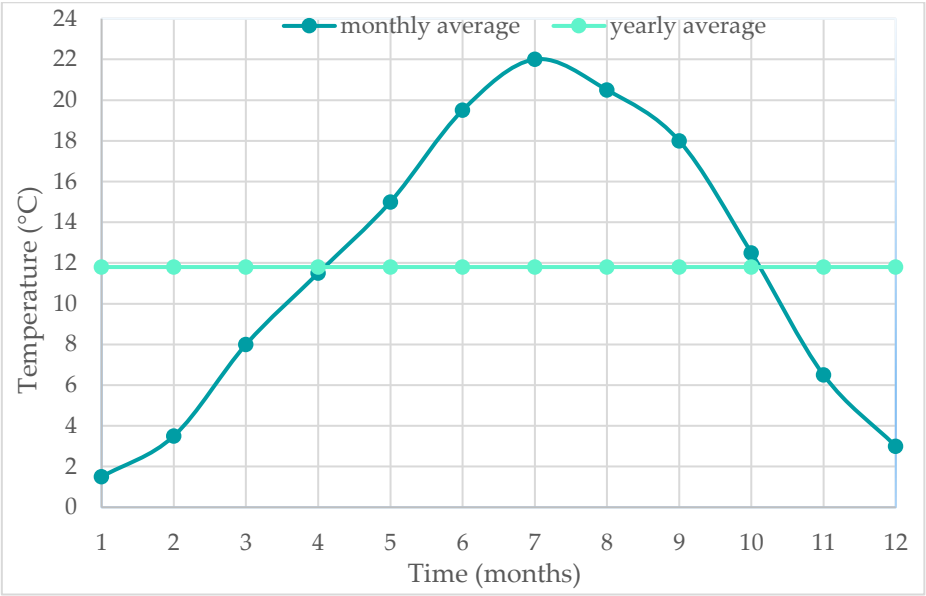

Fig. 1.29 Average annual temperature distribution in Magliano Alfieri (Italy).

In the *Tab. 1* below are summarized the available operational data for the pressure reducing system of the Alba4 plant.

Tab. 1 Natural gas operational parameters at the plant.

PARAMETER	*VALUE*	*U.M.*
Upstream pressure	62	bar
Downstream pressure	5	bar
Inlet temperature	10	°C
Temperature after expansion	5	°C
Average flow rate	1850	m^3/h
Maximum flow rate	2230	m^3/h

1.3.2.1 THE SHELL AND TUBE HEAT EXCHANGER

The preheating system of this small plant is composed of a methane boiler and a shell and tube heat exchanger. Since only these two components are involved in the preheating process (another boiler is installed and kept in stand-by mode as a backup), the operation is quite simple. The gas-fired heater provides the thermal energy necessary to warm up the water. Then, the hot water, which acts as heating carrier fluid, passes into the heat exchanger shell, releasing thermal energy to the natural gas stream which flows in the tube bundle. A schematic representation of the gas preheating system is shown in *Fig. 1.30* below.

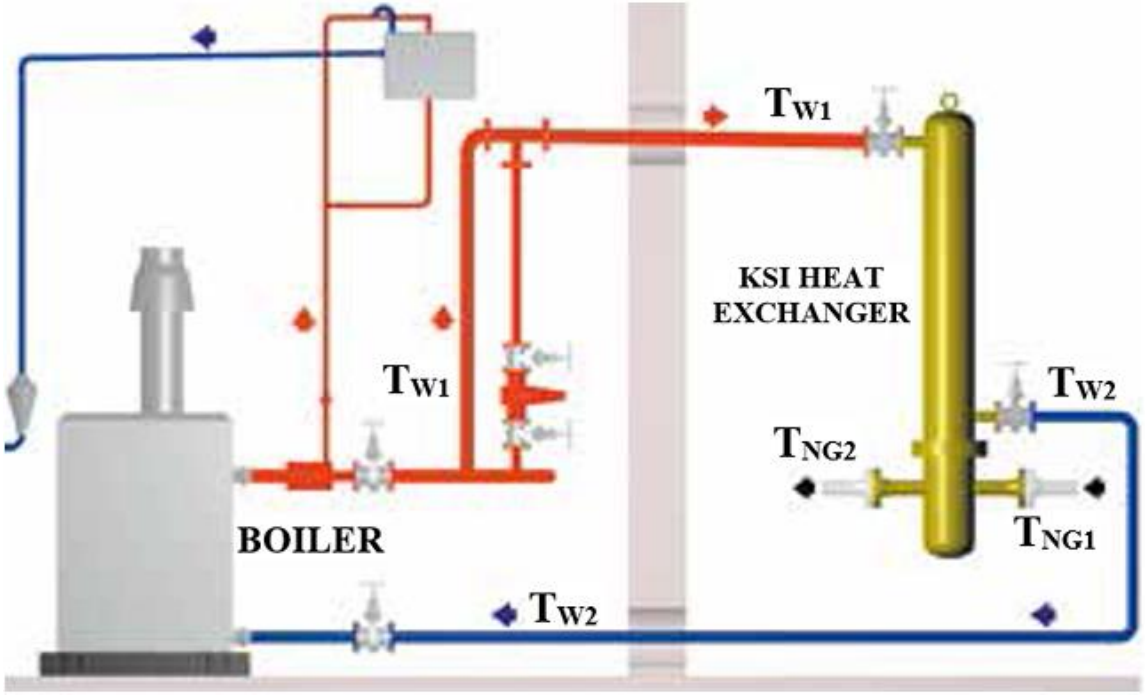

Fig. 1.30 The gas-fired heater, on the left, and shell and tube heat exchanger, on the right.

For installations in natural gas distribution networks, such as in this case, it must be considered the possibility of explosive gaseous mixtures formation inside the pipes, and also the risks related to the emissions of flue gases, which can be flammable or noxious. In order to minimize the fire hazard and the risk of explosions, the heat exchanger installation should have specifications in compliance with the EN 12186 or EN 12279 requirements.

The heat exchanger installed in the preheating system is a KSI-4 model by the Italian manufacturer Pietro Fiorentini. It is a shell and tube heat exchanger specifically designed to preheat natural gas, air, town gases, propane and other not aggressive gases (which, however, must be pre-filtered). The KSI model is BEU type (i.e., it has a U tube bundle fully removable) according to TEMA (Tubular Exchanger Manufacturers' Association) Code.

The main features of this heat exchanger (*from [19]*) are the following:

- hot and superheated water (or steam) as heating fluid;
- maximum working temperature equal to 100 °C (up to 250 °C for superheated water and steam);
- maximum working pressure related to the code and design conditions;
- same pressure values for both shell and tubes sides, with pneumatic actuator, ball valves and shut-off device;
- double connections for preheating of gas on pressure regulators pilot loop;
- connections for condensate drain and relief valves on bottom and top of shell side;
- copper plate for grounding;

The heat exchanger is also equipped with two gas preheating pilot systems: these circuits are independent from the main one and may be used to warm up the natural gas feed for instrumentation.

The heat exchanger operation is straightforward: the cold natural gas enters the first side of the distributor and passes inside the tube bundle which is immersed in the heating fluid. During this passage, the gas absorbs the heat released by water and, after transiting into the other part of the distributor, continues towards the outlet, as it is represented in *Fig. 1.31*.

The heat exchanger is divided in two sections which have different permissible maximum pressure values. The pressure reducing system, installed upstream in the line process, must grant a maximum intervention pressure in case that the inlet gas is overpressure.

The heating fluid has high temperatures and, hence, it is necessary to insulate the external walls of the shell and the water pipes. The insulation of such parts decreases the heat losses and ensures better performance of the whole thermal plant.

Besides, the gas must be previously filtered in order to eliminate the possible presence of solid or liquid impurities which may cause corrosion and fouling phenomena.

To ensure optimal heat exchanger operations, the following accessories are required: the drain valves, the air self-exhausting device and the safety valve on the shell side.

In the *Tab. 2* are listed the geometric features of the KSI-4 shell and tube heat exchanger and its number of tubes, determined as follows:

$$N = \frac{A}{\pi d_o L_T} \tag{1.11}$$

where A is the total heating transfer area, d_o is the tubes outer diameter and L_T is the tubes length. So, there are $N/2$ tubes which perform a double passage (U) into the shell.

Tab. 2 Dimensions of the KSI-4 components.

COMPONENT	*VALUE*	*U.M.*
Shell diameter	323.8	mm
Heating surface	6.746	m^2
Tubes length	1.3	m
Tubes outer diameter	20	mm
Tubes inner diameter	16	mm
Number of tubes	42	-
Tubes pitch	26	mm

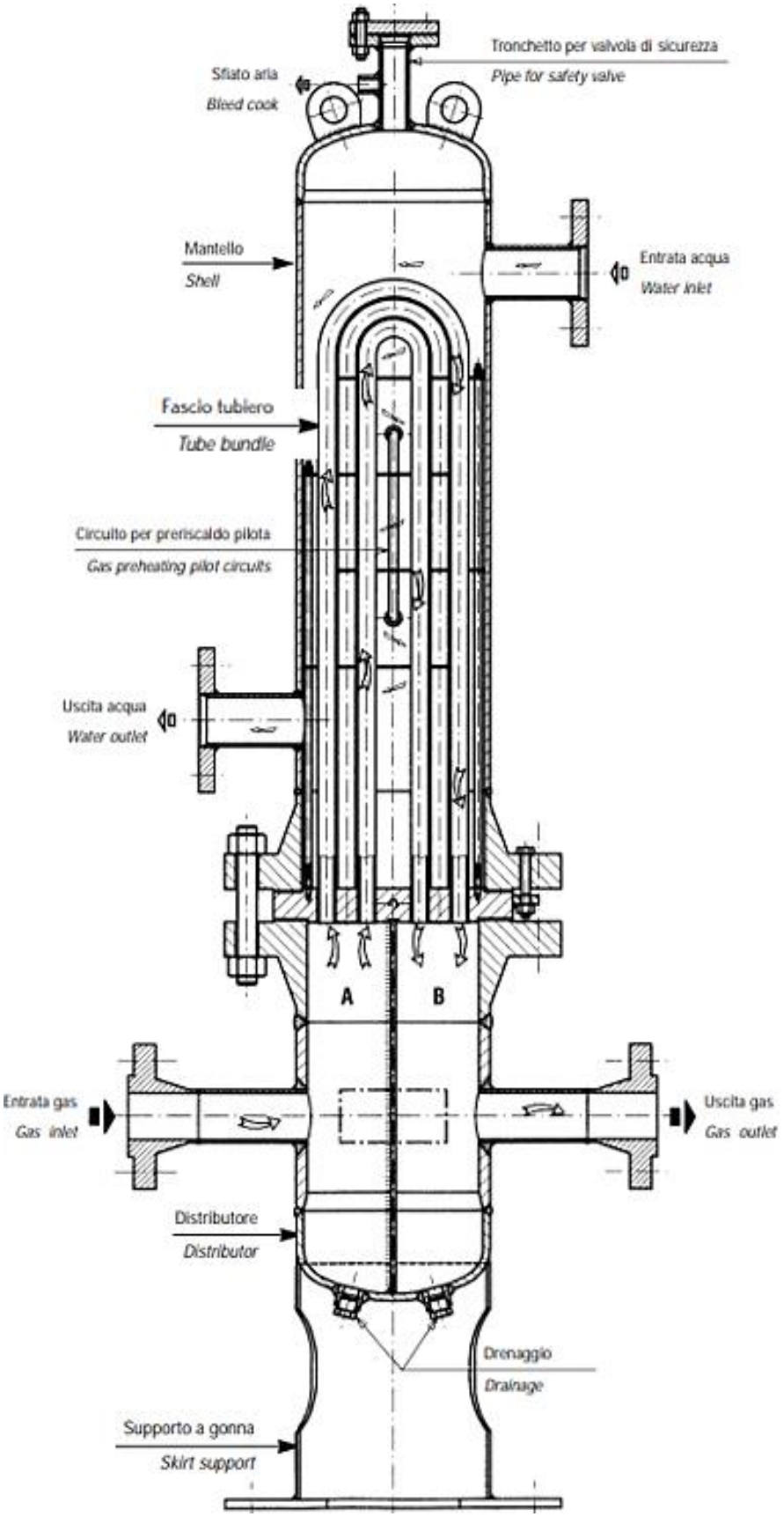

Fig. 1.31 KSI shell and tube heat exchanger (*from [19]*).

2 METHODOLOGY

The methods used to design the different thermal system configurations are presented and described in this section.

In the *Chapter 2.1* the actual preheating system is analysed, and the power required by the thermal plant is calculated using two different procedures. The first one is related to the gas thermodynamic processes, and it is based on the p-h diagram for pure methane. On the other hand, it is also possible to evaluate the thermal load of the gas-fired heater considering fuel consumption data from previous seasons. The study of the shell and tube heat exchanger performance is also presented in this section. The heat transfer processes and the fluids properties are accurately analysed. Moreover, the inlet and outlet temperatures are designed with the Log Mean Temperature Difference method.

Chapter 2.2 is focused on the characterization of the shallow aquifer. The site hydrogeological framework is described and the main hydrodynamic properties of the aquifer are presented. A single-well pumping test, performed in the abstraction well, is evaluated and the resulting data allow to obtain the hydraulic parameters in order to characterize the groundwater flow.

Chapter 2.3 describes the various steps required to size the proposed open-loop system. A first conceptual model is created from the subsoil analysis of the examined area. Then, the aquifer properties are implemented with the numerical code FEFLOW in order to design a 3D model and simulate the groundwater flow and the heat transport, occurring in the subsurface during the geothermal process.

Chapter 2.4 presents the closed-loop geothermal configuration, considered as valid alternative to the conventional preheating system. The sizing procedure for the vertical boreholes is described, with particular reference to the Eskilson model, also known as g-functions method. The Earth Energy Designer software is then presented, since it is based on this semi-analytical model: the program provides numerical simulations of the mean fluid temperatures and the required boreholes length for several patterns. Lastly, the data used to design the closed-loop system, implemented in the thermal plant of a generic pressure reduction station, are set and highlighted.

2.1 THE THERMAL PLANT DESIGN

The thermal plant, consisting in a gas-fired boiler and a heat exchanger, as described in the previous section, must be designed in order to supply the required heat to the gas stream.

The identification of the natural gas thermodynamic properties as well as the examination and calculation of the initial and final pressure and temperature values, are important steps to proceed further in the study.

For simplicity, this thermal plant sizing procedure is based on the following assumptions:

- the pressure at the plant installation site is equal to 1 atm;
- the inlet fuel is at ambient conditions of pressure and temperature;
- the natural gas is formed by pure methane only (other minor compounds were neglected);
- the methane is considered as a perfect gas;
- the operational processes are considered with steady state conditions.

2.1.1 PREHEATING SYSTEM OF THE GAS

First of all, the rapid expansion of the natural gas in the throttling valve can be approximated as an adiabatic, isenthalpic, and irreversible process.

In order to properly design the preheating system, the required operational data are:

- natural gas (methane) density (ρ_{CH4}), at 15 °C and 1 atm, equal to 0.7 kg/m^3;
- maximum gas flow rate ($\dot{G}_{max}$) at standard conditions;
- inlet (P_1) and outlet (P_2) gas absolute pressures;
- natural gas initial temperature (T_{NG1});
- natural gas temperature after the expansion process (T_{NG3});
- enthalpy difference between upstream and downstream gas conditions (Δh).

All the operating parameters are known (listed in *Tab. 1*), except the initial and final enthalpy values of the natural gas.

The enthalpy increase resulting from preheating can be obtained through the use of the methane p-h diagram in *Fig. 2.1*. This important value represents the specific heat amount (expressed in kJ or kcal) which must be supplied to each kilogram of natural gas to increase its temperature before being depressurized.

On the p-h diagram it is possible to highlight the thermodynamic processes corresponding to the change between different thermodynamic states of the natural gas, as represented below.

The three transformations between different gas conditions are summarised as follows:

1) Isenthalpic expansion: from natural gas initial conditions, P_1 and T_{NG1} (point A), till the reduced pressure P_2, with a corresponding temperature value T_{NG4}..
2) Isobaric heating: from the conditions downstream of the pressure regulator, P_2 and T_{NG4} (point B), to the required minimum temperature value of the gas, set to T_{NG3}.
3) Ideal isenthalpic compression: from the final conditions, P_2 and T_{NG3} (point C), to the inlet pressure P_1, with a corresponding temperature value T_{NG2} (point D), which the gas will assume at the heat exchanger outlet (after preheating and before expansion).

Therefore, the gas in the first two conditions (points A and B) is at its initial enthalpy value, while in the other two states (points C and D) the gas is at its final enthalpy condition. The difference between the first specific enthalpy value and the second one exactly corresponds to the required heat that the thermal plant must provide in order to preheat the gas.

The heat exchanger thermal power Q_{th} (kW) can be expressed with the following equation:

$$Q_{th} = \frac{\rho_{CH4}}{\eta_{HE}} \Delta h \, \dot{G}_{max} \tag{2.1}$$

where ρ_{CH4} is the density of methane, Δh is the enthalpy difference between initial and final gas states (kJ kg^{-1}), $\dot{G}_{max}$ ($m^3 s^{-1}$) is the maximum volumetric flow rate of the gas into the line, whereas η_{HE} is the heat exchanger efficiency, assumed to be 90% in conservative condition.

On the other hand, the total power P_{th} (kW) required by the whole preheating system (thus including the gas-fired heater) can be achieved with the following expression:

$$P_{th} = \frac{\rho_{CH4}}{\eta_{HE} \, \eta_{boiler}} \Delta h \, \dot{G}_{max} \tag{2.2}$$

where η_{boiler} is the boiler efficiency, considered equal to 80% in conservative assumptions.

Another possible method, considered for the thermal plant sizing, consists in evaluating the power of the gas-fired heater by calculating its fuel consumption.

The hourly distribution of the methane flow rates for an average day is shown in *Fig. 1.28*. The total thermal duty P_{th} (kW) necessary to preheat the natural gas can be evaluated as follows:

$$P_{th} = \dot{m} \, LHV \, \eta_{boiler} \tag{2.3}$$

where $\dot{m}$ ($m^3 h^{-1}$) is the maximum hourly flow rate of the gas burned in the boiler, whereas *LHV* is the lower heating value of methane, equal to 9.972 kWh/m^3 (*from [21]*).

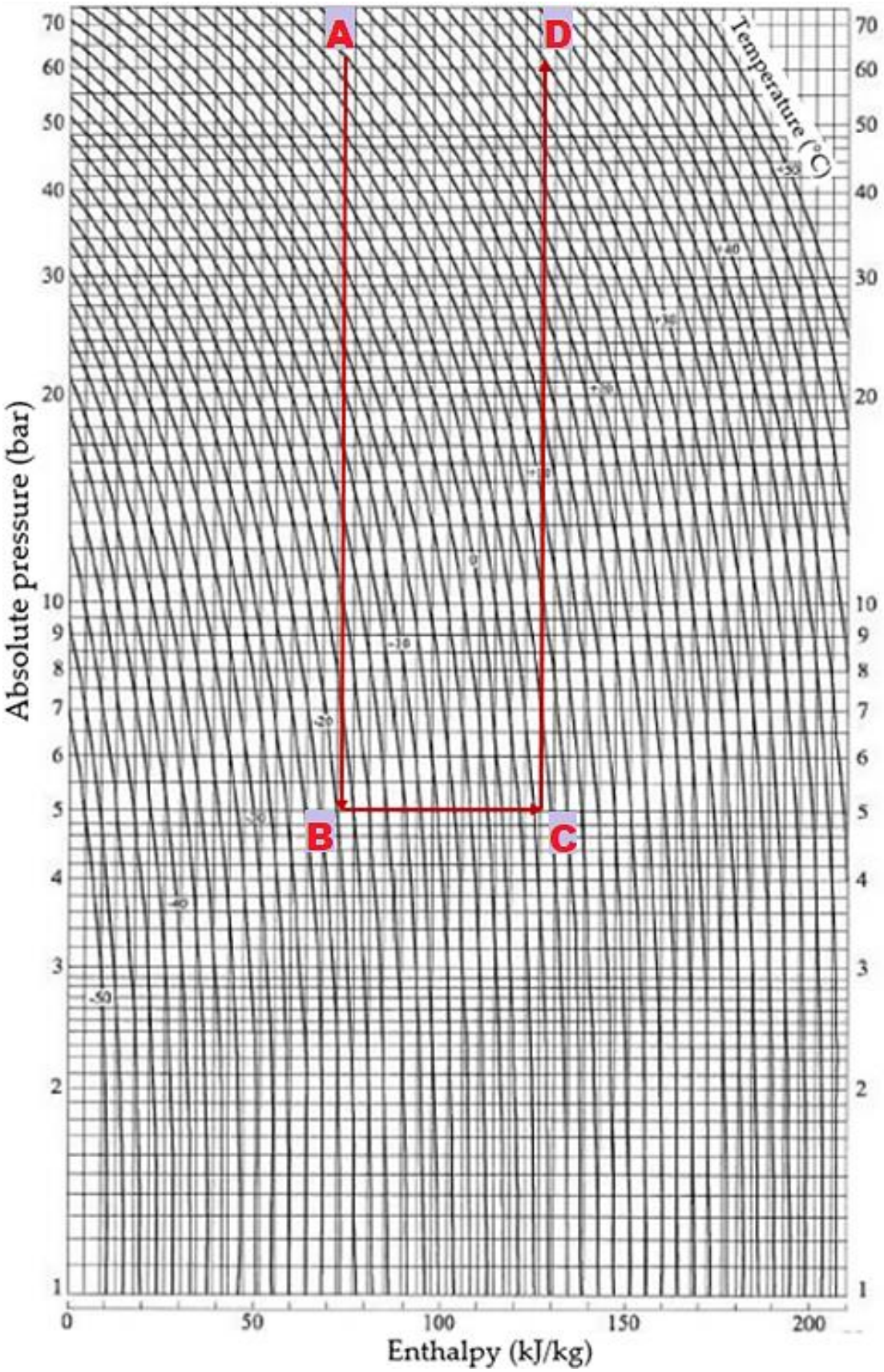

Fig. 2.1 Portion of the methane p-h diagram (*modified from* [20]).

2.1.2 HEAT EXCHANGER PERFORMANCE ANALYSIS

In order to properly design the preheating system, it is important to study the shell and tube heat exchanger operation and its parameters. In addition to the thermal power, it is also necessary to determine the temperature difference between the two fluids, and to evaluate the overall heat transfer coefficient involved in the process. The calculation of the heat transfer coefficient is key to properly size a heat exchanger, however, it is often the most uncertain step of the whole design process. This coefficient can be defined in terms of the conduction and convection resistances to the heat transfer between two fluids that are separated by a wall.

In this sizing procedure, the heat exchanger performance was determined considering the heat transfer and the fluid mechanics processes both into the shell and the tubes of the exchanger. In order to analyse the fluids behaviour, it is important to know their properties and the geometric configuration in exam. During the operation of the heat exchanger, all the surfaces, both of shell and tubes sides, are subjected to rust formation, fouling, and/or other chemical reactions between the fluids impurities and the wall. Subsequently, the deposition of a film on surfaces increases the resistance to the thermal exchange between the two fluids. To make equations easier, such effects were not considered in the following steps, in which the assumption of clean surfaces is made. Moreover, heat conduction through the wall can be neglected, because a thin wall with high thermal conductivity is used in most cases.

Firstly, the gas flow in the tube bundle was examined: as methane moves into pipes, it can be approximated as the case of pure convection in internal flow. The Dittus-Boelter relation can be used, as it applies to a fully developed (hydrodynamically and thermally) turbulent flow in a smooth circular tube (*from [22]*). The Nusselt number can be expressed as follows:

$$Nu = 0.023\, Re_D^{4/5}\, Pr^n \tag{2.4}$$

where n is equal to 0.4 for heating and 0.3 for cooling operations, while Re_D and Pr are the Reynolds and Prandtl numbers respectively. The equation above is valid for the following range of conditions:

$$0.6 \leq Pr \leq 160$$
$$Re_D \geq 10000$$

The Reynolds and Prandtl numbers can be evaluated with the following expressions:

$$Re_D = \frac{\rho\, v\, d_i}{\mu} \tag{2.5}$$

$$Pr = \frac{\mu\, c_p}{k} \tag{2.6}$$

where ρ is the density (kg m^3), v is the velocity (m s^{-1}), d_i is the pipes internal diameter (m), μ is the dynamic viscosity (kg m^{-1}s^{-1}), k is the thermal conductivity (Wm^{-1}K^{-1}) and c_p is the specific heat (J kg^{-1}K^{-1}); therefore, both Reynolds and Prandtl numbers are dimensionless.

The last parameter to be determined is the convection coefficient c ($Wm^{-2}K^{-1}$):

$$c = \frac{Nu\ k}{d_i} \tag{2.7}$$

Regarding the water flow, what happens in the shell of the heat exchanger can be considered equivalent to a flow across a bank of tubes. In fact, because of the position of the baffles, the fluid performs a horizontal flow and moves over the tubes bundle as represented in the configuration in *Fig. 2.2*. The water flow is dominated by wakes which enhance mixing and turbulence phenomena, thus, improving heat transport by convection.

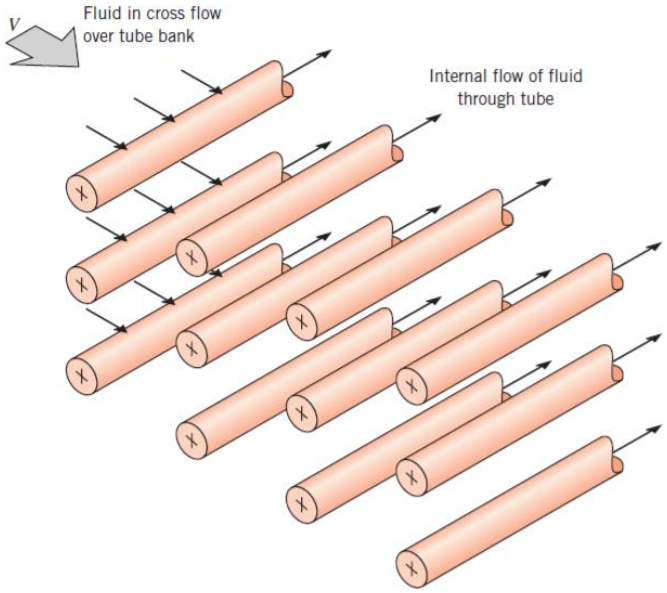

Fig. 2.2 Scheme of a tubes bank in cross flow (*from [22]*).

The average heat transfer coefficient for the whole bundle of tubes can be calculated with the correlation proposed by Zukauskas (*from [22]*) in the following form:

$$Nu_D = F\ Re_{D,max}^{f}\ Pr^{0.36}\left(\frac{Pr}{Pr_s}\right)^{1/4} \tag{2.8}$$

where:

- $F = 0.25$ is a coefficient in function of the tubes rows number and arrangement;
- $f = 0.63$ is a constant depending on the $Re_{D,max}$;
- $Pr_s = 7.09$ is the Prandtl number evaluated at the mean temperature of the surfaces.

The previous equation is valid for:

$$0.7 \leq Pr \leq 500$$
$$10 \leq Re_{D,max} \leq 2 \cdot 10^6$$

The foregoing correlations are based on the Reynolds number which is related to the maximum fluid velocity. The tubes bundle rows were considered aligned in the direction of the water flow, as is shown in the scheme in *Fig. 2.3*, where the transverse pitch S_T is equal to the longitudinal one S_L, while D is equal to the tubes outer diameter (d_o). The highest flow velocity occurs at the transverse section A_1, and can be expressed as below:

$$V_{max} = \frac{S_T}{S_T - d_o} v \tag{2.9}$$

where S_T and d_o are listed in *Tab. 2*. It follows that:

$$Re_{D,max} = \frac{\rho \, V_{max} \, d_o}{\mu} \tag{2.10}$$

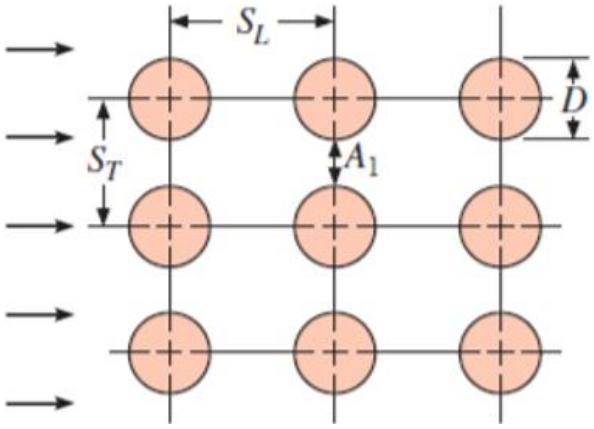

Fig. 2.3 Aligned tubes bundle arrangement (*from [22]*).

The Prandtl number can be calculated with the expression above, the same used for the flow in circular tubes. Lastly, the heat convection coefficient can be evaluated:

$$c = \frac{Nu_D \, k}{d_o} \tag{2.11}$$

Generally, there is a large difference between the two convection coefficients c obtained with the above equations. In particular when a liquid and a gas fluid are present such as in this case: the smaller one dominates in determine the overall heat transfer coefficient U ($Wm^{-2}K^{-1}$), which can be finally expressed as follows:

$$U = \frac{1}{(1/c_{CH4}) + (1/c_{H2O})} \tag{2.12}$$

All the fluid properties used in the sizing procedure are summarized in *Tab. 3* below, both for the methane and the water flows. The two fluids were considered at their average temperature values between the inlet and outlet of the shell and tube heat exchanger.

Tab. 3 Fluids properties into the heat exchanger.

PROPERTIES	*CH_4*	*H_2O*	*U.M.*
Specific heat	2.315	4.178	kJ/(kgK)
Density	0.678	993	kg/m^3
Velocity	73.64	0.26	m/s
Dynamic viscosity	$1.08 \cdot 10^{-5}$	$6.95 \cdot 10^{-4}$	kg/(ms)
Thermal conductivity	0.030	0.628	W/(mK)

2.1.2.1 LOG MEAN TEMPERATURE DIFFERENCE METHOD

The heat exchanger was then designed with the Log Mean Temperature Difference (LMTD) method, to verify the initial and final temperatures of the two fluids. In order to size the heat exchanger and evaluate its performance, the thermal power must be calculated considering the overall heat transfer coefficient, the heating surface and the inlet and outlet temperatures, as expressed in the following equation:

$$Q_{th} = U\, A\, \Delta T_m \tag{2.13}$$

where Q_{th} is the heat exchanger thermal power (W) and A is its heating transfer area (m^2), while ΔT_m is an appropriate average temperature difference (°C), which varies with the position of the hot and cold fluids in the shell and tube heat exchanger.

The subsequent analysis is subject to the assumptions below:

- the heat exchanger is perfectly insulated, hence, the only thermal exchange occurs between the two fluids;
- the specific heat and the overall heat transfer coefficient are constant for both fluids;
- potential and kinetic energy variations of the two fluids and axial conduction along the pipes can be neglected;

The shell and tube heat exchanger was modelled for a counter flow configuration, thus the ΔT_m can be calculated as follows:

$$\Delta T_{lm} = \frac{\Delta T_1 - \Delta T_2}{\ln\left(\Delta T_1 / \Delta T_2\right)} = \frac{\Delta T_2 - \Delta T_1}{\ln\left(\Delta T_2 / \Delta T_1\right)} \tag{2.14}$$

where the subscripts 1 and 2 designate the opposite ends of the heat exchanger, and the temperature differences between the endpoints are defined as below:

$$\begin{aligned} \Delta T_1 &= T_{h,1} - T_{c,1} = T_{h,i} - T_{c,o} \\ \Delta T_2 &= T_{h,2} - T_{c,2} = T_{h,o} - T_{c,i} \end{aligned} \tag{2.15}$$

where the subscripts i and o designate the fluid inlet and outlet conditions, and the subscripts h and c refer to the hot and cold streams.

The temperature distributions of two fluids, related to a counter-current flow heat exchanger, are represented in *Fig. 2.4* below. This configuration is the most effective, since it enhances the heat transfer between the hotter temperatures of the two fluids at one end and the thermal exchange between the colder ones at the other side. It is also important to note that, in the counter flow system, the cold fluid outlet temperature may exceed the hot fluid one.

The LMTD method is a powerful and useful model used to approach and study the heat exchanger, however, it analyses the exchanger operation from a black-box perspective: indeed, this tool does not provide any information about the internal conditions and processes.

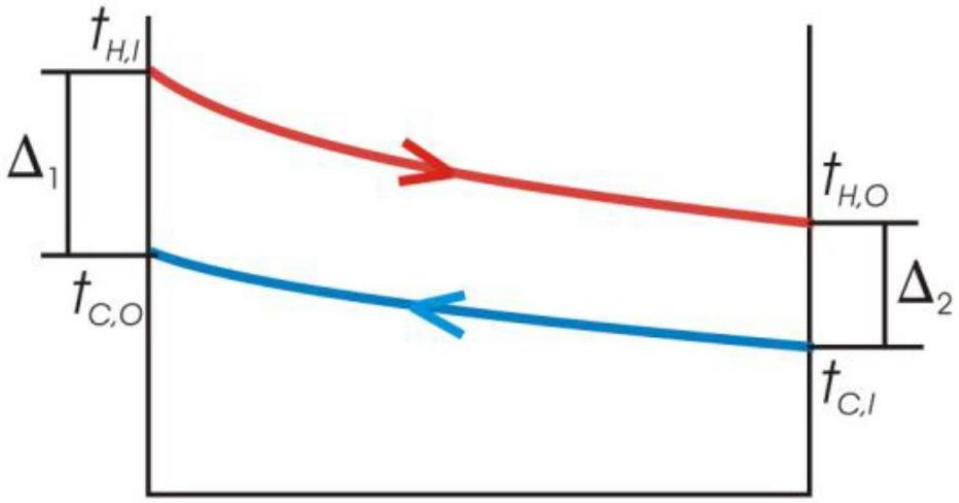

Fig. 2.4 Temperature distributions for a counter flow heat exchanger (*from [4]*).

2.2 CHARACTERIZATION OF THE SHALLOW AQUIFER

An open-loop system is generally sized according to several factors such as the heating need, the local legislation, available spaces and, above all, the hydraulic properties of the aquifer. In particular, the latter are the most important parameters to be determined when considering a groundwater flow. Therefore, the hydrogeological framework of the site in exam was investigated, in order to properly characterize the subsoil and the shallow water table.

A water well is already present close to the pressure reduction station, about 100 meters far away. It is a historical municipal well which never experienced performance issues, but it is currently no longer used for potable purposes because the water quality does not comply with the law requirements, due to the presence of dissolved fertilizers. Therefore, the well is only used for the irrigation of the neighbouring football field. A request for utilization was therefore made to the municipality, which has given the availability to use this well as the extraction well in the open-loop designed configuration. Regarding the injection well, it will be constructed close to the pressure reduction station, at an appropriate distance from the abstraction well in order to avoid the thermal recycling of the reinjected discharge rate. The abstraction well was also used to perform a pumping test, in order to evaluate the aquifer hydrodynamic properties.

2.2.1 HYDROGEOLOGICAL FRAMEWORK

The geological framework of the southern Piedmont is characterised by a substrate consisting in marine sediments within the "Liguria-Piemonte" Tertiary basin, overlain by discontinuous Quaternary alluvial deposits, the latter have generally a reduced thickness. Different stratigraphic units emerge in this area, the substratum of which is made up of several lithologies that are characterised by a marly, clayey and silty composition. The main geological formation (*from [23])* consists in the "Marl of Sant'Agata Fossili", a relatively shallow marine sedimentary succession, consisting in grey-blue marls. The marlstone layers locally emerge in correspondence of the Tanaro riverbed, due to recent erosion processes.

The floodplain has a substrate which is easily eroded by the river action, resulting in gullies and terraced formations. A well-defined and carved bed is typical of rivers that sinuously flow into lowland valleys. The fluvial erosion process involves the surfaces alteration and the modelling of gravitational slopes, caused by the flood events depositing and accumulating large quantities of sediment on the riverbanks. So, following the slow evolution of the Tanaro river, its bed has subsided over the years (*from [24])*. The alluvial deposit lies on the substrate previously described and consists of different materials with a heterogeneous composition: in fact, the grain size is varied, from coarse (sand, gravel and pebble) to fine (clay and silt).

In the recent past, the sediments underwent several natural physical and chemical processes, because of the river dynamics. Due to the large solid load transported by the Tanaro flow rates, the fine sediments can be found mainly over the superficial layers. Thus, resulting in a certain selection of the lithology, based on the granulometric composition. However, in the floodplain there are significant oscillations of the shallow ground stratigraphy from point to point. The local lithostratigraphic reconstruction can be divided in the following main units:

- a soil vegetal cover, in the order of some decimetres;
- a shallow level of sandy loam, with a thickness from decimetres to a few meters;
- the alluvial deposit, consisting in sand, gravels and pebbles, a few meters deep;
- the bedrock composed of silty, clay and marly layers.

The above-described fluvial depositional environment composes the shallow aquifer, while the impermeable marlstone, from a few tens of meters depth, represents the aquifer bottom. The grain size distribution of the alluvial bed is in the range of some millimetres and, due to the presence of gravels and sandy fractions, this layer has high values of permeability. Since the floodplain is bordered by the hills, which are mainly impermeable, the water supplies from the slopes, reaching the land in the valley, feeds the groundwater flow. In this part of the Tanaro valley there are many creeks which perform a draining action from the hills to the plain, flowing then into the river. The Tanaro is also directly in contact with the phreatic surface: there are several water exchanges between the two natural systems, depending on the seasonal oscillations, based on the hydrological regimes and the flow rates. In addition to this natural situation, there is also an extensive network of artificial irrigation channels which cross the land and have several leakages, resulting in further infiltration flows towards the water table. All these streams, either superficial or underground, involve the shallow aquifer; in summary, they can be divided in almost three main local hydrodynamic processes:

- the rainwater runoff which percolates through the soil;
- the draining action of the Tanaro river and the other creeks;
- the water intakes from the canals used to irrigate the crops.

At large-scale, the groundwater flow direction is generally from South-West to North-East, towards the river Tanaro, due to its hydraulic balance with the aquifer. In the central part of the floodplain, the piezometric gradient is in the range of 0.2-0.3%, while getting closer to the river, it reaches values almost equal to 0.5-0.6%. The equipotential lines of the area are represented in *Fig. 2.5*: the potentiometric surface coincides with the water table because the aquifer is unconfined. The average phreatic surface is usually between 2 and 5 m below the ground level, with a maximum excursion of about 1 m. Due to the low aquifer depth, the time of travel of the pollutants is characterised by very small values, in the order of few days. Therefore, this area is particularly vulnerable to the anthropic activities: there are high concentration of nitrates, chlorides and sulphates, due to the agricultural land uses.

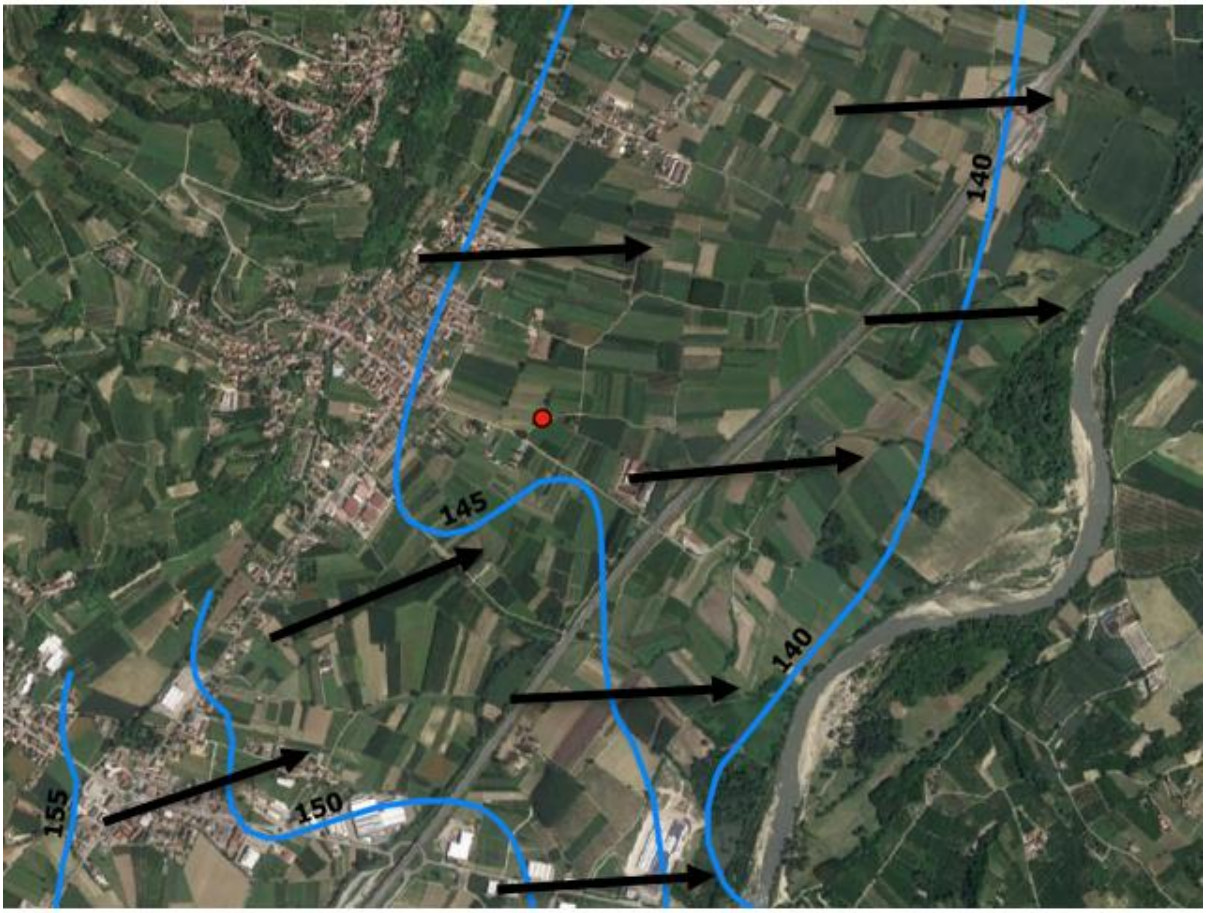

Fig. 2.5 Potentiometric map: equipotential lines in blue and flow lines in black ***(from [25])*****.**

2.2.2 HYDRODYNAMIC PROPERTIES

The hydrodynamic properties of the aquifer were investigated with a pumping test performed in the existing well. This method consists in the abstraction of a constant water discharge rate from a well, inducing a certain drawdown which was measured over time. The aquifer test was carried out for 24 hours and it also included the recovery phase in the 12 hours following the pump interruption, with the analyses of the water table rising, till the static level was recovered. The test was performed with the pump and the equipment already present in the municipal well. The parameters were measured and collected with an automatic acquisition system composed of pressure sensors and data logger, which enabled an optimal definition: the electric piezometer continuously recorded with a scanning frequency of 1 minute and a resolution equal to 1 cm. The results achieved with this pumping test were really good, both in terms of the aquifer productivity and the water table stability, as shown in the *Tab. 4* below. The constant flow rate was set to 4.8 l/s and the resulting drawdown was equal to 22 cm, which occurred in the first 17 minutes, with a subsequent stabilisation of the piezometric levels trend.

Tab. 4 Hydraulic parameters of the aquifer test.

PARAMETER	*VALUE*	*U.M.*
Well diameter	2.5	m
Piezometric level	-4.50	m
Saturated thickness	3.5	m
Flow rate	4.8	l/s
Drawdown	0.22	m
Pumping duration	24	h
Recovery duration	12	h

The pumping test results showed a hydrodynamic behaviour typical of unconfined aquifers. The identification of the physical model is very important for the interpretation of either the pumping and the recovery test. Then, the recorded data were interpreted with the software Aqtesolv, which is a program used to analyse different aquifer typologies (confined, leaky or semi-confined, and unconfined), and to interpret the various aquifer tests such as pumping, recovery, constant-head, slug tests etc.

In order to interpret the recovery test, the superposition principle is normally used: the well is assumed to continue extracting the same constant flow rate even after the pumping stop, and an imaginary recharge well is assumed to start pumping an equal rate. From this interpretation method it was possible to obtain two hydraulic properties of the aquifer: the transmissivity and the storativity. The latter is a dimensionless parameter, also known as storage coefficient (S), and expresses the aquifer ability to release water with gravitational drainage and storage compressibility (*from [26]*). For unconfined aquifers the water release is due to the gravitational drainage only, thus we refer to specific yield ($S = S_y$). In this case, the storage capacity is quite important since it determines the hydrodynamic behaviour of the aquifer:

1) initially, the water supply derives from the aquifer elastic storage;
2) then, there is a phase dominated by delayed gravity drainage;
3) finally, the drawdown starts to increase again depending on the aquifer specific yield.

These three phases are clearly represented in the *Fig. 2.6* below.

On the other hand, the transmissivity T (m^2s^{-1}) measures the aquifer productivity, and it can be defined as follows:

$$T = K \cdot b \tag{2.16}$$

where b is the aquifer's thickness (m) and K is the hydraulic conductivity (ms^{-1}), another important parameter which measures the water circulation capacity into the aquifer. This equation considers the hydraulic conductivity constant along the entire saturated thickness.

Therefore, known the transmissivity of the aquifer and its thickness, it is possible to evaluate the aquifer hydraulic conductivity from the expression above.

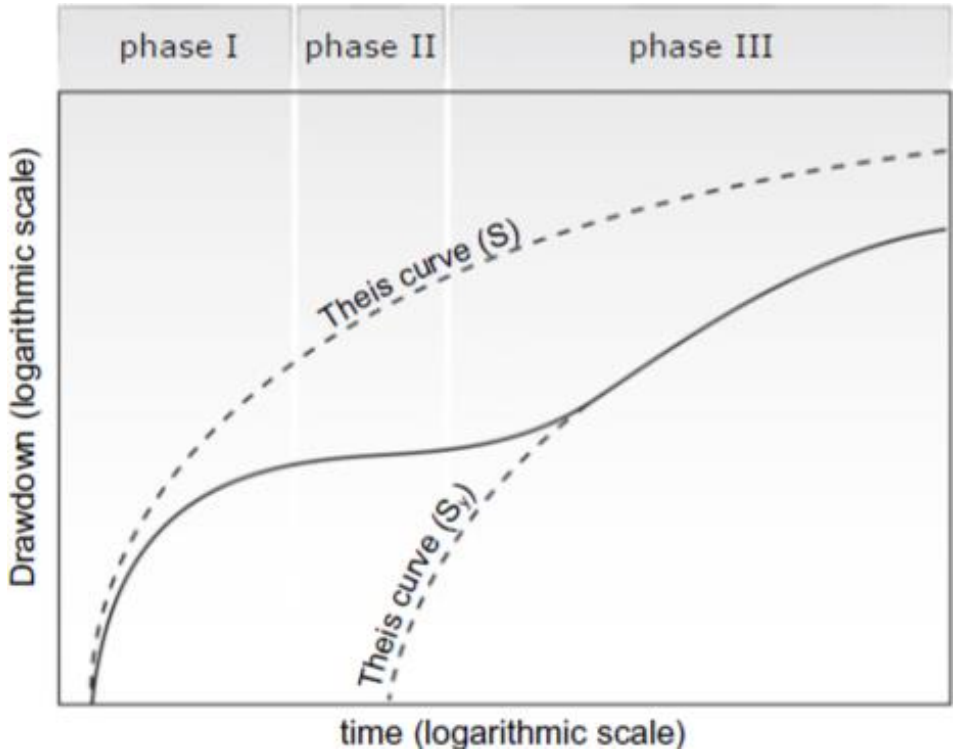

Fig. 2.6 Hydrodynamic behavior of an unconfined aquifer (*from [26]*).

The productivity of the well can be expressed by its specific capacity q_{sp} (m^2s^{-1}), which is the ratio between the pumped discharge (Q) and the corresponding steady-state drawdown (s). In an unconfined aquifer, such as in this case, the well specific capacity is closely related to the aquifer transmissivity:

$$q_{sp} = \frac{Q}{s} \cong T \tag{2.17}$$

2.3 DESIGN OF THE OPEN-LOOP PREHEATING SYSTEM

The open-loop system was proposed to replace the gas boiler in the pressure reduction station. The groundwater heat pump has to provide the required hot water in order to preheat the natural gas stream that flows into the shell and tube heat exchanger. This novel thermal plant configuration is represented in the scheme in *Fig. 2.7* below.

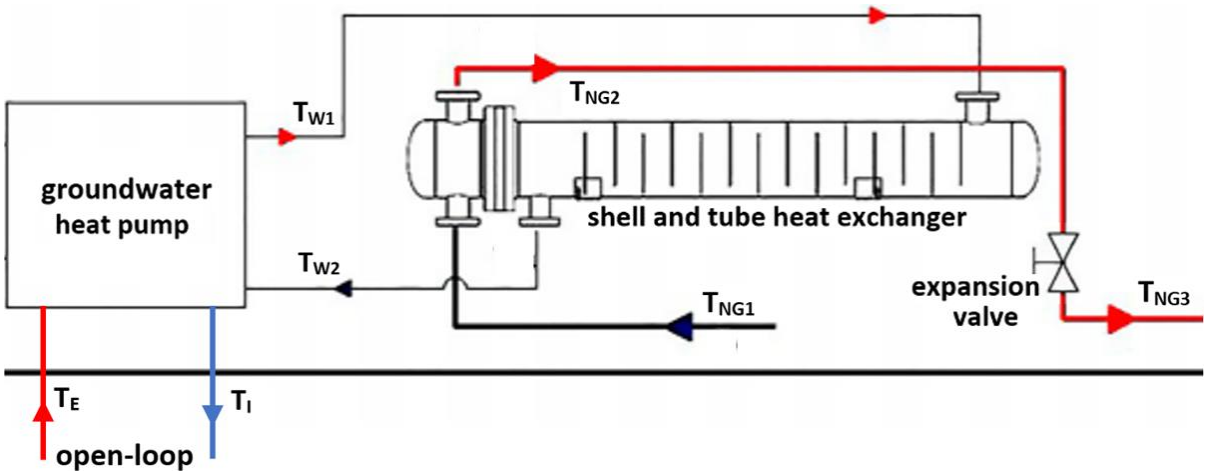

Fig. 2.7 Scheme of the novel thermal plant configuration with the GWHP (*modified from [27]*).

The open-loop system consists in a well doublet configuration, i.e., an abstraction well and a recharge one. This renewable solution enables to preserve the water budget of the aquifer. The groundwater heat pump can exchange a certain amount of thermal power P_{th} (kW), expressed as follows:

$$P_{th} = Q\ \rho_w c_w\ \Delta T \tag{2.18}$$

where Q is the flow rate (m^3h^{-1}) abstracted from the supply well, ΔT is the difference between the extracted (T_E) and the injected (T_I) temperature (K), whereas $\rho_w c_w$ is the groundwater thermal capacity equal to 4.2 MJ/(m^3K), corresponding to 1.167 kWh/(m^3K).

Therefore, in order to properly design the open-loop system, the required input data are: the flow rate and the temperature difference, as well as the hydrogeological characteristics of the aquifer and the hydraulic head distribution in undisturbed conditions.

Then, a model for the desired configuration can be created and implemented with software such as FEFLOW, which enables a numerical simulation of the groundwater flow and the heat transport in porous media. The temperature distribution of the aquifer must be monitored in order to ensure that no thermal recycling will occur over time, as shown in *Fig. 2.8* below.

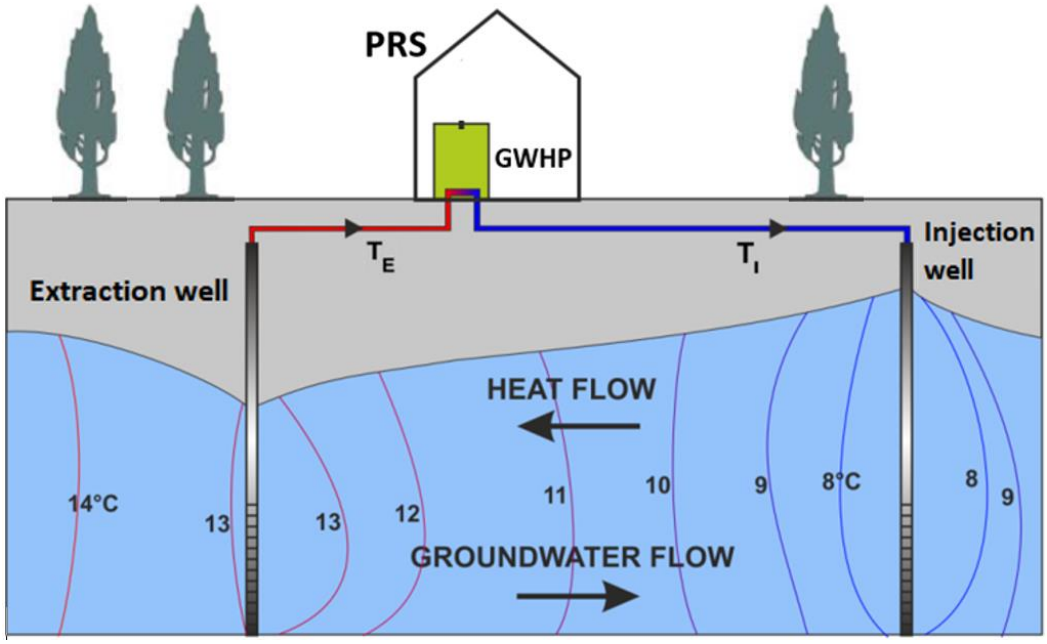

Fig. 2.8 The open-loop system configuration (source *Polytechnic of Turin*).

2.3.1 CONCEPTUAL MODELLING

The first step in model development is the description of the groundwater system conditions. When designing an open-loop system, an important aspect to consider, in addition to the aquifer properties, are the lithological levels and the subsoil geological characteristics which enable to evaluate the groundwater flow. Thus, a simplified lithostratigraphic sequence was assumed, based on several drillings next to the site location. In particular, the Arpa Piemonte surveys on the left bank of the Tanaro river were investigated. The nearest one is that named A14 and it is situated 1 km far from the plant. Moreover, two perforations upstream (A16 and A15) and two downstream (A13 and A12) of the Alba4 station were also considered, as shown in *Fig. 2.9*, in order to include all the hydrogeological features of the area of interest.

The results of this analyses showed a consistent behaviour of the different stratigraphic layers. In this part of the Tanaro valley the ground level decreases from 155 to 140 meters above the sea level, and the pressure reduction station is located at about 150 m a.s.l.. The shallow phreatic aquifer circulates at about 4 m depth from the ground level. The subsoil stratigraphy can be divided in four main layers, as also represented in *Fig. 2.10*:

1) the first one consists in fine sand and has a thickness of about 3 meters;
2) the second level is composed of gravel and pebble, and is about 5 meters deep;
3) the third is a thin layer of silt and clay, and is almost 2 meters thick;
4) the bedrock consists in marlstone till a depth of 50 meters.

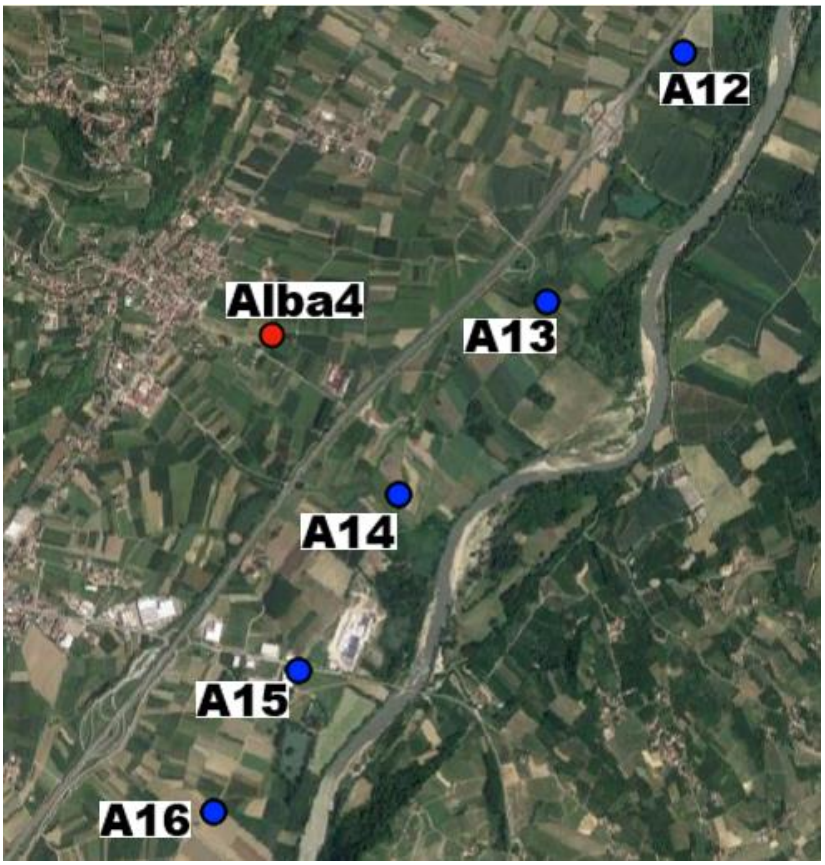

Fig. 2.9 Arpa Piemonte surveys near the plant.

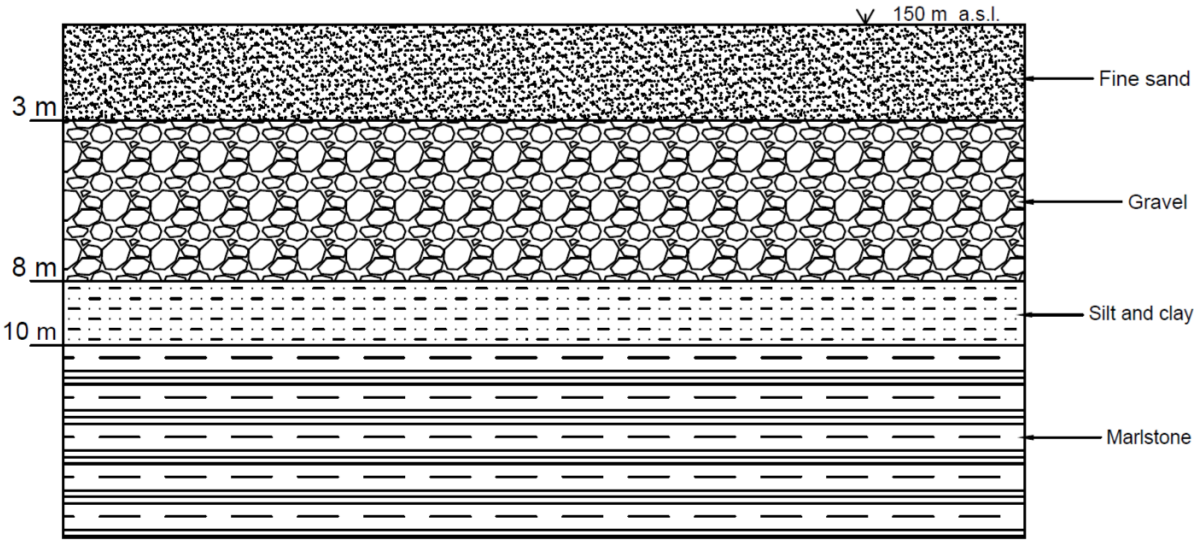

Fig. 2.10 Simplified lithostratigraphic sequence of the local subsoil.

These various levels are characterized by different values of porosity and hydraulic conductivity, depending on the grains size distribution and on the permeability of the lithologies, as schematically shown in the *Fig. 2.11* below.

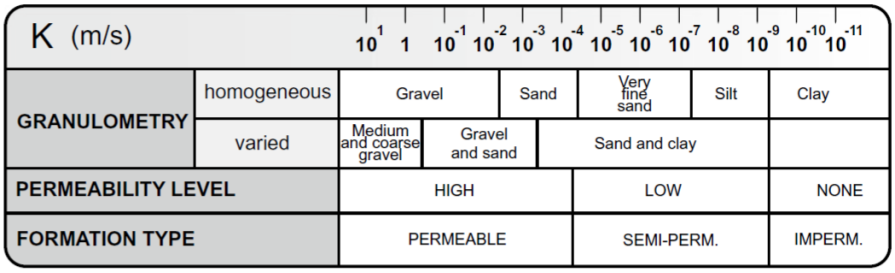

Fig. 2.11 Hydraulic conductivity values of different systems *(from [26])*.

The groundwater circulates into the aquifer under the action of the hydraulic gradient. This is a dimensionless parameter expressed as follows:

$$i = \frac{\Delta h}{\Delta l} \tag{2.19}$$

where Δl is the distance between two equipotential lines, which connect points with the same hydraulic head, and thus, equal piezometric level, while Δh is the hydraulic head drop. In fact, water flows from higher to lower hydraulic heads. Therefore, knowing the magnitude of the hydraulic gradient is essential to evaluate the movement capacity in the aquifer and the direction of the groundwater flow.

In order to prevent that a recycled share of the reinjected discharge rate can affect the abstraction well, the distance L (m) between the two wells must be set at the following value:

$$L > \frac{2Q}{\pi T i} \tag{2.20}$$

It corresponds to the minimum length required to avoid the progressive thermal alteration induced by water recycling.

2.3.2 SETUP OF THE NUMERICAL FLOW AND HEAT TRANSPORT MODEL

Groundwater modelling phases consist in the definition of the domain, the distribution of the material properties and the boundary and initial conditions. The latter define the initial state within the domain (i.e., undisturbed temperature and hydraulic heads), while the boundary conditions determine the exchanges through the domain boundaries. The flow boundaries can be divided in:

- physical: well-defined hydrogeological features which influence the groundwater flow patterns;
- hydraulic: from the groundwater flow distribution and set by the model designer (boundaries with known equipotential lines which represents hydraulic heads).

These boundary conditions are of three types:

1) Dirichlet, for the specified hydraulic head;
2) Neumann, concerning the specified flux;
3) Cauchy, for the specified head-dependent flux.

Once the input data are defined, the main results of the numerical simulation are: the temperatures at certain points (the two wells), the thermal plume and its temporal evolution. In this study the goal consists in solving the coupled flow and heat transport problem, in order to avoid the thermal recycling and the plume propagation in the designed open-loop system. Therefore, the proposed configuration was implemented with the software FEFLOW (Finite Element subsurface FLOW and transport system) to simulate the geothermal process. This numerical tool is provided with a fully-integrated graphical-user-interface and also a graphical presentation of results, with easy parameters specification and modification. On the other hand, it is quite expensive and complex, thus, generally used for large plants.

FEFLOW is a finite elements code and, hence, has the following characteristics:

- properties of the different materials are defined in the grid element by element;
- heads are set by an approximate interpolation function at each point within elements;
- velocities are determined from the derivation of the heads distribution and the properties of the different elements;
- continuity complied with every elements pattern.

Regarding the open-loop system operation, FEFLOW has a special plug-in which applies a predetermined temperature difference between the abstracted water and the reinjected one. The main input required for the model is the Nodal Reference distribution of the two wells. First of all, the spatial domain of the supermesh was created in order to represent the real configuration of the area in exam: a rectangular polygon of 1800 per 600 meters, which starts from the origin (0, 0). The location of the supply well was set in the point *E* (430, 250), while the recharge well position was set in the point *I* (500, 300), as represented in the *Fig. 2.12* below. Then, a 2D mesh with 7855 nodes was generated using the triangular algorithm and, also, a dense refinement of the points around the two wells position, as shown in the *Fig. 2.13* below.

In the next step, the 3D finite-element mesh was created, based on the subsurface conceptual model defined in the previous section. Four layers, delimited by five slices, were set: respectively 3, 5, 2 and 50 meters deep. In fact, the thickness of each layer corresponds to the different lithologies depths represented in *Fig. 2.10*. In order to give to the domain the real sloping, a 0.55% slope was assigned to any slice. Indeed, the upper slice elevations were set equal to 152 meters a.s.l. at the western margin and 142 m at the eastern one. The nodal values were interpolated with the Akima linear method to calculate the elevation of all the mesh points between the two sides. The results are shown in *Fig. 2.14*.

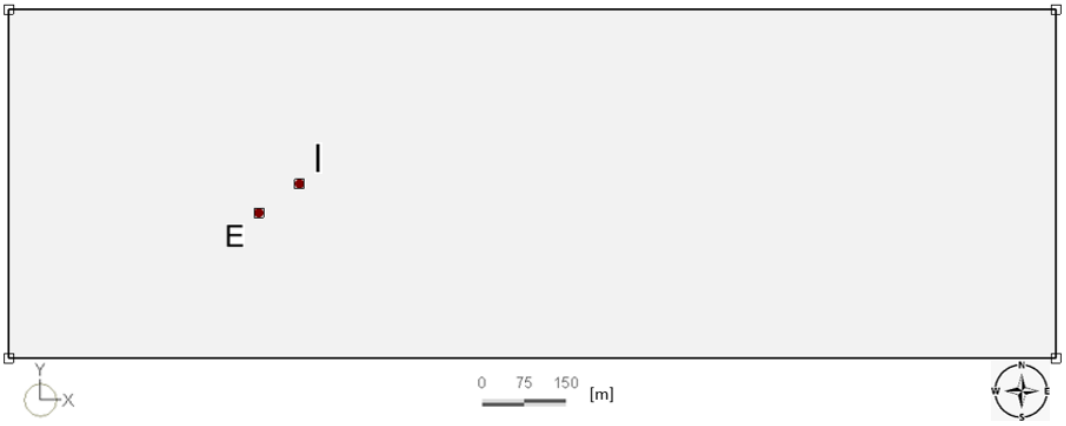

Fig. 2.12 The spatial distribution of the domain with the two wells position.

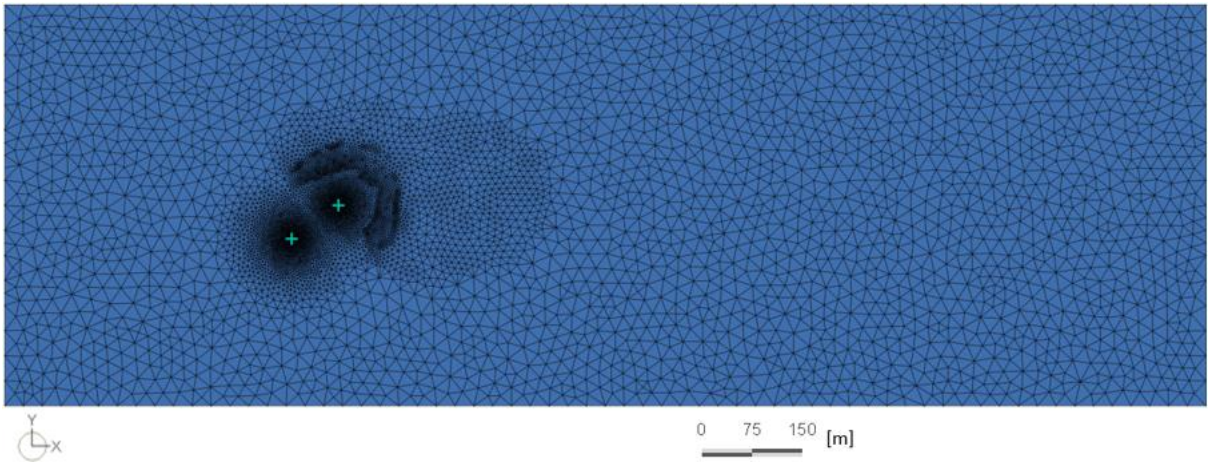

Fig. 2.13 The finite-element mesh with the points refinement around the two wells.

Once the model was created, the initial and the boundary conditions were set. The hydraulic flow boundaries were identified with the equipotential lines: the hydraulic head boundary conditions were set equal to 145 and 140 m along the left and right borders, respectively. Then, the hydraulic heads distribution was attributed along the lines of what was done above to assign the elevation values to the entire domain. The results are represented in *Fig. 2.15*. The undisturbed temperature of the aquifer is equal to 14 °C, so, this value was attributed to all the points of the mesh, in order to set the initial condition for the heat transport.

The main input material parameters to solve the flow problem are the hydraulic conductivity and the effective porosity. These important properties were assigned to the different layers:

1) $K = 5 \cdot 10^{-5}\ m/s$ and $n_e = 0.2$ for the fine sand;
2) $K = 5 \cdot 10^{-3}\ m/s$ and $n_e = 0.25$ for gravel and pebble;
3) $K = 5 \cdot 10^{-7}\ m/s$ and $n_e = 0.1$ for silt and clay;
4) $K = 5 \cdot 10^{-9}\ m/s$ and $n_e = 0.02$ for the marlstone.

The hydraulic conductivities are the same for both the x and y directions, whereas for the z direction these values were set equal to 10% of *K* in all the layers.

The data of the two multilayer wells were also added to the model: the planar and the vertical coordinates of each well were attributed to the two points *E* and *I*. The other required parameters to assign the multilayer well boundary conditions are:

- the radius, equal to 1.25 m for the extraction well and 0.6 m for the injection well;
- the depth, set to 8 m and 3 m for the supply and the recharge wells respectively;
- the pumped rate, equal to 5 l/s for the abstracted rate and -5 l/s for the reinjected one.

Regarding the general settings of the problem class, the fluid flow was simulated in transient state, applying the standard (saturated) groundwater flow equation (the Darcy's equation), including the heat transport. The superficial surface (first slice) of the unconfined aquifer was set to phreatic, while the other slices were "dependent" and the bottom one was fixed.

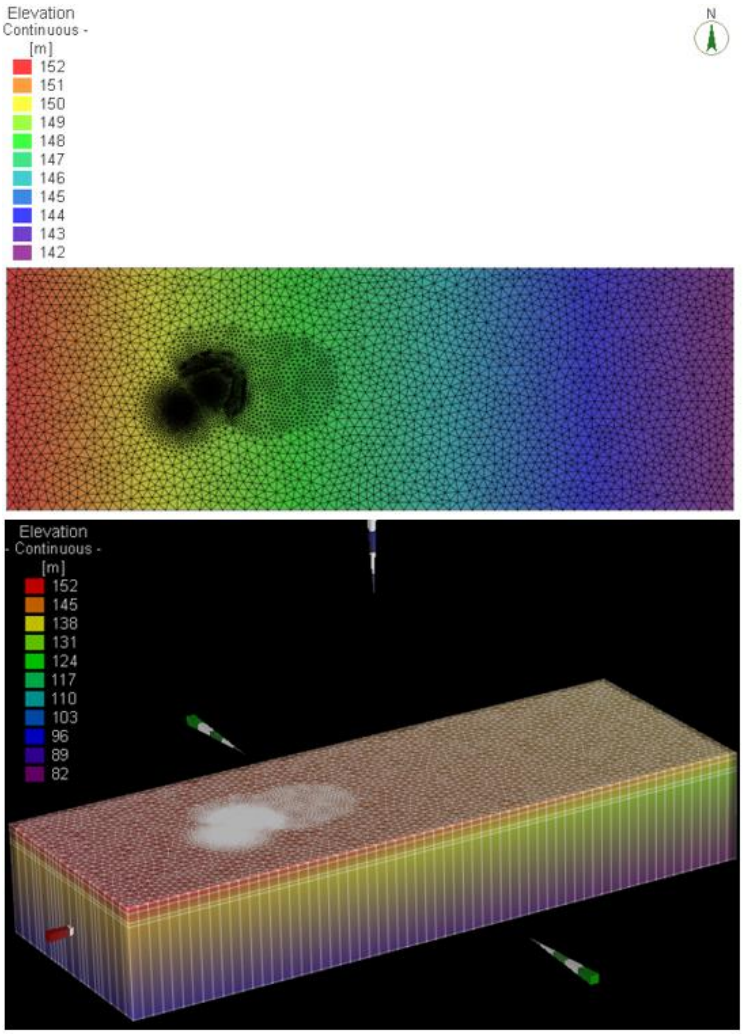

Fig. 2.14 Elevation values for the upper slice (over) and for the 3D model (under).

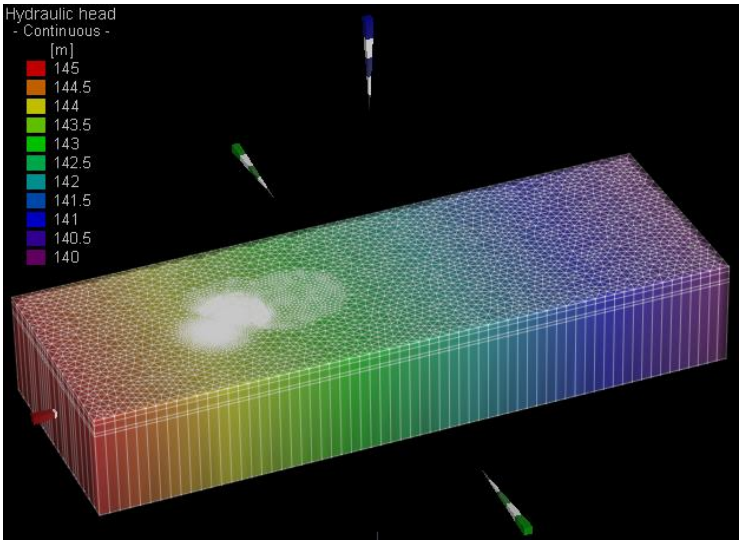

Fig. 2.15 Distribution of the hydraulic head values.

2.4 DESIGN OF THE CLOSED-LOOP PREHEATING SYSTEM

A closed-loop geothermal configuration is also proposed as possible preheating system in the pressure reduction station. The vertical boreholes heat exchangers (BHEs) can be a valid option in such cases in which the aquifer productivity is lower and an open-loop plant is no more so effective. The novel closed-loop preheating system is represented in the scheme in *Fig. 2.16* below.

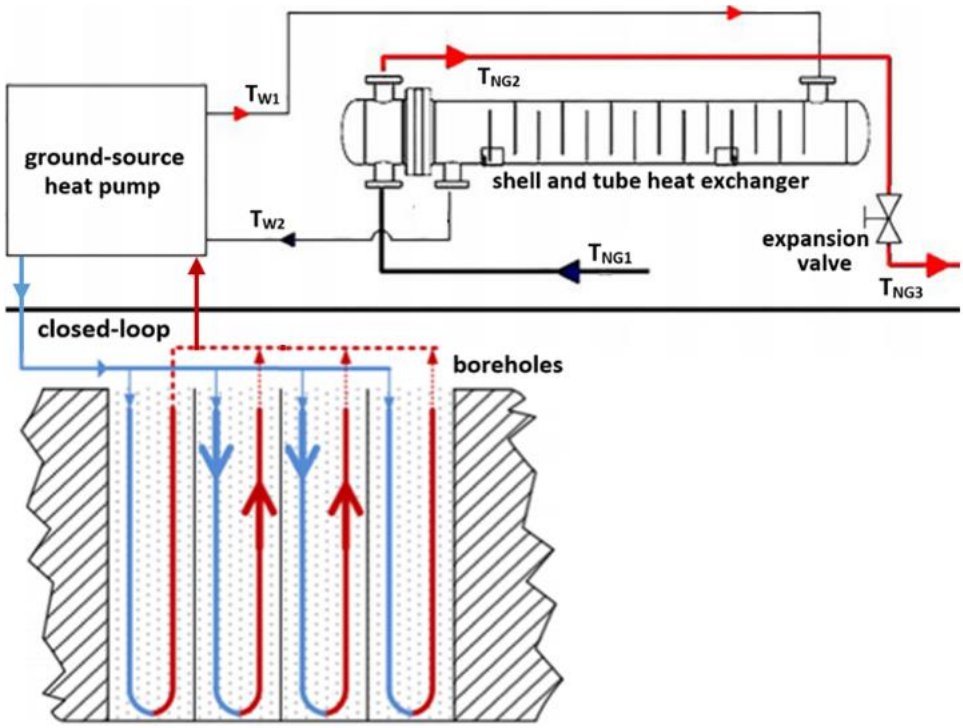

Fig. 2.16 Scheme of the novel thermal plant configuration with BHEs (*modified from [27] and [28]*).

As explained in the introduction, the average annual heat balance of the ground follows a temperature distribution depending on the site climatic conditions and anthropic activities. Vertical BHEs induce a thermal alteration of the ground around them, while at large distances the temperature is undisturbed and remains constant. Consequently, there is a heat transfer between the ground and the boreholes wall: it is associated with thermal and hydrogeological parameters of the soil and the aquifer, and with the material of the tubes. Then, the heat transport occurs in the borehole itself, from the wall to the heat carrier fluid inside the pipes: it depends on the filling thermal resistance and on the fluid properties. Lastly, the fluid temperatures influence the performance of the heat pump.

The closed-loop can exchange with the ground a certain amount of thermal power related to its undisturbed temperature and to its thermal conductivity, which is different according to different lithologies. Typical values for the geothermal heat flux are in the range of 0.05-0.11 W/m^2, while the geothermal gradient is in the order of 1-3 K per 100 m.

In order to design a BHE, there are three main possible methods:

- using default tables, which provide tabulated values of the specific heat extraction;
- using semi-analytical models;
- or numerical simulation of flow and heat transport with software (e.g., FEFLOW).

The Eskilson model was used and it is explained in next paragraph. It is a semi-analytical method based on normalised curves of ground thermal alteration.

2.4.1 ESKILSON METHOD

The Eskilson method is valid for the following assumptions:

- the heat transport is purely conductive, advection and dispersion are negligible;
- homogeneous and isotropic ground properties;
- uniform distribution of the heat flux along the borehole;
- constant undisturbed ground temperature, there is no geothermal gradient;
- standard boreholes geometric configurations;
- constant thermal load.

This model can be compared to an electrical circuit, as shown schematically in the *Fig. 2.17*, where the components behaviour is the following:

- the electrical potentials correspond to the temperatures;
- the electrical resistances correspond to the thermal resistances;
- the nodes correspond to the various elements (ground, wall and fluid);
- the electric current corresponds to the heat flux per unit length.

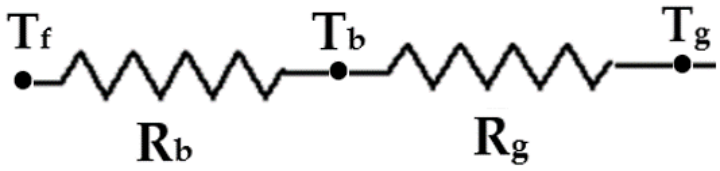

Fig. 2.17 Schematic configuration of the circuit.

Thus, the general equation can be expressed as below:

$$\Delta T = q \cdot R \tag{2.21}$$

where ΔT is the temperature difference between two components, q is the heat flux (Wm^{-1}) and is considered positive when heat is abstracted, and R is the thermal resistance (mKW^{-1}).

As a consequence, the following relations can be established:

$$\begin{aligned} T_g - T_b &= q \cdot R_g \\ T_b - T_f &= q \cdot R_b \end{aligned} \tag{2.22}$$

where the subscripts g, b and f indicate the ground, the borehole wall and the heat carrier fluid, respectively. The ground temperature is considered undisturbed at infinite distance. The thermal resistance of the ground depends on the soil properties and is inversely proportional to its conductivity. The heat carrier fluid temperature is the average value between the borehole inlet and outlet. Lastly, the borehole wall resistance is considered as a function of different parameters: it is based on the borehole and tube diameters, the distance between the pipes, the filling resistance and other factors such as the fluid properties and the Reynolds number. Typical values are in the range of 0.1-0.15 mK/W for the 1U, and 0.07-0.12 mK/W for the 2U configuration.

The Eskilson method is also called g-functions model because it is associated with numerical functions of the boreholes geometry, as represented in the charts of *Fig. 2.18* below.

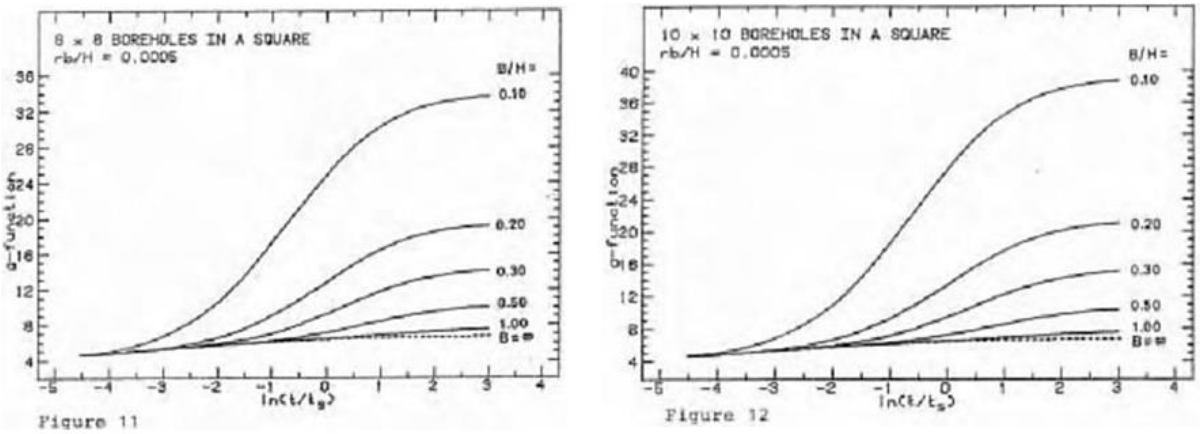

Fig. 2.18 Graphic representation of the g-functions.

The graphs are presented in function of different arrangements of the borehole fields (aligned or square configuration) and represent the following parameters:

- the normalized thermal alteration of ground at the borehole wall (g-function) on the vertical axis:

$$g = 2\pi\lambda_g R_g = \frac{T_b - T_0}{\frac{q}{2\pi\lambda_g}} \tag{2.23}$$

  where λ_g is the ground thermal conductivity ($Wm^{-1}K^{-1}$);

- the logarithm of the normalized time $\ln\left(\frac{t}{t_s}\right)$ on the horizontal axis:

$$t_s = \frac{H^2}{9\alpha} = \frac{H^2 \rho_g c_g}{9\lambda_g} \tag{2.24}$$

where H is the borehole depth and α is the ground thermal diffusivity (m^2s^{-1});

- different curves for each B/H factor, on the basis of the distance between the boreholes and their depth.

In those cases in which the thermal loads are variable, the superposition principle can be implemented. If the load is divided in several steps q_0, q_1, q_2, … q_n which start at different times $t_0 < t_1 < t_2 < \ldots < t_n$, the value of T_b at a certain time t can be expressed as follows:

$$T_b(t) = T_g - q_0 R_g(t - t_0) - (q_1 - q_0) R_g(t - t_1) - \ \ldots - (q_n - q_{n-1}) R_g(t - t_{n-1}) \tag{2.25}$$

2.4.2 EARTH ENERGY DESIGNER SOFTWARE

The Eskilson method was then implemented in the Earth Energy Designer (EED) program: this is a software for vertical BHEs design, based on the g-functions model. It is a useful tool because of its quick calculations times, a short learning curve and an easy-to-use interface, as shown in the *Fig. 2.19* below.

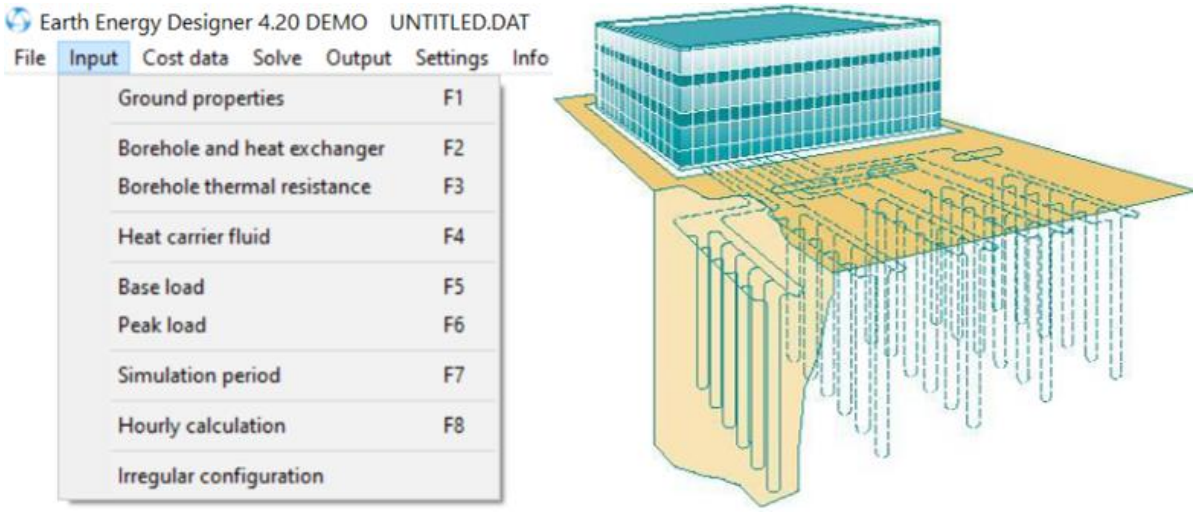

Fig. 2.19 Graphic interface of Earth Energy Designer.

EED is associated with the g-functions and, thus, its numerical simulation model results in analytical solutions for a wide range of geometry configurations. Thermal interferences are given by neighbouring BHEs and depend on their number, depths and spacing: indeed, the g-functions are based on the B/H factor values. The database supplies the necessary boreholes parameters, from the pipes materials to the heat carrier fluids properties.

The software provides typical values for the ground surface temperature and the geothermal heat flux for several locations, while for the ground thermal conductivity and the specific heat capacity, the data files give a range and recommended values for each lithology. In porous media the water content highly affects these properties, thus, a TRT (thermal response test) should always be preferred. Moreover, this program provides the required boreholes size and layout either for small and large geothermal systems. Finally, EED is also able to evaluate the variation of any load for heating, cooling and the domestic hot water with a hourly resolution.

The software input data are the following:

- ground properties;
- borehole parameters and geometry configuration;
- characteristics of the pipes;
- heat carrier fluid properties;
- annual energy and monthly profile for heating and cooling base loads;
- peak heat and cool power and duration;
- simulation period and hourly calculation;
- costs data;
- fluid temperature constraints.

The borehole thermal resistance is calculated based on the arrangement, the filling and the pipes material. In output there is a printed report with graphical processing of the design data: the mean fluid temperatures, the required boreholes length and the costs optimization are provided. In fact, the sizing procedure consists in a trade-off between longer BHEs, which reduce the thermal disturbance and, hence, achieve a better performance, and shorter or less numerous BHEs, which are cheaper. Moreover, to avoid the freezing of the heat carrier fluid, the design must consider the threshold value for the minimum temperature.

2.4.3 CONFIGURATION SETTINGS ON EED

In order to properly design the vertical boreholes heat exchangers, a generic location in Italy was considered. Input data were chosen according to average values for the ground properties and standard geometric parameters for the boreholes arrangement. Regarding the heating base load of the plant, it was implemented the thermal power monthly profile and the average annual energy required by the preheating system object of this thesis work.

The project input data provided to EED for the closed-loop model are summarized below.

Regarding the ground, a saturated sand was considered and its properties are listed in *Tab. 5*.

Tab. 5 Ground properties for a saturated sand.

PROPERTIES	*VALUE*	*U.M.*
Thermal conductivity	2.4	W/(mK)
Volumetric heat capacity	2.5	MJ/(m^{3}K)
Ground surface temperature	14	°C
Geothermal heat flux	0.07	W/m^2

The vertical heat exchangers are arranged in an L array. The boreholes diameter is equal to 130 mm. A double-U configuration was selected: pipes in PE, with a nominal diameter equal to 32 mm, a wall thickness of 3 mm, and thus a SDR (standard dimension ratio between the pipe outside diameter and its thickness) equal to 11. The thermal conductivity of the U-pipes is 0.42 W/(mK). The shank spacing between the two pipes was set to 90 mm, as shown in *Fig. 2.20*. Thermal grout was considered as filling material and its thermal conductivity is equal to 1.47 W/(mK). Concerning the heat carrier fluid, an antifreeze solution must be used and the mono-ethylene glycol at 25% was chosen. The flow rate was set to 1.5 l/s per each borehole. The working fluid properties are summarized in *Tab. 6* below.

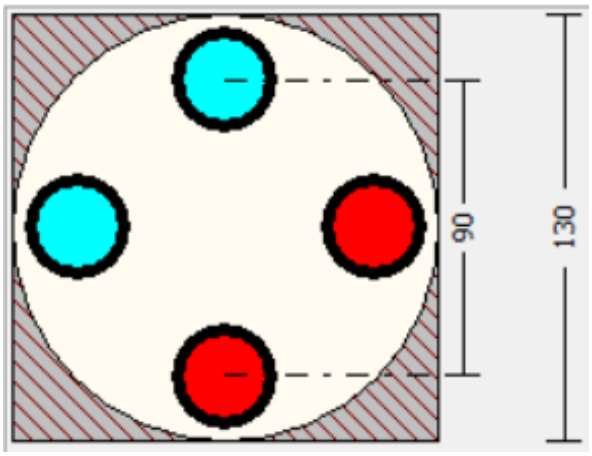

Fig. 2.20 Upward (red) and downward (blue) channels inside the borehole.

Tab. 6 Heat carrier fluid properties.

PROPERTIES	*VALUE*	*U.M.*
Thermal conductivity	0.48	W/(mK)
Specific heat capacity	3.795	kJ/(kgK)
Density	1052	kg/m^3
Viscosity	0.005	kg/(ms)
Freezing point	-14	°C

Finally, according to the fuel consumption for each month of the year 2018, shown in *Fig. 2.21*, the corresponding thermal energy demand E_{th} (kWh) was calculated as follows:

$$E_{th} = m \cdot LHV \cdot \eta \tag{2.26}$$

where m (m^3) represents the monthly amount of gas consumed by the line-heater, LHV is the lower heating value of methane, equal to 9.972 kWh/m^3, and η is the efficiency of the boiler, considered of 80% in order to size the thermal plant in conservative conditions.

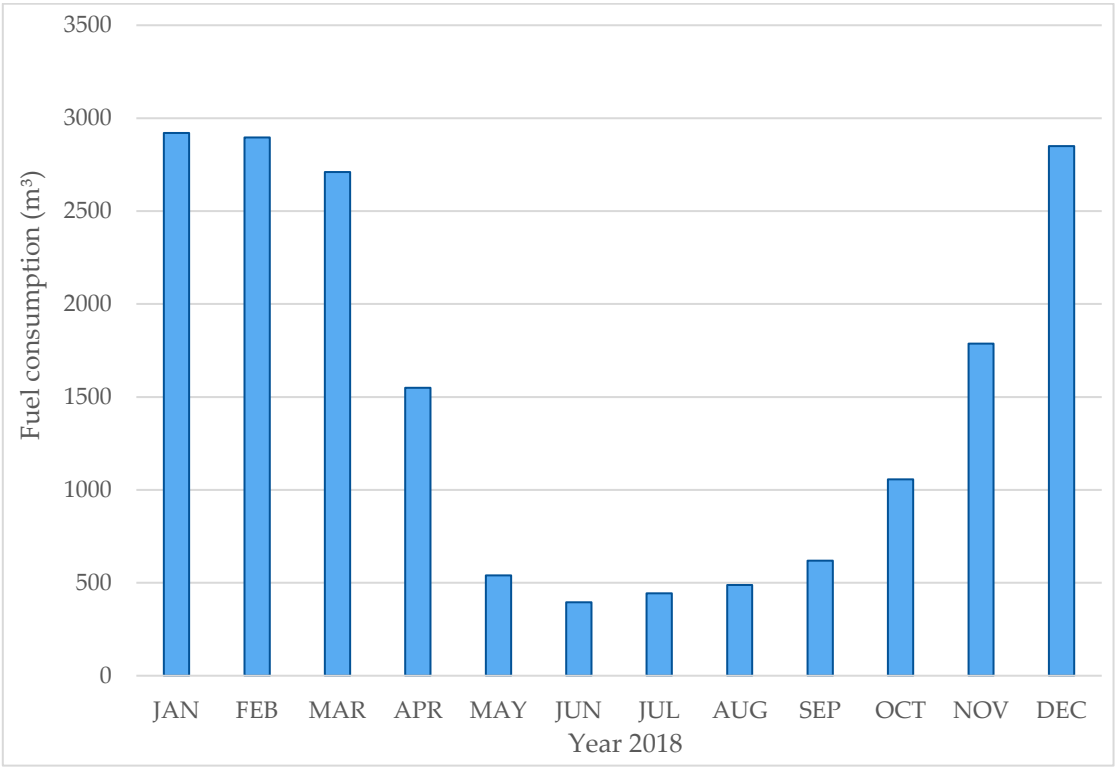

Fig. 2.21 Monthly distribution of the Alba4 plant fuel consumption in 2018.

3 RESULTS AND DISCUSSION

In this section, the results obtained for the different thermal plant configurations are discussed.

First of all, the operational parameters of the conventional preheating system are presented in the *Chapter 3.1*. The total power is evaluated either for the thermal plant and the shell and tube heat exchanger. The overall heat transfer coefficient for the exchanger is calculated, and the temperature distributions of both gas and water streams are defined with the LMTD method.

Chapter 3.2 presents the hydrodynamic properties of the shallow aquifer, interpreted with Aqtesolv, and the hydraulic parameters which are required to design the open-loop system. In this section, also the results obtained with the FEFLOW model are presented and analysed.

Chapter 3.3 is focused on the design of the closed-loop system with vertical boreholes, the EED software provides the optimal configuration for the heating base load of the plant in exam.

Moreover, in *Chapter 3.4* and *Chapter 3.5* the environmental and economical assessments are evaluated: the GHG emissions released by different preheating systems are compared and the geothermal heat pumps pay-back times are calculated.

3.1 THERMAL PLANT OPERATIONAL PARAMETERS

As explained in the *subchapter 2.1.1*, the total power required by the thermal plant is related to the enthalpy difference between upstream and downstream thermodynamic conditions of the natural gas. The specific enthalpy increase resulting from preheating was evaluated with the methane p-h diagram in *Fig. 2.1*. Considering the operating data involved in this process (listed in *Tab. 1*), the thermodynamic states, which correspond to the different gas transformations, are summarized below:

A) $P_1 = 62$ bar and $T_{NG1} = 10$ °C, with a corresponding enthalpy value $h_1 = 72$ kJ/kg;
B) $P_2 = 5$ bar and $T_{NG4} = -20$ °C, with a corresponding enthalpy value $h_1 = 72$ kJ/kg;
C) $P_2 = 5$ bar and $T_{NG3} = 5$ °C, with a corresponding enthalpy value $h_2 = 127$ kJ/kg;
D) $P_1 = 62$ bar and $T_{NG2} = 30$ °C, with a corresponding enthalpy value $h_2 = 127$ kJ/kg.

Thus, the enthalpy difference between initial and final conditions of the natural gas is equal to 55 kJ/kg, which represents the amount of energy to be supplied to preheat the gas stream. Since the gas temperature before expansion must be almost equal to 30 °C it is not possible to perform a "free heating", i.e., with the only shell and tube heat exchanger as line-heater. Indeed, the water inlet temperature at the shell side must exceed the gas outlet temperature.

Therefore, the water flow rate abstracted from the extraction well must be previously warmed up with the designed water-water heat pump.

Once the specific enthalpy value is known, it was possible to calculate the thermal power of the heat exchanger and the total duty of the whole preheating system, evaluated with the following equations:

$$Q_{th} = 0.7\frac{kg}{m^3} \cdot 55\frac{kJ}{kg} \cdot \frac{2230}{3600}\frac{m^3}{s} \cdot \frac{1}{0.9} = 26.5\ kW \tag{3.1}$$

$$P_{th} = 0.7\frac{kg}{m^3} \cdot 55\frac{kJ}{kg} \cdot \frac{2230}{3600}\frac{m^3}{s} \cdot \frac{1}{0.9 \cdot 0.8} = 33.1\ kW \tag{3.2}$$

$$P_{th} = 4.4\frac{m^3}{h} \cdot 9.972\frac{kWh}{m^3} \cdot 0.8 = 35.1\ kW \tag{3.3}$$

This last equation is that related to the fuel consumption of the methane boiler installed in the plant. Then, the thermal power of the heat exchanger was implemented with a safety margin of 1.25, resulting equal to 33 kW. On the other hand, the total thermal duty for the whole preheating system was set equal to 40 kW in conservative assumptions, in order to consider also possible higher peak demands of gas passing through the line.

Concerning the heat exchanger performance analyses, the overall heat transfer coefficient was determined with the sizing procedure and the equations presented in the *subchapter 2.1.2*, and the results are summarized in the *Tab. 7* below. Moreover, in order to design the shell and tube heat exchanger operation, an iterative approach was used to find the appropriate range for the water temperatures at the shell side.

Tab. 7 Performance values of the heat exchanger.

PARAMETER	***CH_4***	***H_2O***	***U.M.***
Prandtl number	0.83	4.62	-
Reynolds number	$7.4 \cdot 10^4$	$3.3 \cdot 10^4$	-
Nusselt number	168	275	-
Convection coefficient	315	8635	W/(m²K)
Heat transfer coefficient	304		W/(m²K)

As can be seen from the Reynolds numbers, both the flows into the pipes and the shell are characterized by turbulence conditions. The water convection coefficient is much larger than the methane one, thus the definition of the overall heat transfer coefficient was dominated by the convection coefficient of the gaseous fluid stream.

Then, the inlet and outlet temperatures of water at the shell side were calculated using the LMTD method. The log mean temperature difference was evaluated as follows:

$$\Delta T_{lm} = \frac{Q_{th}}{U \cdot A} = \frac{33 \cdot 10^3\ W}{304 \frac{W}{m^2 K} \cdot 6.746\ m^2} = 16\ K \tag{3.4}$$

The shell and tube heat exchanger was designed with the counter flow configuration: indeed, the temperature differences between the two opposite endpoints were assessed equal to 10 °C for the hotter side (ΔT_1) and almost 24 °C for the colder one (ΔT_2). These values were calculated with an iterative process, considering a temperature difference of about 6 °C for the water stream at the shell side. Therefore, knowing the initial and final gas temperatures (T_{NG1} and T_{NG2}) at the tubes side, the inlet water temperature value, which must be supplied by the heat pump, is equal to 40 °C, whereas the outlet one resulted in almost 34 °C.

3.2 OPEN-LOOP SYSTEM EVALUATION

In order to study the hydrodynamic properties of the shallow aquifer, the experimental data resulting from the pumping test were interpreted with the software Aqtesolv. The Theis solution was implemented via a type curve matching method, as shown in *Fig. 3.1*, which represents a log-log graph of time versus drawdown. As represented in the graph, the curve did not reach a well-defined stabilization. However, this interpretation method provided the required values for the transmissivity and the storage coefficient, or specific yield, equal to 0.017 m²/s and 0.156, respectively. Once the transmissivity is known, it was possible to calculate the aquifer hydraulic conductivity, expressed as follows:

$$K = \frac{T}{b} = \frac{0.017 \frac{m^2}{s}}{3.5\ m} = 4.91 \cdot 10^{-3} \frac{m}{s} \tag{3.5}$$

Using the results of the single-well pumping test, it was also possible to evaluate the specific capacity of the well and thus its productivity, which is quite similar to the transmissivity value:

$$q_{sp} = \frac{Q}{s} = \frac{4.8 \cdot 10^{-3} \frac{m^3}{s}}{0.22\ m} = 0.022 \frac{m^2}{s} \tag{3.6}$$

The aquifer transmissivity value is very high, thus, it could be confirmed that the well productivity and the aquifer performance are excellent; also considering that the water table is quite shallow and the unconfined aquifer has a reduced saturated thickness. In this case, most probably, the anthropic activity has significantly contributed to feed the groundwater flow: in fact, the irrigation network supplies large water discharges through its several channels across the neighboring fields.

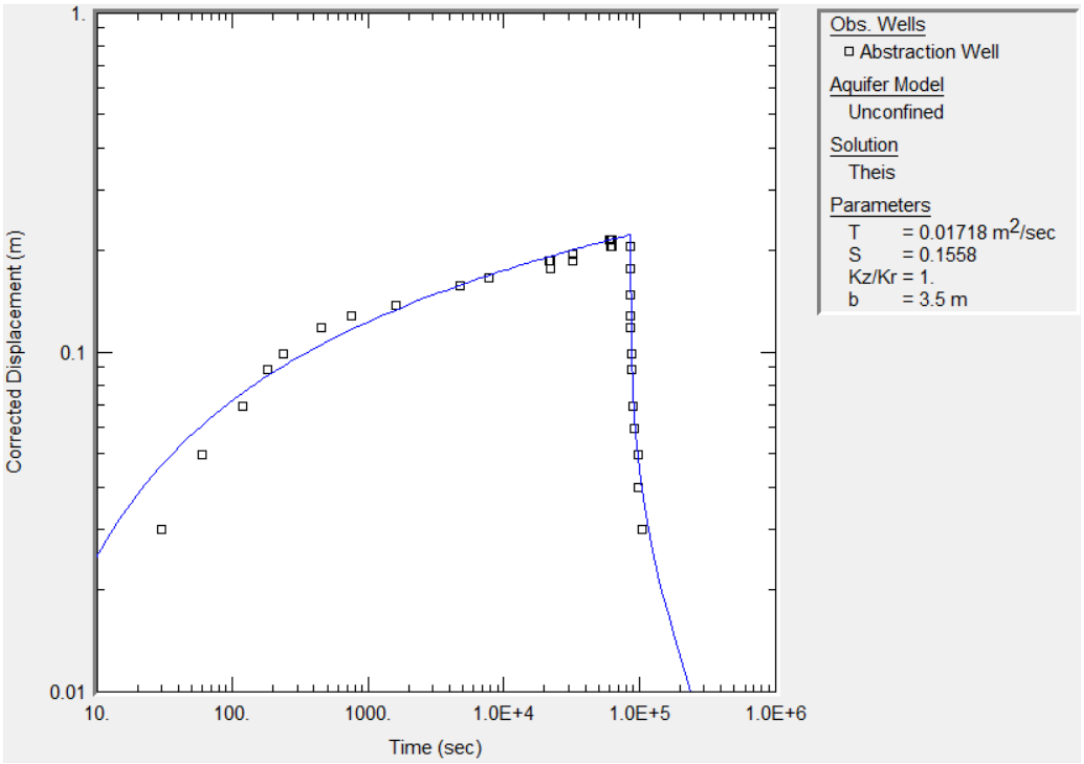

Fig. 3.1 Aquifer diagnostic curve interpretated with Aqtesolv.

As it is shown in the *Fig. 2.5*, the site is located between the equipotential line corresponding to hydraulic heads of 145 m and the line which connects points with hydraulic heads equal to 140 m. The distance between these two imaginary lines is approximately equal to 1800 meters. Therefore, it was possible to determine the hydraulic gradient which is about 3‰. The properties of the shallow aquifer are summarized in the *Tab. 8* below.

In accordance with the results of the single-well pumping test, the open-loop configuration was designed with a pumped rate equal to 5 l/s. The temperature difference between the extraction and the injection wells can be expressed as follows:

$$\Delta T = \frac{P_{th}}{Q \cdot \rho_w c_w} = \frac{40\ kW}{\frac{5 \cdot 3600}{1000}\frac{m^3}{h} \cdot 1.167\frac{kWh}{°C\ m^3}} = 2\ °C \tag{3.7}$$

This thermal alteration, induced in the aquifer, complies with technical regulations, which require a maximum variation for the water temperature of $\pm 7\ °C$.

Moreover, in order to avoid the recycling of the cold plume, the minimum distance between the abstraction well and the reinjection one must be equal to the following length:

$$L = \frac{2Q}{\pi T i} = \frac{2 \cdot 5 \cdot 10^{-3}\frac{m^3}{s}}{\pi \cdot 0.017\frac{m^2}{s} \cdot 2.8 \cdot 10^{-3}} \cong 67\ m \tag{3.8}$$

However, the supply well is already present near the pressure reduction station, and its position may not be changed. Concerning the recharge well, it will be drilled in the property of the Alba4 plant, thus, the designed distance between the two wells is fixed at approximately 90 meters. This length will ensure that a null share of the reinjected flow rate will be recycled.

Tab. 8 Hydrodynamic properties of the aquifer.

PROPERTIES	*VALUE*	*U.M.*
Transmissivity	$1.72 \cdot 10^{-2}$	m^2/s
Storage capacity	$1.56 \cdot 10^{-1}$	-
Hydraulic conductivity	$4.91 \cdot 10^{-3}$	m/s
Specific capacity	$2.18 \cdot 10^{-2}$	m^2/s
Hydraulic gradient	$2.78 \cdot 10^{-3}$	-

All the parameters presented above were then implemented in the FEFLOW model described in *Chapter 2.3.2*, in order to verify the correct operation of the designed open-loop system. The simulation time was set to 20 years and the thermal plant was assumed to work with a constant power of 40 kW and pumping flow rates equal to 5 l/s and -5 l/s for the extraction and the reinjection wells, respectively. The numerical simulation of groundwater flow and heat transport provided the temperatures over time at the two wells points, which are represented in the graph in *Fig. 3.2*, and the distribution of the thermal plume after 20 years of operation, as shown in the *Fig. 3.3*. The aquifer temperature was of 14 °C, whereas the reinjected water temperature was initially at 12 °C and, subsequently, gets colder and colder. In fact, during the system operation, the temperature of the abstracted flow rate decreases due to the cold plume propagation. In particular, the temperature of the supply water decreases of about 1 °C in the first three years of operation and, then, remains quite constant in the range of 13.5-12.5 °C in next years. Obviously the recharge water temperature undergoes to the same trend, but it is 2 °C lower, because of the constant temperature change imposed by the groundwater heat pump. The temperature variations, caused by the reinjected water flow rates, are not so high and the resulting cold plume extension is limited and towards the groundwater flow direction, thus, the extraction well is not affected by hydraulic and thermal recycling phenomena, as can be seen in the *Fig. 3.4* below.

This shallow open-loop configuration seems to be a good and sustainable solution in order to replace the conventional preheating system of the Alba4 plant. However, the hydrological framework should be analysed more in detail: in particular, the piezometric levels should be monitored over time and also other wells near the site should be investigated, in order to properly evaluate the aquifer hydraulic heads and the groundwater flow direction.

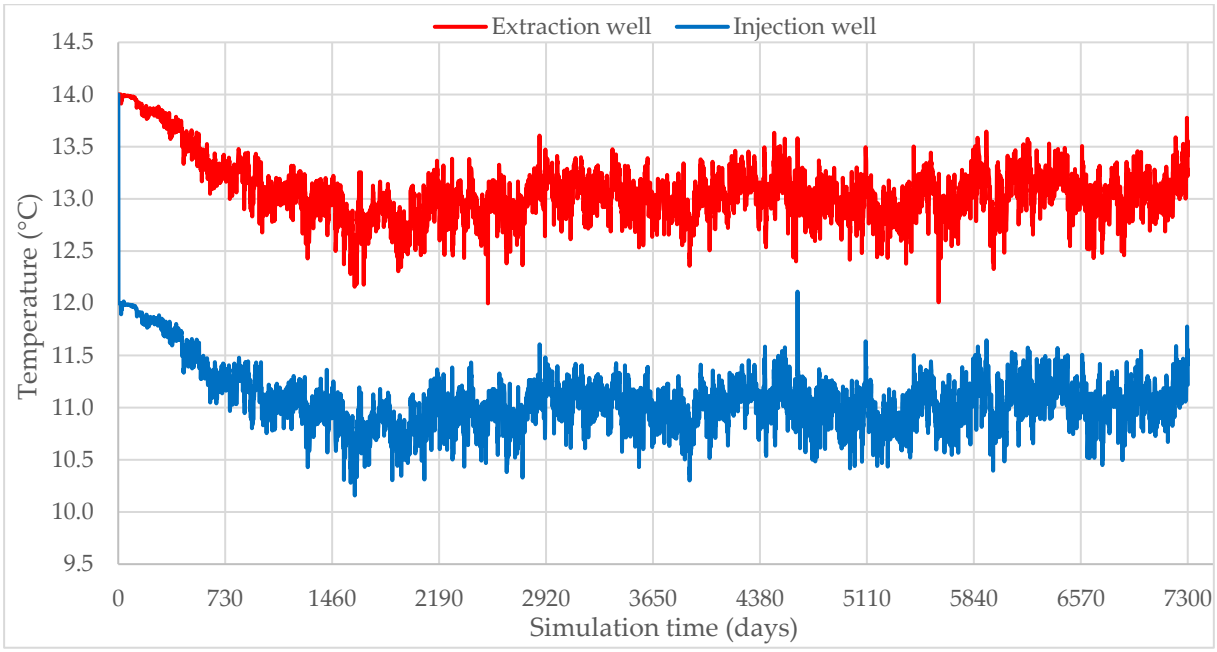

Fig. 3.2 Temporal distributions of the wells temperatures during 20 years of operation.

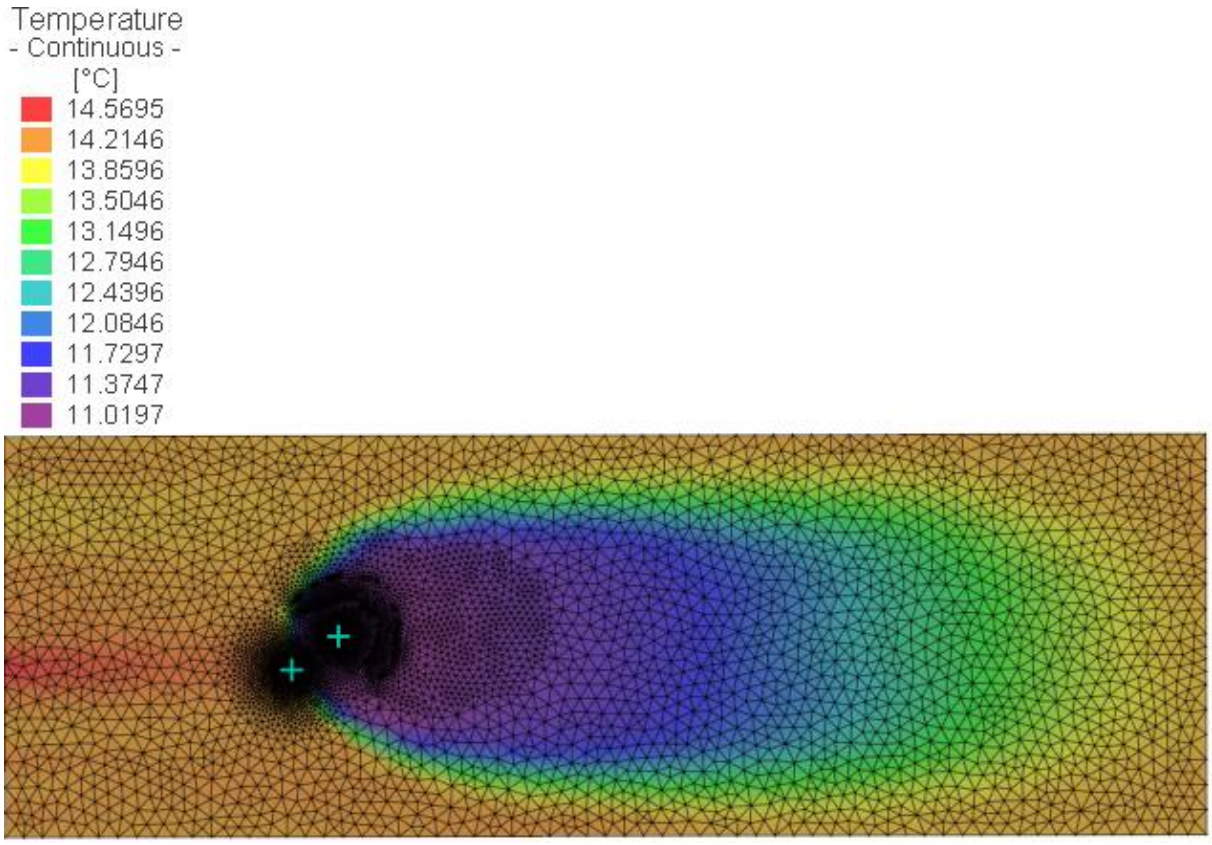

Fig. 3.3 The resulting extension of the thermal plume at the end of the simulation.

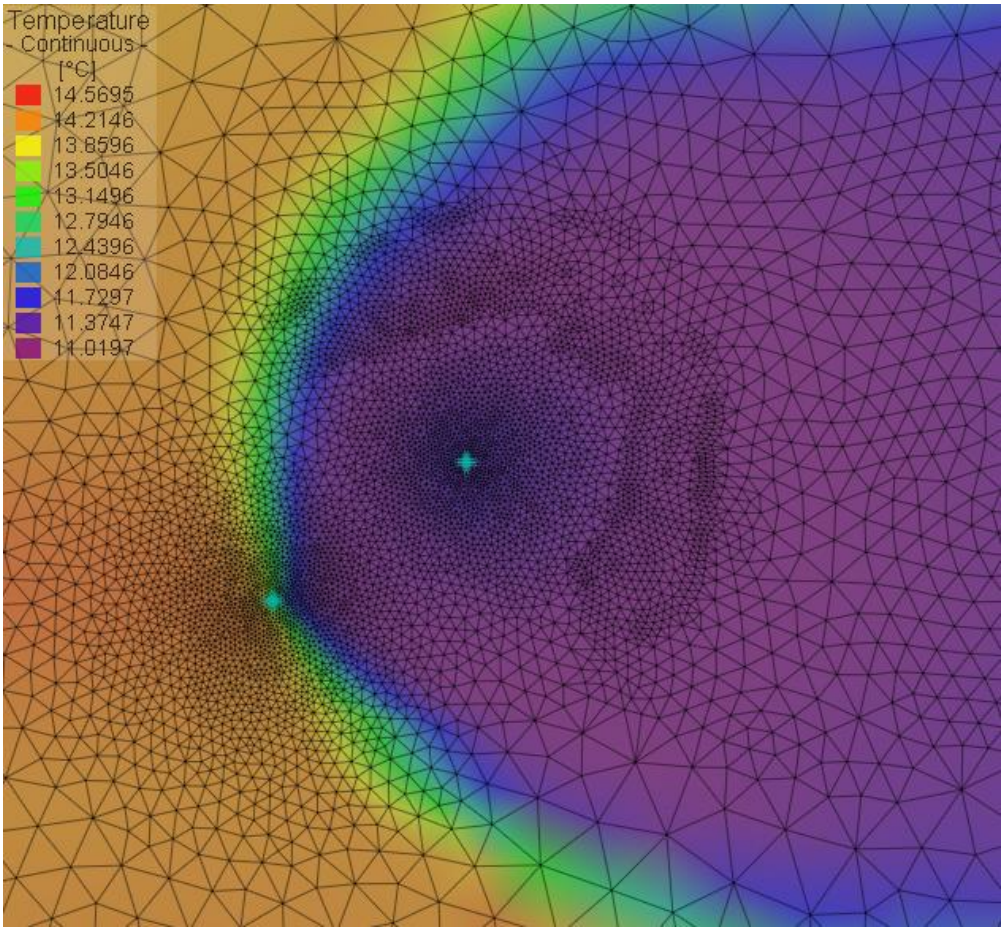

Fig. 3.4 Zoom on the temperature distribution at the two wells points after 20 years.

3.3 CLOSED-LOOP SYSTEM EVALUATION

The design of the closed-loop preheating system was performed with the EED software which provided the proper geothermal configuration for a simulation time of 20 years. The resulting L array consists in 4 vertical ground heat exchangers with 2x3 arrangement. The spacing between each borehole is of 15 m and their depth is about 127 m.

The BHEs thermal resistances were calculated, considering the internal heat transfer between upward and downward channels, and the resulting effective resistance is of 0.05 mK/W.

Based on monthly average values of fuel consumption in 2018, shown in *Fig. 2.21*, it was possible to calculate the heating base load of the Alba4 station. The total annual energy required by the thermal plant is about 146 MWh_{th}, and the EED software divided it into two parts: the heat extracted from the ground is about 3/4, equal to approximately 109.5 MWh_{th}, while the thermal energy demand provided by the heat pump is the remaining 1/4, about 36.5 MWh_{th}. This is due to the heat pump SPF (Seasonal Performance Factor) which was set to 4, equal to the COP, because in this case the heat pump operation is always in heating mode.

According to the plant heating base load, which is represented in *Fig. 3.5* below, the maximum specific heat extraction rate is of about 47 W/m in January, while the minimum value occurred in June and is equal to 6.4 W/m. The thermal energy demand is very low during the warmer months of the year: this cyclical load helps the geothermal system to operate over long time.

In the graph in *Fig. 3.6* are represented the mean temperatures of the heat carrier fluid during 20 years of operation. At the end of this period, the maximum value is 7.24 °C in August, while the minimum one occurs in February and is equal to -5 °C, which is the minimum constraint imposed for the fluid temperature. The temperature variations of the heat transfer fluid are an important parameter to evaluate because the geothermal heat pump efficiency is affected by the source side (ground loop) temperature.

The heat amount absorbed by vertical BHEs is highly related to the soil thermal properties. Since these parameters are constant over time and the power exchanged by the preheating system is fixed, the working fluid temperature decreases every year because the ground heat is always extracted and no part of it is then reinjected. The ground heat balance gets colder and also the total annual thermal energy abstracted with vertical BHEs has a descending behaviour over time. The heat pump needs more electricity and, hence, the performance of the closed-loop system are higher in the first years of operation.

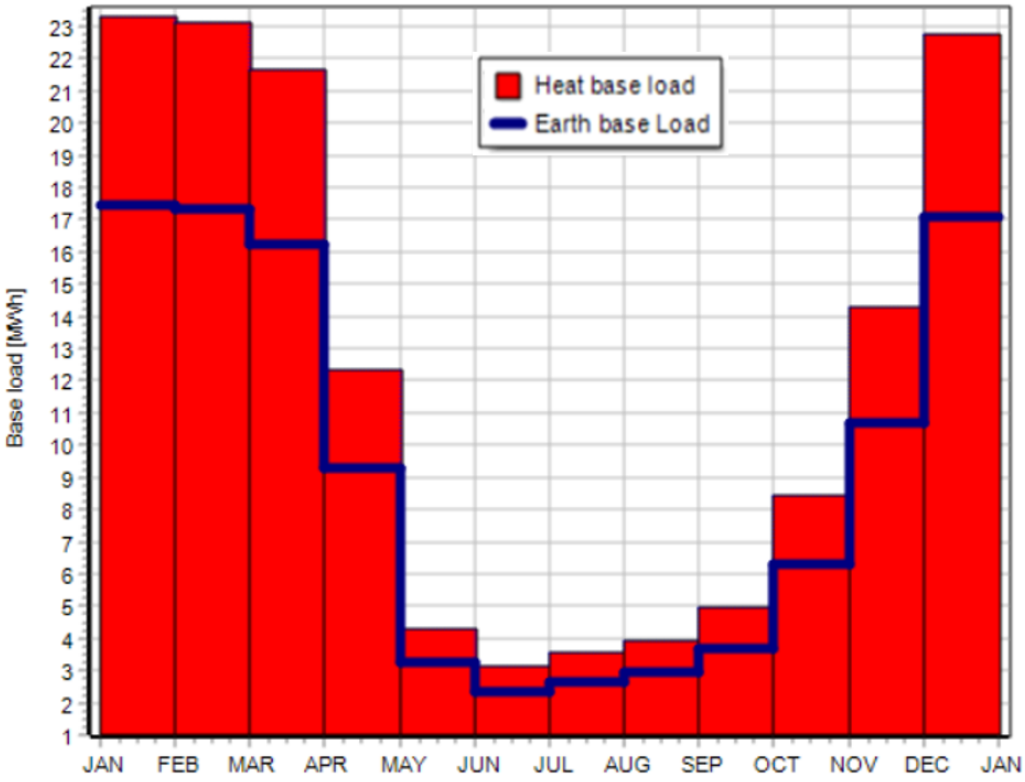

Fig. 3.5 Heating monthly base load for the 2018.

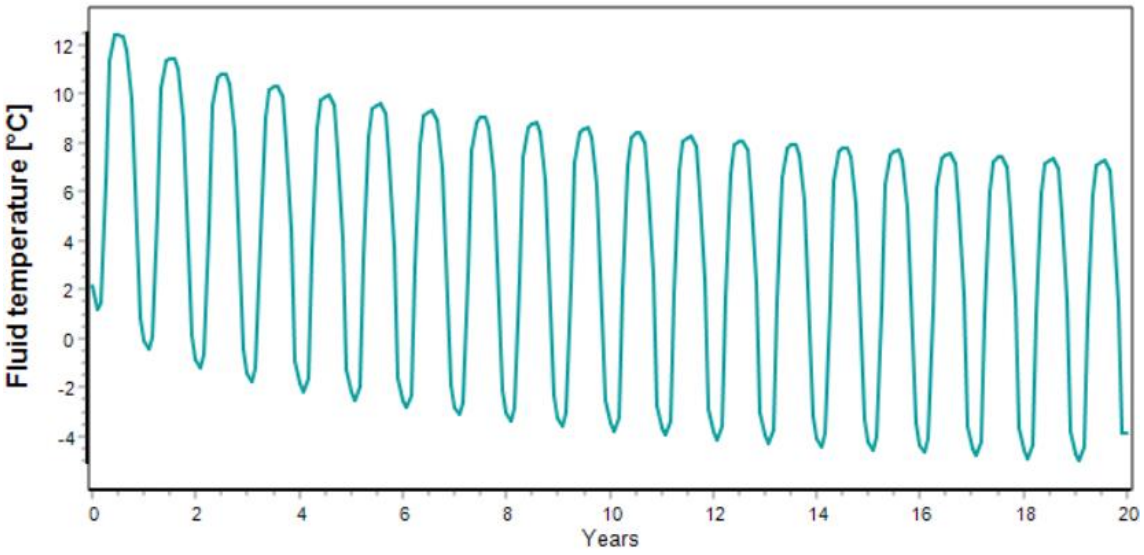

Fig. 3.6 Mean temperatures of the heat carrier fluid during 20 years of system operation.

3.4 ENVIRONMENTAL ASSESSMENT

The environmental assessment for the pressure reduction station was carried out considering the amount of greenhouse gases emissions released into the atmosphere by the preheating system. Production and dispersion of air pollutants are important aspects to consider in order to evaluate the sustainability of the plant. Replacing conventional fossil fuels-based boilers with renewable energy resource systems can lead to a substantial reduction of NO_x, PM2.5, PM10 and CO_2 emissions. The latter is the main GHG, cause of global warming and climate change, thus, the GHGs emission factor was calculated as the equivalent amount of CO_2 produced per unit of thermal energy (gCO_2eq/kWh). For fossil fuels, the GHG emission factor depends on their supply chain, the gas leakages during extraction and transportation (e.g., methane leakages from pipelines), the combustion reaction and the efficiency of the burners. Reference values for the emission factor of gas-fired boilers can be assumed in the range of 200-240 gCO_2eq/kWh_{th}.

Concerning heat pumps, the emission factor of GSHP systems (EF_{HP}) was defined as follows:

$$EF_{HP} = \frac{EF_{el}}{COP} \tag{3.9}$$

where COP is the heat pump efficiency for the heating mode, whereas EF_{el} (gCO_2eq/kWh_{el}) is the emission factor of the electrical energy. In fact, heat pumps do not release pollutants on site, since electricity is the only energy source required for their operation. In order to evaluate their GHG emission factors, it is necessary to consider the amount of electrical energy produced with fossil fuels in thermal power plants. As a consequence, the heat pump emission factors decrease with the increasing share of electricity coming from renewable energies.

In the next steps, the GHG emission factors were assumed equal to 240 and 270 gCO_2eq/kWh (*from [29]*) for the line-heater and the electrical energy, respectively. As stated in the previous sections, the gas boiler efficiency was considered of 80%, while the lower heating value of methane is 9.972 kWh/m^3. The average COP were set equal to 4.8 and 4 for the open-loop and the closed-loop geothermal systems, respectively. Regarding the annual thermal energy required by the plant, it was considered the monthly distribution of fuel consumption in 2018, represented in *Fig. 2.21*. The electrical energy needed by the groundwater and the ground-coupled heat pumps was calculated and the results are summarized in *Tab. 9*. The amount of CO_2 released by the gas-fired line-heater was compared with that produced by the two geothermal plant configurations. The resulting annual GHG emissions are of about 35 tCO_2 equivalent for the methane boiler and about 8.2 and 9.8 tCO_2 equivalent for the groundwater heat pump and the vertical boreholes, respectively. Therefore, the average annual reduction of pollutant emissions is approximately 76% using the open-loop system and about 72% with the closed-loop one. The mean distribution of the CO_2 produced in each month of the year is shown in the graph in *Fig. 3.7* below.

Tab. 9 Annual electrical energy required by geothermal heat pumps.

Year	m^3	kWh_{th}	kWh_{el} GWHP	kWh_{el} GCHP
Jan	2920	23294.59	4853.04	5823.65
Feb	2897	23111.11	4814.81	5777.78
Mar	2711	21627.27	4505.68	5406.82
Apr	1549	12357.30	2574.44	3089.33
May	540	4307.90	897.48	1076.98
Jun	396	3159.13	658.15	789.78
Jul	443	3534.08	736.27	883.52
Aug	489	3901.05	812.72	975.26
Sep	620	4946.11	1030.44	1236.53
Oct	1056	8424.35	1755.07	2106.09
Nov	1787	14255.97	2969.99	3563.99
Dec	2850	22736.16	4736.70	5684.04
TOTAL	18,258	145,655	30,345	36,414

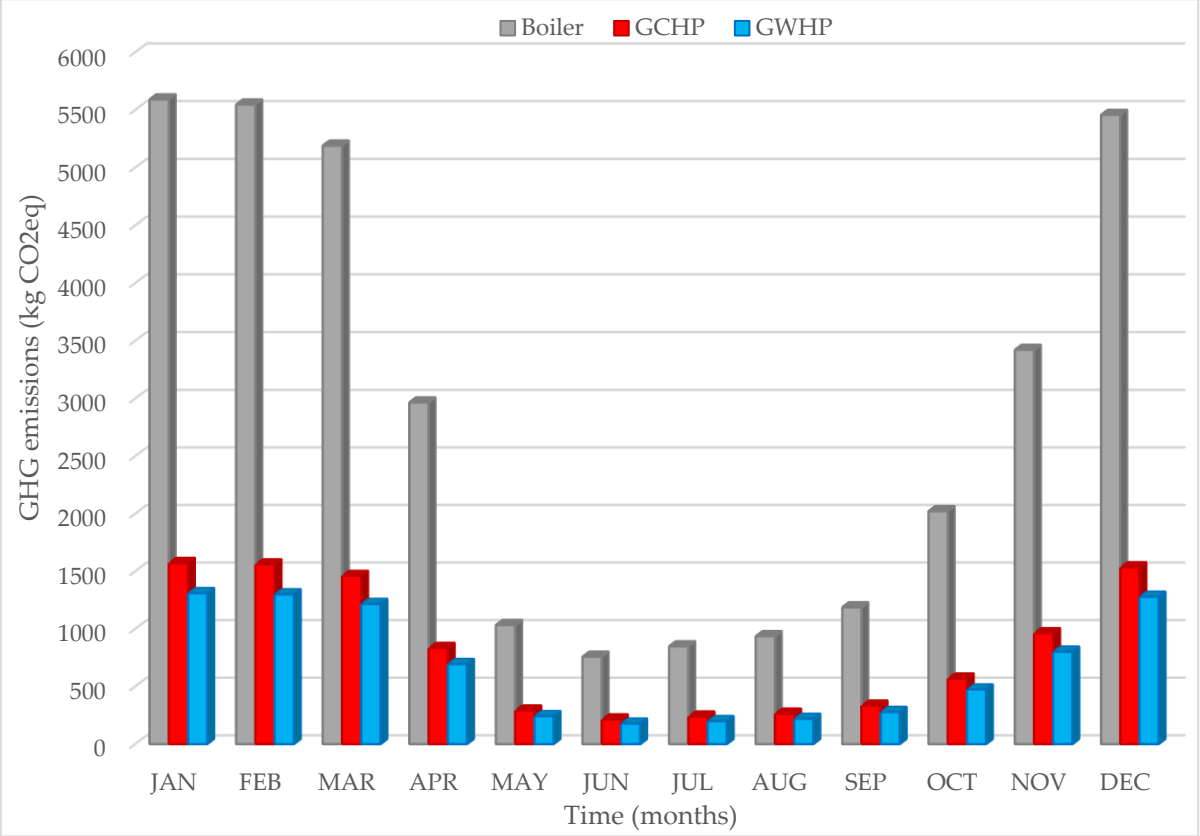

Fig. 3.7 Average monthly distribution of CO_2 emissions released by different systems.

3.5 ECONOMIC ASSESSMENT

In order to evaluate the possibility of use different preheating configurations, the economic assessment was analysed. The costs related to the amount of gas burned by the line-heater were compared to the heat pumps electricity consumption of the two geothermal systems. The thermal plant of the Alba4 pressure reduction station has an average fuel consumption (m) of about 18260 m^3 per year. In order to evaluate and compare the costs associated with this very old item, the boiler efficiency was assumed about 70% in the next steps. Considering the methane lower heating value equal to 9.972 kWh/m^3, as previously stated, the annual heating need (E_{th}) is about 130 MWh_{th}.

The other parameters required for the economic assessment were assumed as follows:

- average COP for the open-loop system equal to 4.8;
- average COP for the closed-loop system equal to 4;
- electricity cost (C_{el}) for non-household consumers equal to 0.221 €/kWh (*from [30]*);
- cost of natural gas (C_{gas}) for industrial consumers equal to 0.762 €/m^3 (*from [31]*).

The yearly operation costs of the gas line-heater (Co_{gas}) were expressed in relation to the annual fuel consumption:

$$Co_{gas} = m \cdot C_{gas} \tag{3.10}$$

whereas the methane boiler unit cost (Cu_{gas}) was calculated as the ratio between operational costs and the heating need:

$$Cu_{gas} = \frac{Co_{gas}}{E_{th}} \tag{3.11}$$

On the other hand, the heat pumps unit costs (Cu_{HP}) were defined as the ratio between the cost of electrical energy and the seasonal performance factor:

$$Cu_{HP} = \frac{C_{el}}{COP} \tag{3.12}$$

while the annual operation costs (Co_{HP}) were evaluated as follows:

$$Co_{HP} = Cu_{HP} \cdot E_{th} \tag{3.13}$$

The results concerning unit costs and yearly operational costs for both fossil fuel-based and geothermal systems are summarized in the *Tab. 10* below.

The unit costs of the groundwater and the ground-coupled heat pumps are respectively -57% and -48% compared to the unit cost of the methane boiler. Moreover, there are substantial annual operation savings with ground source heat pumps, compared to the gas-fired heater: about 7900 and 6700 € per year using the groundwater and the ground-coupled heat pump, respectively.

Tab. 10 Unit and operational costs for the different systems.

COST		***VALUE***	***U.M.***
Unit	GAS	107	€/MWh$_{th}$
	GWHP	46	€/MWh$_{el}$
	GCHP	55	€/MWh$_{el}$
Operation	GAS	13900	€/year
	GWHP	6000	€/year
	GCHP	7200	€/year

In order to evaluate the feasibility of the projects, the pay-back periods (PBP) for the proposed geothermal configurations were calculated according to the investment costs of the systems. The total initial capital consists in the cost of heat pumps, installation, drilling and the design.

The price of the water-water heat pump is the same for both the GWHP and the GCHP and was set as follows (*from [32]*):

$$Price_{HP} = 5000 + 300 \cdot P_{th} = 17000\ € \tag{3.14}$$

where P_{th} is the peak thermal power of the preheating system, equal to 40 kW, as stated in the previous sections.

Installation costs include all the machineries and materials used for the installing works of shallow geothermal systems. In fact, the drilling equipment must be transported and placed at the construction site. This investment cost share also includes hydraulic flow tests and the monitoring performed in the boreholes, in order to analyse the hydro-chemical properties of water and the hydrogeological parameters of soil. The installation costs were assessed of about 18000 € for the open-loop system and about 15000 € for the closed-loop configuration.

Drilling costs are one of the main share of the initial investment, especially for deep boreholes. In order to compare the two shallow geothermal systems, a new well-doublet was considered for the open-loop plant, while the BHEs arrangement is the same previously presented. Thus, the extraction and the reinjection wells were assumed to be about 10 m deep each, with large diameters in order to avoid their obstruction over long time operation. As explained in the introduction, percussion is the most effective technique for large-diameter wells at small depths, so, it was chosen for the drilling of the two wells. The drilling cost for nominal diameters of 1200 mm was set equal to 650 €/m (*from [33]*), hence, resulting in an overall cost of 13000 € for the open-loop configuration. On the other hand, the four vertical boreholes of the closed-loop system have a depth of about 127 m. The drilling cost was set to 55 €/m (*from [33]*), so, their total cost is about 28000 €.

Lastly, the cost for the plants design was set equal to 20% of the installation and drilling costs, thus resulting in 6200 € for the well-doublet and about 8600 € for the BHEs configuration.

In conclusion, the total investment costs are equal to 54200 € for the shallow open-loop and about 68500 € for the closed-loop geothermal system. The corresponding PBPs were evaluated equal to approximately 6.8 and 10.2 years respectively, which are acceptable times if we consider a period of almost 20 years for the plant operation.

4 CONCLUSION

This work assessed the techno-economic feasibility and the benefits of replacing gas boilers with shallow geothermal energy systems in a gas pressure reduction station (PRS). As explained in the thesis, all gas PRSs must have a preheating system to avoid the icing of gas after its expansion. However, the uses of gas boilers to perform this task results in higher costs, higher GHG emissions, and the risk of fires and explosions.

Natural gas is expanded in PRSs, passing from high-pressure (about 60 bar) to low-pressure values (almost 5 bar), before being delivered to the end-users. As a consequence, a temperature drop, directly proportional to the reduction of pressure in the throttling valve, occurs between the upstream and the downstream. If the natural gas temperature decreases below 0 °C, hydrates condensation appears and could damage pipelines. Therefore, the gas stream must be preheated before the expansion process: the required temperature outgoing the pressure regulator must be almost equal to 5 °C. This minimum value is strongly related to the initial pressure and temperature of the gas, which depend on the local climatic conditions and, thus, are variable throughout the year.

The case study of the Alba4 REMI plant, located in Magliano Alfieri (NW Italy) and managed by the local utility EGEA, was analysed. In order to size the preheating system, average annual values for the gas flow rate, pressure, and temperature at the PRS inlet were considered. The average fuel consumption of the methane boiler is of almost 18500 m^3 per year. The annual heating need and peak thermal power are of approximately 150 MWh_{th} and 40 kW, considering a line-heater efficiency at 80%, in conservative assumption. This sizing procedure, implemented with a safety margin, allows to consider also possible higher gas demands during the system operation. A detailed calculation was performed considering the actual volume of gas treated and the thermodynamic characteristics of natural gas (p-h diagram).

The heat transfer to the natural gas before expansion is performed with a specifically designed shell and tube heat exchanger. The calculations performed with the LMTD method provided, as a result, inlet and outlet temperatures of 40 °C and 34 °C for the hot stream (i.e., technical water from the boiler or, in the future, the heat pump) and of 10 °C and 30 °C for the cold stream (i.e., the natural gas to be preheated). These operating temperatures are suitable for a geothermal heat pump.

However, since the average temperature of the local shallow aquifer is about 14 °C, it is not possible perform a direct heat exchange between the well loop and the gas. This option would have led to virtually zero energy demand for the preheating system, that is, only the energy for pumping from well would have been needed.

A groundwater heat pump (GWHP) was proposed to replace the old boiler. A single-well pumping test was interpreted with the software Aqtesolv and provided the hydrodynamic properties needed to design the open-loop system. The unconfined aquifer has a high transmissivity ($1.7 \cdot 10^{-2}$ m^2/s) and the hydraulic conductivity is approximately equal to $5 \cdot 10^{-3}$ m/s. A numerical model was implemented with the software FEFLOW, to simulate groundwater flow and heat transport occurring during the operation of the geothermal system. The flow rate was set to 5 l/s and the thermal power exchanged by the groundwater heat pump (40 kW) was assumed constant throughout the operation time. A very limited thermal and hydraulic impact was observed, with no thermal recycling.

The study also considered a ground-coupled heat pump (GCHP) to assess the techno-economic feasibility in the absence of a productive aquifer. With the monthly heating base load related to the thermal plant consumption, the sizing was performed with the software Earth Energy Designer (EED), resulting in an optimal configuration of four vertical boreholes heat exchangers, of 127 m each.

The GWHP and the GCHP allow to achieve an annual reduction of CO_2 of about 76% and 72%, respectively, compared to the amount of pollutant emissions released by the gas-fired line-heater. As for the economic feasibility, based on the estimation of installation and operational costs of all options, pay-back times of about 7 and 10 years were found, respectively, for the GWHP and the GCHP compared to the currently used gas boiler.

Therefore, as demonstrated in this thesis, shallow geothermal energy systems have a great potential to improve the sustainability of the gas network.

GLOSSARY

List of acronyms

BHE: Borehole Heat Exchanger
CNG: Compressed Natural Gas
COP: Coefficient Of Performance
EED: Earth Energy Designer
EER: Energy Efficiency Ratio
EF: Emission Factor
GCHP: Ground Coupled Heat Pump
GHG: Green House Gas
GSHP: Ground Source Heat Pump
GWHP: Ground Water Heat Pump
LHV: Lower Heating Value
LMTD: Log Mean Temperature Difference
LNG: Liquefied Natural Gas
PBP: Pay-Back Period
PRS: Pressure Reduction Station
REMI: "REgolazione e MIsura"
RES: Renewable Energy Source
SPF: Seasonal Performance Factor

List of symbols: Latin letters

A: Heating surface of the heat exchanger, m^2
b: Saturated thickness of the aquifer, m
c: Heat convection coefficient, $Wm^{-2}K^{-1}$
c_p: Specific heat, J $kg^{-1}K^{-1}$
Co: Operational cost, €/y
Cu: Unit cost, €/MWh
d: Diameter of the exchanger tubes, m
E_{th}: Heating need of the thermal plant, kWh
g: g-function of the boreholes
$\dot{G}_{max}$: Maximum gas flow rate, m^3s^{-1}
h: Specific enthalpy, J kg^{-1}
i: Hydraulic gradient
k: Thermal conductivity of the fluids, $Wm^{-1}K^{-1}$
K: Hydraulic conductivity, m s^{-1}
L: Minimum distance of the wells, m
L_T: Length of the exchanger tubes, m
m: Fuel consumption of the boiler, m^3
$\dot{m}$: Maximum methane flow rate, m^3s^{-1}
n_e: Effective porosity
N: Number of the exchanger tubes
Nu: Nusselt number
P: Pressure of the natural gas, bar
P_{th}: Power of the thermal plant, W
Pr: Prandtl number
Q: Water flow rate, m^3s^{-1}
Q_{th}: Thermal power of the exchanger, W
q: Generic heat flux, Wm^{-1}
q_{sp}: Specific capacity of the well, m^2s^{-1}
R: Generic thermal resistance, m K W^{-1}
Re: Reynolds number
s: Drawdown of the piezometric level, m
S: Storage capacity
S_T: Pitch of the exchanger tubes, m
T: Hydraulic transmissivity, m^2s^{-1}
T_{lm}: Log mean temperature difference, K
T_{NG}: Temperature of the natural gas, K
v: Flow velocity of the fluids, m s^{-1}
U: Overall heat transfer coefficient, $Wm^{-2}K^{-1}$

List of symbols: Greek letters

η_{boiler}: Efficiency of the methane boiler
η_{HE}: Efficiency of the heat exchanger
λ: Thermal conductivity of solids, $Wm^{-1}K^{-1}$
μ: Dynamic viscosity of the fluids, kg $m^{-1}s^{-1}$
μ_{JT}: Joule-Thomson coefficient, °C Pa^{-1}
ρ: Density of the fluids, kg m^{-3}

REFERENCES

[1] European Commission. Joint Research Centre. Institute for Environment and Sustainability e European Technology Platform on Renewable Heating and Cooling, *2020-2030-2050, common vision for the renewable heating and cooling sector in Europe*. LU: Publications Office, 2011.

[2] D. Banks, *An introduction to thermogeology: ground source heating and cooling*, 2nd ed. Hoboken, NJ: John Wiley & Sons, Ltd, 2012.

[3] «Water2Energy-References». http://www.veoliawater2energy.com/en/references/heat-pumps/ (consulted feb. 03, 2021).

[4] «Evaporators and condensers: counter-current or co-current arrangement?», *UNILAB - Heat Transfer Software*, 2019. https://www.unilab.eu/articles/technical-articles/thermodynamic-engineering-articles/counter-current-co-current-arrangement/ (consulted feb. 04, 2021).

[5] «How to decide whether the given shell and tube heat exchanger is a counter flow or parallel flow - Quora». https://www.quora.com/How-do-I-decide-whether-the-given-shell-and-tube-heat-exchanger-is-a-counter-flow-or-parallel-flow/ (consulted feb. 04, 2021).

[6] «Basics of Shell & Tube Heat Exchangers», *Arveng Training & Engineering*, ott. 10, 2015. https://arvengtraining.com/en/basics-of-shell-tube-heat-exchangers/ (consulted feb. 04, 2021).

[7] Casasso e Sethi, «Groundwater-Related Issues of Ground Source Heat Pump (GSHP) Systems: Assessment, Good Practices and Proposals from the European Experience», *Water*, vol. 11, n. 8, pag. 1573, lug. 2019, doi: 10.3390/w11081573.

[8] H.-J. G. Diersch, *FEFLOW*. Berlin, Heidelberg: Springer Berlin Heidelberg, 2014.

[9] B. Misstear, D. Banks, e L. Clark, *Water Wells and Boreholes*. Chichester, UK: John Wiley & Sons, Ltd, 2017.

[10] «Natural Gas Information – Analysis», *IEA*. https://www.iea.org/reports/natural-gas-information-overview/ (consulted feb. 12, 2021).

[11] «Le infrastrutture di Snam». https://www.snam.it/it/chi-siamo/infrastrutture-snam/ (consulted feb. 15, 2021).

[12] «La rete di trasporto». https://www.snam.it/it/chi-siamo/infrastrutture-snam/trasporto/ (consulted feb. 15, 2021).

[13] «Impianti RE-MI e GRF: Progettazione - Conduzione - Manutenzione», *Blog della IN.CO. Edile Soc. Coop.*, apr. 13, 2015. http://incoedile.altervista.org/blog/impianti-remi-e-grf-progettazione-conduzione-manutenzione/ (consulted feb. 16, 2021).

[14] «Architettura del sistema». http://www.lifegreengasnetwork.com/it/architettura_del_sistema (consulted feb. 16, 2021).

[15] «decompressione_misura.pdf». Consulted: feb. 18, 2021. [Online]. Available on: https://www.cpl.it/wp-content/uploads/2018/03/decompressione_misura.pdf.

[16] «Valves-Pressure Reducing Valves», *CTG Technical Blog*, 2012. https://techblog.ctgclean.com/2012/04/valves-pressure-reducing-valves/ (consulted feb. 19, 2021).

[17] M. Farzaneh-Gord, R. Ghezelbash, M. Sadi, e A. J. Moghadam, «Integration of vertical ground-coupled heat pump into a conventional natural gas pressure drop station: Energy, economic and CO2 emission assessment», *Energy*, vol. 112, pagg. 998–1014, ott. 2016, doi: 10.1016/j.energy.2016.06.100.

[18] M. Olfati, M. Bahiraei, e F. Veysi, «A novel modification on preheating process of natural gas in pressure reduction stations to improve energy consumption, exergy destruction and CO2 emission: Preheating based on real demand», *Energy*, vol. 173, pagg. 598–609, apr. 2019, doi: 10.1016/j.energy.2019.02.090.

[19] «559_ksi_ct_eng_may07.pdf». Consulted: feb. 20, 2021. [Online]. Available on: https://www.fiorentini.com/media/files/559_ksi_ct_eng_may07.pdf.

[20] «allegato_dimensionamento_remi.pdf». Consulted: feb. 20, 2021. [Online]. Available on:

https://www.snam.it/export/sites/snam-rp/repository-srg/file/Codice_di_rete/01_Area_Capitoli_Codice_di_Rete/Capitolo_10/10_Allegati/allegato_dimensionamento_remi.pdf.
[21] M. F. Torchio, *Tabelle di termodinamica applicata e trasmissione del calore*, CLUT, 2012.
[22] T. L. Bergman, A c. di, *Introduction to heat transfer*, 6th ed. Hoboken, NJ: Wiley, 2011.
[23] F. Piana, G. Fioraso, A. Irace, e P. Mosca, «Geological map of Piemonte Region (NW Italy)».
[24] «Idrogeologia del Piemonte.pdf». Consulted: jan. 15, 2021. [Online]. Available on: https://www.arpa.piemonte.it/approfondimenti/temi-ambientali/acqua/acque-sotterranee/IdrogeologiadelPiemonte.pdf.
[25] «Piano di Tutela delle Acque – Revisione 2018», *Regione Piemonte*. https://www.regione.piemonte.it/web/temi/ambiente-territorio/ambiente/acqua/piano-tutela-delle-acque-revisione-2018/ (consulted jan. 12, 2021).
[26] R. Sethi e A. Di Molfetta, *Groundwater Engineering: A Technical Approach to Hydrogeology, Contaminant Transport and Groundwater Remediation*. Springer International Publishing, 2019.
[27] Y. Noorollahi, G. Ghasemi, F. Kowsary, S. Roumi, e S. Jalilinasrabady, «Modelling of heat supply for natural gas pressure reduction station using geothermal energy», *International Journal of Sustainable Energy*, vol. 38, n. 8, pagg. 773–793, set. 2019, doi: 10.1080/14786451.2019.1585434.
[28] M. Farzaneh-Gord, R. Ghezelbash, A. Arabkoohsar, L. Pilevari, L. Machado, e R. N. N. Koury, «Employing geothermal heat exchanger in natural gas pressure drop station in order to decrease fuel consumption», *Energy*, vol. 83, pagg. 164–176, apr. 2015, doi: 10.1016/j.energy.2015.02.093.
[29] «Fattori di emissione per la produzione ed il consumo di energia elettrica in Italia — Italiano». http://www.sinanet.isprambiente.it/it/sia-ispra/serie-storiche-emissioni/fattori-di-emissione-per-la-produzione-ed-il-consumo-di-energia-elettrica-in-italia/view (consulted feb. 21, 2021).
[30] «Electricity price statistics - Statistics Explained». https://ec.europa.eu/eurostat/statistics-explained/index.php/Electricity_price_statistics#Electricity_prices_for_non-household_consumers/ (consulted mar. 1, 2021).
[31] «ARERA - Prezzi finali del gas naturale per i consumatori industriali - UE e area Euro». https://www.arera.it/it/dati/gpcfr2.htm/ (consulted mar. 1, 2021).
[32] M. Rivoire, *Dynamic simulation and economic analysis of geothermal HVAC systems in different climate zones*, Polytechnic of Turin: Master Thesis, Mar. 2017.
[33] «Preziario ANIPA 2021 | A.N.I.P.A.» https://www.anipapozzi.com/it/preziario-anipa-2021 (consulted mar. 1, 2021).
[34] R. Ghezelbash, M. Farzaneh-Gord, H. Behi, M. Sadi, e H. S. Khorramabady, «Performance assessment of a natural gas expansion plant integrated with a vertical ground-coupled heat pump», *Energy*, vol. 93, pagg. 2503–2517, dic. 2015, doi: 10.1016/j.energy.2015.10.101.
[35] E. L. Cascio, Z. Ma, e C. Schenone, «Performance assessment of a novel natural gas pressure reduction station equipped with parabolic trough solar collectors», *Renewable Energy*, vol. 128, pagg. 177–187, dic. 2018, doi: 10.1016/j.renene.2018.05.058.
[36] P. Danieli, G. Carraro, e A. Lazzaretto, «Thermodynamic and Economic Feasibility of Energy Recovery from Pressure Reduction Stations in Natural Gas Distribution Networks», *Energies*, vol. 13, n. 17, pag. 4453, ago. 2020, doi: 10.3390/en13174453.
[37] E. Ashouri, F. Veysi, E. Shojaeizadeh, e M. Asadi, «The minimum gas temperature at the inlet of regulators in natural gas pressure reduction stations (CGS) for energy saving in water bath heaters», *Journal of Natural Gas Science and Engineering*, vol. 21, pagg. 230–240, nov. 2014, doi: 10.1016/j.jngse.2014.08.005.
[38] A. Franco, «Natural gas consumption and correlation with the uses of thermal energy: Analysis of the Italian case», *Journal of Natural Gas Science and Engineering*, vol. 31, pagg. 703–714, apr. 2016, doi: 10.1016/j.jngse.2016.03.094.

ACKNOWLEDGMENTS

I would like to acknowledge the contributions of Marco Orsi, who supplied the data necessary for this study, and my supervisors Alessandro, Bruno, and Edoardo, for their valuable advices.

I also would like to gratefully thank all my friends, my girlfriend, and my family, for their unfailing support during this time and throughout the past years.